ALMA MATER STUDIORUM
UNIVERSITÀ DI BOLOGNA

in cotutela con Instytut Geofizyki Polskiej Akademii Nauk

DOTTORATO DI RICERCA IN

Ingegneria civile, chimica, ambientale e dei materiali

Ciclo XXXVII

Settore Concorsuale: 08/A1 - Idraulica, Idrologia, Costruzioni Idrauliche e Marittime

Settore Scientifico Disciplinare: ICAR/01 - Idraulica

Onset of motion of compact-shaped microplastics in open-channel flows

Presentata da: Arianna Varrani

Coordinatore Dottorato

Prof. Enrico Sassoni

Supervisori

Prof. Paweł M. Rowiński
Prof. Massimo Guerrero

Co-supervisore

dr.ing. Magdalena Mrokowska

Esame finale anno 2025

Onset of motion of compact-shaped microplastics in open-channel flows

Arianna Varrani

A thesis presented for the degree of
Doktor Nauk / Philosophiae Doctor

Institute of Geophysics, Polish Academy of Sciences
Department of Hydrology and Hydrodynamics

Alma Mater Studiorum, Università di Bologna
Department of Civil, Chemical, Environmental and Materials Engineering

Supervisor: Professor Paweł M. Rowiński
Co-supervisor: Associate Professor Massimo Guerrero
Auxiliary supervisor: Associate Professor Magdalena Mrokowska

Institute of Geophysics
Polish Academy of Sciences

ALMA MATER STUDIORUM
UNIVERSITÀ DI BOLOGNA

DIPARTIMENTO DI INGEGNERIA
CIVILE, CHIMICA, AMBIENTALE E
DEI MATERIALI

Warsaw, February 2025

to Ian, and Michael

Acknowledgements

My thanks go to Paweł Rowiński, for accepting me as Ph.D. candidate, knowing I already quit once, and fostering collaboration with Magdalena Mrokowska, which I think enriched me in many different forms. My sincere thanks also to Massimo Guerrero, for accepting the challenges of mentoring me, for a second time. I shall treasure those Italian-spoken truths about life in Academia. To my supervisors and hidden mentors: thank you. I deeply value the advice and thought-provoking comments in the writing exercise resulted in this thesis. I really appreciate the support you offered me in these turbulent years of pandemic, and will keep all lessons learned for future collaborations, to allow a much smoother transition than the one I embodied.

What was achieved here would surely not have been possible without the kind words, help (and time) of Alessio Radice, who hosted me in the hydraulic laboratories of Politecnico di Milano for a first tentative experiment on incipient motion. I am deeply grateful to have crossed path with him, and I hope I'll have a chance to return kindness.

A mention is due to the secretaries overseeing the Cotutelle procedure, especially Ms. Anna Cygan, Ms. Angela Maritato and Mr. Antonio Spagnuolo without whom this 1500 km-long collaboration couldn't have been formally set and prolonged.

Through my experimental journey, I benefitted from the help of many people who stepped in unconsciously for different aspects of this endeavour. The hands: Andrzej Skrzyński and Alberto Boninsegni for their technical support during experiments preparation. The eyes: Gabriella Gaeta for spotting crucial files and helping sieving a portion of the plastics used. The hands and ears: Łukasz Przyborowski for the time spent in the laboratory in Warsaw doing the first tests, and then experiments, and for embracing the "save the world from plastics" quest I joined when starting my Ph.D. journey. The mouth: Slaven Conevski for a "magic word" at the beginning of my data analysis struggles.

I am grateful to have met, through my journey, so many inspiring humans, whom I list here, for their gentle listening, precious advice, encouragement and friendship: Frank Molkenthin, Daniel Caviedes-Voullième, Grzegorz Sinycin, Hossein Hamidifar, Marie Burckbuchler, Stéphane Fischer, Daniel Valero, Alnilam Fernandez, Toktam Zand, Ilya Bruchkouski.

This journey got its kick-off during the pandemic times, and I am especially grateful for the casual remote support team I became part of: Anne, Cornelle, Hagit, thank you for listening and growing together.

I would not have moved to Warsaw if not for two very unique humans: Michael thank you for your patience, unconditional support and for the rock you are, and Ian, I hope this inspires you to pursue your dreams.

Special thanks to the family I chose some many years ago. I am so thankful and deeply grateful for the unconditional support through these years, and I look forward to the next chapter of our adventure together. May it be blissful as in our shared vision.

Finally, I am grateful for my family in Italy, who tried to keep track of my path along with their own highs and lows. Grazie per avermi sostenuto anche quando non poteva essere fra le vostre priorità.

Contents

List of Figures ix
List of Tables xiii
List of Symbols xv
List of Acronyms xix

1 Outline **1**
1.1 Problem's statement 1
1.2 Thesis' layout 2
1.3 On the terms *incipient motion* and *remobilisation* 2

2 Introduction **5**
2.1 Motivation and scope 5
2.1.1 Plastics as new sedimentary material 6
2.1.2 The overlooked story of plastics incipient motion experiments 7
2.2 Literature review 10
2.2.1 Historical excursus on the importance of incipient motion studies . . . 10
2.2.2 Incipient motion of sediments in flowing waters: parameters' choice . . 11
2.2.3 Incipient motion of sediments in flowing waters: a classification of approaches 26
2.2.4 Incipient motion measurements: weighted vs visual estimation 28
2.2.5 Microplastics remobilisation and incipient motion studies: an overview 28
2.2.6 On the many, different definitions for incipient motion 29
2.3 A semi-probabilistic definition of threshold conditions for mobilisation 30

3 Methodology **33**
3.1 Experimental programme and experiments' design 33
3.1.1 Measuring apparatus 34
3.1.2 Materials 34
3.2 HML flume experiments: flat bed 36
3.2.1 Plastics homogeneous bed experiments 37
3.2.2 Natural bed experiments: microplastics on a clastic bed 41

3.3 Data analysis fundamentals . . . 45
3.3.1 Analysis of velocity data . . . 45
3.3.2 Analysis of videos for particles' detachments . . . 47

4 Plastic grains over a plastic bed 51
4.1 Introduction . . . 51
4.2 Experiments . . . 53
4.2.1 Experimental conditions . . . 53
4.3 Experimental results . . . 54
4.3.1 Bed shear velocities . . . 54
4.3.2 Bed changes . . . 55
4.3.3 Threshold conditions . . . 57
4.4 Discussion . . . 59
4.5 Summary . . . 61

5 Remobilisation of plastic particles from a clastic bed 63
5.1 Introduction . . . 63
5.2 Experiments . . . 65
5.2.1 Experimental conditions . . . 66
5.3 Experimental results . . . 71
5.3.1 Bed shear velocities . . . 72
5.3.2 Microplastics' surface concentration changes . . . 73
5.3.3 Threshold conditions on clastic bed . . . 74
5.3.4 Microplastics mobility . . . 75
5.3.5 Dimensional analysis and PCA . . . 75
5.4 Discussion . . . 79
5.4.1 From analogy to analysis . . . 81
5.5 Summary . . . 83

6 Conclusions and further developments 85
6.1 Incipient motion of microplastics from homogeneous bed . . . 85
6.2 Remobilisation of plastic particles from a clastic bed . . . 86
6.3 Are compact microplastics talking sedimentary processes' language? . . . 86
6.4 Further work . . . 86

Bibliography 89

Appendices 105

A Glossary 106
A.1 List of key terms . . . 106

B Summary tables **107**
B.1 Incipient motion experiments: plastics on plastics bed 107
B.2 Incipient motion experiments: plastics on clastic bed 110
B.2.1 Gravel: PA6 110
B.2.2 Gravel: POM 111
B.2.3 Sand: PA6 111
B.2.4 Sand: POM 112
B.3 Logarithmic fit parameters for different beds 113
B.3.1 Homogeneous: PA6 113
B.3.2 Homogeneous: POM 114
B.3.3 Gravel: PA6 115
B.3.4 Gravel: POM 116
B.3.5 Sand: PA6 117
B.3.6 Sand: POM 118

C Experimental protocol **119**
C.1 Movable bed experiments with plastic granules 119
C.1.1 Bed layer preparation 119
C.1.2 Flume filling up to working conditions 120
C.1.3 Flow field characterisation 120
C.1.4 Bed movements and cover changes detection 122
C.2 Fixed bed experiments with plastic granules: clastic bed 123
C.2.1 General protocol for experiments with MPs on clastic beds. 123
C.2.2 Flow field characterisaton 125
C.2.3 Bed cover changes detection 126

List of Figures

2.1 Hjulström diagram showing the dependency between the sediment grain-size and the (critical) velocity required for its erosion, transport or deposition. Source Wikipedia, licensed with CC-by-SA-3.0, GFDL. 13

2.2 Schematic illustrations of various forces acting on a single grain for zero-sloped beds. (after Armanini, 2018). 18

2.3 Original Shields' diagram, modified from Shields, 1936 PhD Thesis to highlight near-bed regimes, from left to right: in light blue smooth-wall, in violet transitional and in pink rough wall regime. 21

2.4 Higher resolved Shields' diagram, modified from Armanini, 2018 reporting the original dataset plotted by Shields'. 22

2.5 Probability distributions for the particle resisting shear stress (discontinuous probability function) and the ambient fluid shear stress (continuous probability function) acting on bed particles. The probabilities of instantaneous bed shear stress due to flow turbulence $\bar{\tau}$ and shear stress needed to dislodge the particles $\bar{\tau}_C$ are determining the sensitivity of grains to mobilisation (original from Grass, 1970, as reported in Cecchetto, 2017). 31

3.1 Sketch of the HML flume, planar view. Sections S_{1-4} starting from a distance of 2.0 m from the inlet, where measurements were taken. At the outlet, a sediment trap was located, collecting transported particles. 36

3.2 Experimental setup during PA6 experiments, the transducers for velocity measurements are placed at an intermediate vertical position in the first available cross-section. 39

3.3 Isolines of near-bed UVP-measured longitudinal velocities for PA6 experiments. The water depth (highlighted in light blue) was around 60 mm. 40

3.4 Example of gravel bed covered by PA6 grains at 1% surface cover. It is visible how the MPs are distributed randomly and uniformly over the bed. The image was not used for further processing. 43

3.5 Camera field of view over the region of interest (ROI) for detecting the mobilisation of microplastics on a gravel bed. 44

3.6 Workflow from dataset selection to image analysis. If the image has more than two colours, preprocessing is needed, and colour thresholding is done in the CieLAB colour space. The analysis sees the computation of pixel-wise mean $M_{1,px}$ and standard deviation $M_{2,px}$ that are later used to identify areas where significant change in the colour intensity occurred. Once filtered by size, these areas correspond to particle-sized cover changes. 48

3.7 Cumulative sum of bed changes detected at each time-window (for the dataset PA6_Q2t3). 49

4.1 PA6 (black) and POM (red) particles chosen for the experiments. 53

4.2 Distribution of mean flow velocities measured via UVP at increasing elevations from the mean bed for Section 3 in PA6 experiments (lighter plastic grains). . . 55

4.3 Example of time-averaged bed shear velocities computed from UVP measurements and cumulative bed changes for the minimum (a) and maximum (b) discharges tested on PA6 bed. The scale indicates how long in the time intervals single particles were not in their initial position (light grey meaning unchanged bed cover and yellow meaning sheet-flow occurring throughout the whole experiment). 56

4.4 Experimental data points for PA6 (orange) and POM (pink) bedded tests versus literature data derived with similar methodology. The Shields' curve range (dashed) follows the relation proposed by Paphitis, 2001. 57

4.5 Proxy distribution of experimental data points for PA6 (black) and POM (red) bed changes frequency $\dot{n}/N$ vs bed shear velocities u^*, computed for time intervals of 5 s for all experiments. The variability of bed shear velocities is evident for both plastic materials. 58

4.6 Experimental data points for PA6 and POM bedded tests versus Graf and Pazis, 1977 data for other plastics homogeneous bed tests. The Shields' curve range (dashed) follows the relations by Paphitis, 2001. The particle Reynolds number and Shields' number calculated for all tests for the two plastics are sorted by discharge (size of symbols). Downward triangles indicate the incipient motion threshold identified with the *semi-probabilistic approach* proposed. 60

5.1 Example of plastic PA6 particles on flat gravel (left) and sand (right) bed. . . . 66

5.2 Experimental data points for PA6 (orange) and POM (pink) flat-bed tests versus homogeneous bed experiments (updated from Figure 4.4). Data on sand and gravel bed (full points and big circles) are visibly below the theoretical Shields' curve. 72

5.3 Violin plots showing the observed bed shear velocities u^* for PA6 (black, lower density) and POM (red, higher density) on the three different types of beds. The general trend with a decrease in observed u^* with decreasing geometric roughness (and grain-size) moving along the x-axis from homogeneous bed to gravel and sand bed is evident. 73

5.4 Detected number of changes for PA6 on gravel flat-bed tests sorted by MPs surface concentration at a discharge $Q = 2$ l/s. 73

5.5 Modification of Figure 5.2 with threshold conditions derived from a fixed $\dot{n}/N = 10^{-2}s^{-1}$. Threshold for the chosen MPs on both sand ($*$) and gravel ($\lozenge$) beds lies below the theoretical Shields' curve. 74

5.6 Detected frequency of particle motion $\dot{n}$ $[s^{-1}]$ for PA6 (first row) and POM (second row) on gravel (first column) and sand (second column) beds. Data are sorted by discharge, where increasing darkness of blue means increasing discharge. On the x-axis the concentration increases from $c_1 = 0.05\%$ to $c_5 = 1\%$. 75

5.7 PC analysis of all experiments on homogeneous and clastic bed: first two principal components PC1 and PC2 on the x- and y-axis respectively. Dimensionless parameters used are from Equation 5.5 substituting the stream power Ω to Re. Only those with the highest relevance are shown. 78

5.8 Percentage of variability in the data explained by the first 3 principal components. 78

5.9 Threshold conditions for the PA6 (yellow) and POM (pink) particles determined in this work versus literature data (grey). Most of the values fall in the same region but PA6 on sand. The symbols show thresholds conditions on different bed, where literature data, and $\triangledown$, $\lozenge$ and $*$ represent our derived thresholds on homogeneous, gravel and sand bed respectively. 79

5.10 Experimental data points for PA6 (black) and POM (red) flat-bed tests for homogeneous bed (full $\circ$), plastics on gravel ($\lozenge$) and plastics on sand ($*$), the symbol size indicates the (increasing) surface concentration in the tests with values equal to 0.05%, 0.1%, 0.2%, 0.5%, 1%. Data on sand and gravel bed, due to the lower surface concentration, show a higher relative mobility (higher values of $\dot{n}/N$). . 80

5.11 PC analysis of all experiments on homogeneous and clastic bed: first two principal components PC1 and PC2 on the x- and y-axis respectively. Dimensionless parameters used are the same as in 5.7 with the exclusion of $Re_{s,MP}$, only those with the highest relevance are shown. 83

C.1 Ubertone® online drive GUI 121

C.2 Positioning of the measurement apparatus: a) details on the UBLab P transducers by Ubertone®, b) camera and its support. 122

C.3 Scheme of manual seeding method: seeding lines (violet) inclined 45° to the longitudinal axis of the flume. 125

C.4 UVP transducer and camera setup during gravel bed experiments. Flume seen from the side. 126

List of Tables

2.1 Overview of studies using lightweight materials in physical models to scale morphodynamic processes in time. Edited and updated from Henry and Aberle, 2018. 8

3.1 Results from the sieve analysis for the two microplastics used 35

3.2 Summary of microplastic particles' characteristics 35

3.3 Granulometric distribution of the chosen gravel for HML flat bed experiments. Data from the producer. 35

3.4 Granulometric distribution of the chosen sand for HML flat bed experiments. Data from the producer. 36

3.5 General ranges for the hydraulic conditions in the plastic bed experiments. Discharge Q, water depth y, bed elevation from the flume rigid bottom Z_{Bed}, water surface elevation from the flume rigid bottom h 38

3.6 Tested MPs surface concentrations **c1** - **c5** (in percentage of area covered by MPs) on clastic beds. 41

3.7 General ranges for the hydraulic conditions in the gravel bed experiments. Discharge Q, water depth y, bed elevation from the flume rigid bottom Z_{Bed}, water surface elevation from the flume rigid bottom h. 42

3.8 General ranges for the hydraulic conditions in the sand bed experiments. Discharge Q, water depth y, bed elevation from the flume rigid bottom Z_{Bed}, water surface elevation from the flume rigid bottom h. 43

4.1 Discharge-wise ranges for the hydraulic conditions in the plastic bed experiments for PA6 and POM particles at Section 3: discharge Q, water depth y, flow Reynolds' number Re, time-averaged bed shear velocity U^*, particle Reynolds' number Re^* and Froude number Fr. For other conditions see Appendix B.1 . . 54

4.2 PA6 and POM threshold conditions on homogeneous bed: $\frac{\dot{n}}{N}|_{cr}$ is the chosen (threshold) for bed changes frequency, $P_{cr}|_{\dot{n}/N}$ is its associated probability of occurrence, u^*_{cr} corresponds to $u^*|P_{cr}$ identified by the chosen threshold for frequency of bed changes $P_{cr}|_{\dot{n}/N}$, and $\tau_{0,cr}$ was computed for the obtained values of threshold bed shear velocities u^*_{cr}. For completeness, also the particle's Reynolds' number Re^* and threshold Shields' parameters θ_{cr} are shown. 59
4.3 Plastic sediments data, and experimantal conditions, from Graf and Pazis, 1977. 61

5.1 Discharge-wise ranges for the hydraulic conditions in the gravel bed experiments for PA6 particles: discharge Q, water depth y, flow Reynolds' number Re, time-averaged bed shear velocity U^*, bed Reynolds' number Re^* and Froude number Fr. For other conditions see Appendix B.1 67
5.2 Discharge-wise ranges for the hydraulic conditions in the gravel bed experiments for POM particles: discharge Q, water depth y, flow Reynolds' number Re, time-averaged bed shear velocity U^*, bed Reynolds' number Re^* and Froude number Fr. For other conditions see Appendix B.1 68
5.3 Discharge-wise ranges for the hydraulic conditions in the sand bed experiments for PA6 particles: discharge Q, water depth y, flow Reynolds' number Re, time-averaged bed shear velocity U^*, bed Reynolds' number Re^* and Froude number Fr. For other conditions see Appendix B.1 69
5.4 Discharge-wise ranges for the hydraulic conditions in the sand bed experiments for POM particles: discharge Q, water depth y, flow Reynolds' number Re, time-averaged bed shear velocity U^*, bed Reynolds' number Re^* and Froude number Fr. For other conditions see Appendix B.1 70

List of Symbols

$\%C$	Bed surface concentration of movable material (MPs)	[−]
χ_B	Dimensionless degree of motion of a fraction on a mixed bed	[−]
Δ	Submerged relative density of sediments	[−]
δ	Thickness of viscous sublayer	[−]
Δ_{MP}	Submerged relative density of microplastics	[−]
κ	Von Kármán constant	[−]
ν	Kinematic viscosity coefficient of water	[m^2 s^{-1}]
Ω	Stream power	[kg m s^{-3}]
Ω_{cr}	Threshold stream power	[kg m s^{-3}]
ϕ	Surface packing density, percentage of imaged bed area covered by surface grains	[−]
Φ_D	Depositional flux	[m^2 s^{-1}]
Φ_E	Erosional flux	[m^2 s^{-1}]
ρ	Density of water	[kg m^3]
ρ_S	Bulk sediment density	[kg m^3]
ρ_{MP}	Bulk density of microplastics	[kg m^3]
σ_z	Standard deviation of the bed elevation	[m]
τ	Shear stress	[kg $m^{-1}s^{-2}$]
τ_0	Bed shear stress	[kg $m^{-1}s^{-2}$]
$\tau_{0,cr}$	Threshold bed shear stress	[kg m^{-1} s^{-2}]

θ^*	Shields' mobility parameter	[−]
θ^*_{cr}	Threshold Shields' mobility parameter	[−]
$\theta_{cr,i}$	Shields' critical parameter of the i-th fraction	[−]
$\theta_{cr,m}$	Shields' critical parameter of the representative sediment class	[−]
ϑ	Threshold value for pixel (colour) intensity	[−]
$\forall_p$	Solid particle volume	[m^3]
ξ_i	Hiding exposure function for the i-th fraction	[−]
A	Surface area imaged in the ROI	[m^2]
A_p	Area of the particle exposed to the flow	[m^2]
$a_{1,2}$	Major and minor axes of the plastic ellipsoidal grains	[m]
C_1, C_2	Regression coefficients	[−]
C_D	Particle drag coefficient	[−]
C_L	Particle lift coefficient	[−]
$c_{c,s}$	Cohesivity coefficient by Zanke 1977	[−]
$c_{packing}$	Packing coefficient by White 1940	[−]
c_{turb}	Turbulence coefficient by White 1940	[−]
CU	Coefficient of uniformity of sediment size in the bed uppermost layer	[−]
d	Grain diameter	[m]
D^*	Dimensionless grain diameter	[−]
d^*_{MP}	Dimensionless diameter of the MPs	[−]
d_i	Diameter of the i-th class	[m]
d_m	Representative diameter of the sediment mixture	[m]
d_{50}	Median diameter of a graded sediment mixture	[m]
d_{eq}	Sphere equivalent diameter of the plastic particles	[m]
e	Grain exposure	[m]
e_s	Nikuradse bed roughness height	[m]

exp	Exponential function	[−]
f_1, f_2	Generic functional relationships	[−]
F_D	Drag force	[kg m s^{-2}]
F_L	Lift force	[kg m s^{-2}]
f_{cr}	Function at initiation of motion	
$F_{tr,cr}$	Threshold tractive force	[kg m s^{-3}]
F_{tr}	Tractive force	[kg m s^{-3}]
Fr	Froude number	[−]
Fr^*_S	Particle densimetric Froude number	[−]
h	Mean water surface elevation	[m]
$M_{1,px}$	Mean of pixelwise color value	[−]
$M_{2,px}$	Standard deviation of pixelwise color value	[m]
n	Number of bed changes in each Time Window	[−]
N_{Tot}	Total number of movable particles on the bed surface	[−]
p	Grain protrusion	[m]
Q	Mean flow discharge	[m^3 s^{-1}]
q_S	Solid discharge per unit width	[m^2 s^{-1}]
Q_{cr}	Threshold discharge	[m^3 s^{-1}]
Q_{seed}	MPs seeding discharge on clastic bed	[m^3 s^{-1}]
Re	Reynolds' number	[−]
Re^*	Particle's Reynolds number	[−]
Re^*_{Bed}	Bed Reynolds' number	[−]
Re^*_{MP}	Microplastics (mobile particles) Reynolds' number	[−]
$Re_{s,MP}$	Mobile particle sedimentary Reynolds' number	[−]
Rs	Rouse number	[−]
S_b	Bed slope	[−]

S_e	Slope of the energy grade line	[−]
t	Time interval	[s]
U	Mean flow velocity	[m s^{-1}]
u	Longitudinal velocity	[m s^{-1}]
u^*	Bed shear velocity	[m s^{-1}]
u_p	Near-bed velocity at the particle level	[m s^{-1}]
U_{cr}	Threshold mean flow velocity	[m s^{-1}]
u_{cr}	Near-bed threshold flow velocity	[m s^{-1}]
$u_{p,cr}$	Threshold flow velocity at the particle level	[m s^{-1}]
$v_{b,cr}$	Near-bed velocity at onset of transport (critical)	[m s^{-1}]
w_s	Particle settling velocity	[m s^{-1}]
y	Mean water depth	[m]
z	Generic elevation from the bed	[m]
z_0	Hydrodynamic roughness length	[m]
z_b	Bed surface elevation	[m]
Z_{Bed}	Elevation of the mean bed from the flume rigid bottom (reference)	[m]
CSF	Corey Shape Factor	[−]
KUP	Kramer's uniformity parameter	[−]

List of Acronyms

CIELAB	CIELAB color space. Defined by the International Commission on Illumination: L* stays for lightness (black to white on a scale of 0 - 100), while a* and b* represent chromaticity with no specific numeric limits spanning green to red and blue to yellow.
FOV	Field of View
HML	Hydrodynamic Models Laboratory, Institute of Geophysics Polish Academy of Sciences
IG-PAS	Institute of Geophysics, Polish Academy of Sciences
MP	Microplastic
PA6	Polyamide 6
PC	Principal Component
POM	Polyoxymethylene
RGB	Red Green Blue color space
ROI	Region of Interest
TW	Time Window
UVP	Ultrasonic Velocity Profiler

Chapter 1

Outline

"For the world is changing: I feel it in the water,
I feel it in the earth, and I smell it in the air."

J.R.R. Tolkien, 1954

1.1 Problem's statement

Historically, scientific and technical research devoted special attention to the conditions at which grains, resting at the riverbed, begin to move forced by the overflowing water (Dey and Ali, 2019). For obvious reasons, most studies investigated such threshold conditions (i.e. incipient motion condition) in the case of natural sediments. In this Thesis, instead, incipient motion and remobilisation conditions of anthropogenic particles, which can be found presently among river-bed sediments (J. Li et al., 2018, Frei et al., 2019, Koelmans et al., 2019) are investigated. For their size, the material used can be referred to as microplastics (i.e. plastic particles in the range 1 μm - 5 mm), and, having a lower density than natural sediments, it is therefore more mobile in a wide range of flow conditions.
A series of flume experiments is here presented and the results discussed, with the goal of setting a basis for understanding the dynamics of plastic particles present in the bed sediments, also paying attention to the relative effects of the bed sediments grain-size distribution on the remobilisation of plastic particles having different densities.

Research questions

The work in this thesis aims at addressing the flow-induced mobilisation of plastic particles from a loose bed, and its dependency upon the bed grain-size characteristics. Specifically, the presence of both lightweight plastic and natural clastic sediments poses the following questions when plastics mobilisation is considered: **Q1.1** - How can we define the critical threshold for incipient

motion of microplastic particles? **Q1.2** - How to relate it to the hydraulic conditions? **Q2.1** - Can we use the same threshold definition for different bed compositions? **Q2.2** - Does the threshold value depend on the content of MPs potentially moving on the bed surface?

1.2 Thesis' layout

The Thesis is subdivided into chapters, building a narrative around the microplastics' incipient motion and remobilisation in open channel flows. Chapter 2, introduces to the problem and the main research aims, and contains a synopsis to present knowledge about the incipient motion of sediments. The most adopted methods are classified and described and the framework for our proposed method is given. In Chapter 3, the research facilities and experimental methodology are described, with details about the measuring equipment and bed materials used. The chapter also contains key aspects of the data analysis and assessment procedures, as well as the main assumptions in processing data. In Chapter 4, our approach to define the mobility threshold for uniform sediment is introduced, with reference to artificial grains, and the results of its first application are reported and discussed. This chapter provides the answer to **Q1.1** and **Q1.2** and the definition of incipient motion reported there serves later as baseline conditions for assessing microplastics mobility on different types of beds. In Chapter 5, the proposed framework is adopted to study threshold conditions of microplastics on various beds. The experimental results are presented and analysed, and factors influencing the behaviour of the entire sediment mixture and individual fractions are examined. Here the answer to **Q2.1** and **Q2.2** is provided. Chapter 6 contains the conclusions from the research undertaken, together with suggestions for future developments to complement the knowledge of microplastics sedimentary processes. The Appendices contain detailed protocols to carry out experimental work of microplastics' mobilisation and transport in laboratory flumes (Appendices C), summary tables of data measured for all experiments (Appendices B), and a glossary for the most recurrent terms (Appendix A) when dealing with erosion and remobilisation of sediments.
The datasets are available in the IG-PAS public repository
(https://dataportal.igf.edu.pl/group/about/lab_microplastics_ncn).

1.3 On the terms *incipient motion* and *remobilisation*

In this work, the term "incipient motion" is appropriately used only in the case of sediments which cannot be distinguished by the ones composing the bed layer, while we address with "remobilisation" the phenomenon of any type of other sedimentary material getting into motion on a loose solid boundary by the action of a forcing fluid. We deem it important to be clear about this point, since a variety of terminologies is available in the literature, which sows ambiguity to a dichotomous problem per se, i.e. onset of motion of particles, and as a result, does not support further efforts in addressing the more complex cases of bimodal bed composition in terms of

particles' materials.

Chapter 2

Introduction

"The root cause of this unfortunate proliferation and diversity of ideas is evidently the absence of any sound and indisputable quantitative basis of reasoning compatible both with the facts and with the laws of nature and therefore commonly acceptable. Consensus of opinion, which varies from decade to decade, is no satisfactory substitute."

R. A. Bagnold, 1966

2.1 Motivation and scope

"Plastics are used extensively because of their highly functional properties — they can be moulded into many shapes and are lightweight, hygienic, cheap to make and good insulators. For these reasons, plastics production is increasing sharply. In the past two decades it has doubled to more than 450 million tonnes annually" ("UN plastics treaty: don't let lobbyists drown out researchers", 2024). Plastic pollution has been recognised as a global problem by the United Nations in 2022 (UNEP, 2022), thanks to the large body of evidence built in the past 20 years on the presence of plastic in all environmental compartments (Thompson et al., 2004; Horton et al., 2017; Hurley et al., 2020; Horton, 2022, among others). The field of plastic research is therefore rather new and many uncertainties are still to be resolved around long-term effects and environmental consequences (Wagner et al., 2014). Uncertainty does not involve only the biological and ecotoxicological aspects of plastic pollution (Adam et al., 2019), but it spreads through all facets of the problem: from monitoring of quantity and evaluation of single polymers in samples to quantification and budgeting at both small and large scales (Wagner et al., 2014; Schmidt et al., 2017; González-Fernández et al., 2023).

It is well known that plastic materials leaked into the environment undergo weathering and fragmentation (Pfohl et al., 2022), forming smaller particles named microplastics (Liro et al., 2023; Andrady et al., 2022) and, further down in size, nanoplastics (Wohlleben et al., 2024). The

processes of ageing, weathering and fragmentation are likely to change not only the toxicological effects of microplastics, but also, as recently outlined by Wang et al. (2024), the transport processes, and specifically the incipient motion conditions.
Besides the increasing evidence featuring the presence of plastic particles and debris in freshwater systems (Zbyszewski and Corcoran, 2011; Dris et al., 2015; J. Li et al., 2018; and Lechner, 2020), little is known about the interactions between plastics and natural clastic particles. Such interactions can be classified as physical, like the interplay between microplastics' and sediment transport (Waldschläger and Schüttrumpf, 2019a; Boos et al., 2021; Russell et al., 2023), or chemical, e.g. the absorption of heavy metals and contaminants (Rochman et al., 2014; Alimi et al., 2018 and B. Li et al., 2024).
While comprehensive and sustained efforts in monitoring and measuring plastics appear, e.g. Lechner et al. (2014) report the abundance of plastics in the Danube river, which help describe the magnitude of the plastic problem beyond what is well known for the ocean (Dris et al., 2015), the amount of resources invested in understanding transport processes among compartments, to inform models and eventually monitoring strategies is much scarcer, for the inherent complexity that plastic materials show.
This Thesis aims to add one small brick to reduce this knowledge gap, based on experimental work: the estimation of the mobility threshold used in formulae for the estimation of sediment transport (e.g. Meyer-Peter and Müller 1948, Van Rijn 1984). Since those formulae are implemented in numerical models, the results here obtained could be later used to estimate fluxes of microplastics at the water-bed interface of open channel flows.

2.1.1 Plastics as new sedimentary material

Sediment derives from the Latin *sedēre*, with the meaning of "to deposit". Sediments are all those particulate matter and substances which, present in a fluid under a gravitational field, tend to reach the lowest solid boundary. Within this definition, not only naturally occurring particles fit, but also granular materials or debris deriving from anthropic activities, such as e.g. ceramic fragments and plastic nurdles.
The literature on sediment transport discerns between the two environments in which sediment is immersed, mobilised and transported, namely water and air. Different approaches have been developed and adopted when dealing with transport in the two media (Shields, 1936; Einstein, 1950; Bagnold, 1954), with attempts to unify sediment transport models (among the first Bagnold,1979, and more recent contributions are e.g. Lu et al., 2005; Houssais and Jerolmack, 2017; Pähtz and Durán, 2020 and Pähtz et al., 2020). The transferability of sediment transport models (in both environments) to plastics transport has not been questioned, and adaptations of available theories are being developed (e.g. Goral et al., 2023a; Luo et al., 2022) to transfer methods to the new field of *plastics transport*.
Sediment transport dynamics depend on their physical and geometrical properties (e.g. size, density and shape), and, for natural sediments, the range of variability in grain-sizes generally

outweighs the variability of the other two properties. On the other hand, when considering other types of sedimentary materials, such as heavy minerals and anthropogenic particles, like microplastics, density and shape vary widely and can therefore play a greater role in determining transport dynamics (e.g. Komar et al., 1981; Viparelli et al., 2015 and Waldschläger et al., 2022). Gabbott et al. (2020) advance the proposition to treat plastic debris as a geological material due to the "ubiquity, longevity and abundance" that geological materials entail, which could also be among the properties of plastic debris. A rather recent review by Akdogan and Guven (2019) collecting literature sources from Web of Science, highlighted how the proven ubiquity and persistence of plastics in the environment require attention, not only in terms of toxicological effects, but also in terms of understanding their fate and transport. Another review on the presence of plastics in the environment (P. Li et al., 2021) highlighted the ubiquity of plastics in all environmental compartments, calling for more research in freshwater, terrestrial, and atmospheric systems, as marine plastics pollution has received much attention. In an assessment of the state of policies to safeguard the integrity of planet Earth's systems, Persson et al. (2022) refer to novel entities (among which plastics) as "entities that are novel in a geological sense and that could have large-scale impacts that threaten the integrity of Earth system processes".
Growing evidence of the presence and accumulation of plastic and microplastics in rivers at the river-bed interface (Liedermann et al., 2018; Drummond et al., 2022 and Duong et al., 2023), calls for an in-depth understanding of microplastic transport processes, and recent studies on microplastics transport dynamics (Waldschläger and Schüttrumpf, 2019a; Boos et al., 2021) started to answer such pressing need. Still, even when the usage of plastic products will be drastically reduced, the legacy of such materials leaked from our hands into the environment will likely last for ages to come (Bertling et al., 2018; Nyberg et al., 2023). Understanding the sedimentary processes of erosion, transport and deposition alongside all efforts into the more environmental and toxicological aspects of such materials in natural systems is paramount to mitigate and reduce exposure and risks (Wagner et al., 2014; de Souza Machado et al., 2018; UNEP, 2022).

2.1.2 The overlooked story of plastics incipient motion experiments

The use of artificial material for sediment motion studies dates back to the first USWES 1936 investigations, with the use of lightweight materials for bedload experiments (Bettess, 1990; Henry and Aberle, 2018) and Bagnold (1955) on the "characterisation of the effects of grains' low density on transport processes". Apart from the scientific merit of investigating incipient motion and transport of materials with diverse densities, the use of lightweight materials did not take hold until the 1970s when the increased need for engineering design of river management works required scaling sediments, and the "cohesion problem" did not allow for scaling by particle size only. Indeed, lightweight materials, such as plastic granules, allow for reproducing significant morphological processes at reduced time scales, due to the higher mobility for their lower density at a given size (i.e., larger than 60-100 μm to avoid possible cohesive force).

Dynamic scaling involves (i) the identification of a set of dimensionless variables, needed for a complete description of the studies process, and (ii) to design such model so that these variables have the same value both in the model and in the (field) prototype (Paola et al., 2009).
Scaling of flow involves either Froude (Fr) or Reynolds (Re) similarity, with the two dimensionless numbers equal to Equations 2.1 and 2.2

$$Fr = \frac{U}{gL} \tag{2.1}$$

$$Re = \frac{UL}{\nu} \tag{2.2}$$

while to scale sediment transport, Rouse number (Equation 2.3) and Shields' number (see later, 2.2.2.3, Equation 2.38) are to be considered

$$Rs = \frac{w_s}{\kappa u^*} \tag{2.3}$$

In Equations 2.1, 2.2 U is the mean flow velocity, g is the gravity constant, L is a length scale, usually the mean flow depth y is chosen, the coefficient of kinematic viscosity $\nu = 10^{-6}\ m^2/s$. In Equation and 2.3 w_S is the settling velocity in quiescent fluid, κ is the Von Kàrman constant and u^* is the bed shear velocity.
Scaled experiments with lightweight (plastic) materials have various advantages, and Table 2.1 reports an incomplete list of published works in which plastic grains were used as bed material. Although the focus was not specifically on the onset of transport, the *history* of lightweight-scaled experiments offers a starting point to understand microplastics sedimentary dynamics.

Table 2.1: Overview of studies using lightweight materials in physical models to scale morphodynamic processes in time. Edited and updated from Henry and Aberle, 2018.

Name	Process studied	Modelling approach	Sediments characteristics
Juez et al., 2018	Sediment supply-triggered hysteresis	Froude scaling. Unsteady flow.	polyurethane grains, diameters d_{50} = 200, 160, 80 μm and ρ_S = 1.16 g/cm^3
Berni et al., 2017	Bed destabilization under waves	Shields and Rouse number scaling	angular shaped grains with median diameter d_{50} = 0.64 mm and bulk density ρ_S = 1.18 g/cm^3
Finotello, 2017	Tidal channel evolution	No scaling	median diameter d_{50} = 250μm with bulk density ρ_S = 1.35 g/cm^3
Viparelli et al., 2015	Sediment sorting and selective transport by weight	No scaling. Use of lightweight sediments for testing sorting/transport processes	sediments mixtures of different densities spanning ρ_{S1} = 1.5 – 4.0 and ρ_{S2} = 2.6 - 3.3 g/cm^3
Gorrick and Rodrìguez, 2014	Mixed-load transport	Geometric and Froude scaling	similar grading mixture as prototype with ρ_S = 1.3 g/cm^3

Petruzzelli et al., 2013	Beach profiles morphodynamics	Froude scaling and distorted geometry	various angular and spherical particles with diameter and density range of d = 0.07 - 1.5 mm and ρ_S = 1.15 - 2.52 g/cm^3
Thélusmond et al., 2013	Sedimentary processes	Distorted Froude	ground melamine formaldehyde grains, size range d = 0.4 - 1.4 mm and density ρ_S = 1.49 g/cm^3
Meyering, 2012	Sediment density effect on scouring	Flow intensity U/u^* and densimetric Froude scaling	ellipsoidal and cylindrical granules with grain-size d = 2.7 mm and d = 2.6 mm and density ρ_S = 1.04 g/cm^3 and ρ_S = 1.39 g/cm^3 respectively
Gill and Pugh, 2009	Sediment transport processes	Modified-Froude model, sediment density and slope adjusted to scale on dimensionless transport rate	crushed coal sediments with d = 0.88 mm and ρ_S = 1.27 g/cm^3 to scale 51-mm-clastic sediments
Radice et al., 2008	Scouring at rectangular abutment	No scaling	grains with median diameter d_{50} = 1.9 mm and density ρ_S = 1.57 g/cm^3
Maynord, 2006	Morphodynamics for river engineering	Distorted Froude micromodels	a) coal beads and b) plastic granules with d = 0.25 - 1.2 mm ρ_S = 1.48 g/cm^3
Kocyigit et al., 2005	Sediment transport in harbours	No proper scaling	cation resin grains with median diameter d_{50} = 0.73 mm and density ρ_S = 1.21 g/cm^3
Peters, 1990	Sediment transport in large alluvial rivers with very low slopes	Distorted Froude scaled lightweight sediments. Velocity adjustment to trigger scouring	bakelite and polystyrene particles
Seng Low, 1989	Bed load transport	No scaling. Description of the transport of lightweight sediments	cylinder shaped particles with median dimension d_{50} = 3.5 mm and range of density ρ_S = 1.0 - 2.5 g/cm^3
Graf and Pazis, 1977	Erosion and deposition	No proper scaling	rounded PVC grains with median dimension d_{50} = 3.02 mm and density ρ_S = 1.41 g/cm^3
Bagnold, 1954	Transport processes	No scaling. Exploratory work on transport of very lightweight material	spherical particles with grain-size d = 1.32 mm and density ρ_S = 1.0 g/cm^3
USWES, 1936	Bed load material	Investigation of the suitability of lightweight materials to simulate bed load transport	

The use of plastic media is therefore not new to hydraulic laboratory environments (as evident in a first survey report by Bettess, 1990 and later by Henry and Aberle, 2018) and hydromorphodynamic studies, but the research questions behind it have now changed. A shift is

needed from "plastic sediments as a proxy of (clastic) sediments", to plastic sediments as anthropogenic sediments leaking into the natural environment, for which transport processes are still poorly understood, and the potential harm is still to be thoroughly assessed. Understanding the sedimentary behaviour of plastic grains *per se* is slowly becoming the scientific focus of a new branch of sedimentary research, and the work in this Thesis aims to contribute to this both old and new research thread.

2.2 Literature review

2.2.1 Historical excursus on the importance of incipient motion studies

The beginning of transport of sediments has been investigated in a systematic way, to date, for around a century, still, no coherent definition is available, which allows to definitely set such a threshold (1966 and much more recently Dey and Ali, 2019), provided it exists after all (Lavelle and Mofjeld, 1987 and Paphitis, 2001). The threshold concept itself has been questioned (Lavelle and Mofjeld, 1987), since, due to the cohesionless nature of riverbeds, the process is highly stochastic, and a single value is a rather poor descriptor of what happens to grains subject to a flowing fluid. As outlined already in the founding studies by Shields (1936), stochasticity is embedded in the process, and when looking at grain mobilisation from a loose bed, the descriptors chosen should account for it. In the century passed since the first studies, multifarious approaches appeared on the scene of “incipient motion and beginning of transport” and this section aims at wandering among those and finding some commonalities and the main differences.
Historically, the first studies into the beginning of transport are closely connected to the field of river geomorphology and morphodynamics. This tradition dates back to Davis and Gilbert (Grant et al., 2013), respectively with a qualitative classification of the landscape changes (Davis, 1909), and a more physical, processes-oriented framework to explain such variability in the landscape (Gilbert, 1914). Gilbert (1914) carried out laboratory experiments to investigate the transport capacity of rivers by gradually increasing input discharge, defining incipient motion by the discharge conditions mobilising few grains. From those landmarks, the present field of geomorphology stemmed, and sediment transport studies can be considered a branch of it.
On another, related, front within the field of *hydraulics*, the first systematic studies into sediment transport date back to the beginning of the XX century with Forchheimer (1908 and 1926) and Schoklitsch (1914 and 1926) investigating sediments movements in flowing waters, but not before the 30’s a clear framework was available to estimate and predict erosion (see Hjulström, 1932 and Shields, 1936). Shields’ milestone study set a divide and a standard in approaching and investigating sediments’ onset of transport, by providing a clear method for assessing such a condition. From there on, the standard approach for the definition of the threshold for sediment motion required a measurement of either shear velocity or bed shear stresses, be they cross-sectional averaged, or local or very punctual values, and a proxy measurement of the solid flux. With this said, we can now walk through the sediment motion studies scene, and meet the different

characters in this story, keeping in mind that all of them shaped the current understanding of the process.

2.2.2 Incipient motion of sediments in flowing waters: parameters' choice

The definition of incipient motion conditions requires establishing a relationship between particles' mobility (or alternatively solid discharge) and hydrodynamic conditions triggering mobility. Throughout the last 90 years, the problem of incipient motion and onset of transport has been approached with a highly diverse choice of parameters, resembling the background and education of the various researchers tackling such a topic, spanning from geography and geomorphology to civil engineering and physics. Hereby, combining multiple sources (Shvidchenko, 2000; Armanini, 2018; Dey and Ali, 2019; Witz et al., 2019) a summary is presented of those parameters' choices which had a sequel.

2.2.2.1 Hydrodynamics' descriptors

The earliest formulation, as reported in Dey (2014), with reference to the incipient motion of granular material resting at the bed can be found in Brahms (1754) and suggests a proportionality between the grain weight (volume and density) and the near-bed velocity in the form

$$v_{b,cr} \propto (\rho_S, \forbidden_p)^{1/6} \tag{2.4}$$

where $v_{b,cr}$ is the near-bed velocity triggering grains' motion, ρ_S is the particle density and $\forbidden_p$ is the solid particle volume. This first formulation contains both particle information (density and volume, which is directly related to the grain-size in the case of uniform sediments), and flow characterisation, being, *de facto*, the basis for all successive research.

Threshold velocity

As seen above, the near-bed velocity was the first parameter adopted to explain particles' threshold for motion. As a natural evolution of Brahms' velocity threshold, few authors adopted near-bed velocity thresholds, as hereafter briefly outlined. For example, Carstens et al. (1964) propose a relationship between threshold velocity at the particle level $u_{p,cr}$, sediment and bed characteristics in the form:

$$u_{p,cr} \approx 1.9 \cdot g\Delta d^{1/2}(\tan\phi \cos S_{b,\alpha} - \sin\phi)^{1/2} \tag{2.5}$$

where d is a representative diameter for the particle, $\Delta = (\rho_S - \rho)/\rho$ is the submerged relative density of the particle, ϕ and $S_{b,\alpha}$ are the bulk friction angle of the sediment and the bed slope in degrees, respectively. In a discussion among many authors (see Neill et al., 1966) it was proposed to relate the near-bed threshold velocity u_{cr} only to the bed particles' density ρ_s and size d, as

follows:

$$u_{cr} = 3.3 \cdot \Delta^{1/2} d^{4/9} \tag{2.6}$$

Another thread for the estimation of the threshold near-bed velocity sees its relation to the settling velocity of the particle w_s observed for the first time by Rubey (1933). There he noticed similarity between bed shear and settling velocities magnitudes, which was later used to derive empirical formulae for bed shear velocity estimation. As an example, Egiazaroff (1965) assumes the threshold velocity at the particles' level $u^*_{p,cr}$ to equal the particles' settling velocity w_s in the case of homogeneous beds with sustained transport, obtaining

$$u^*_{p,cr} = w_s \tag{2.7}$$

Although very simplistic, this formulation has been reworked and is especially useful to discern modes of transport for a variety of natural minerals as outlined in Komar and Clemens (1986) and has been adopted for resuspension criterion (as in e.g Lane and Kalinske, 1939 and Komar, 1985).

$$\frac{u^*}{w_s} \begin{cases} > 1 & \text{suspended transport occurs} \\ \approx 1 & \text{threshold to suspension} \\ < 1 & \text{bedload transport occurs} \end{cases} \tag{2.8}$$

As an example, Yang's formulation (1973), depending on the settling velocity, was derived through forces balance on a spherical sediment particle on a loose bed. By balancing drag, lift, friction and gravity at the particle level he comes up with a relation

$$\frac{U_{cr}}{w_s} = \begin{cases} \left(\frac{2.5}{\log Re^* - 0.06} + 0.66\right) & Re^* \in [0, 70) \\ 2.05 & Re^* \geq 70 \end{cases} \tag{2.9}$$

where Re^* is the particle Reynolds' number computed as

$$Re^* = \frac{u^* d}{\nu} \tag{2.10}$$

For the purpose of this Thesis, resuspension limits are not further investigated. Still, for sake of completeness, a relation between bed shear velocity and settling velocity is to be mentioned, due to the particular characteristics and variety of microplastics, and the growing literature on microplastics settling velocity estimation in both still and turbulent water (Waldschläger et al., 2020; Goral et al., 2023b; Lofty et al., 2024).
Although Rubey already in 1938 concluded that *"The velocity in the immediate vicinity of the particle on the stream bed is more significant for this [particles' onset of motion] inquiry than the mean velocity of the entire stream"*, threshold mean velocity relations were derived for various

conditions thereafter (Dey, 2014). Such formulation had the advantage of being easier to estimate, overcoming the inherent difficulty in near-bed velocity estimates both in the laboratory and in field conditions.
As a first example, the Hjulström diagram (1932) represents the earliest systematic application of a velocity threshold. Through experimental data, the critical mean flow velocity U_{cr} was derived by Hjulström (1932) for a wide range of diameters, at a constant water depth of 1 m. The Hjulström diagram (Figure 2.1) is still widely used for approximate assessment of erosional depositional processes in rivers, even though its independence from flow depth does not allow scaling to conditions different from those for which it was initially determined.

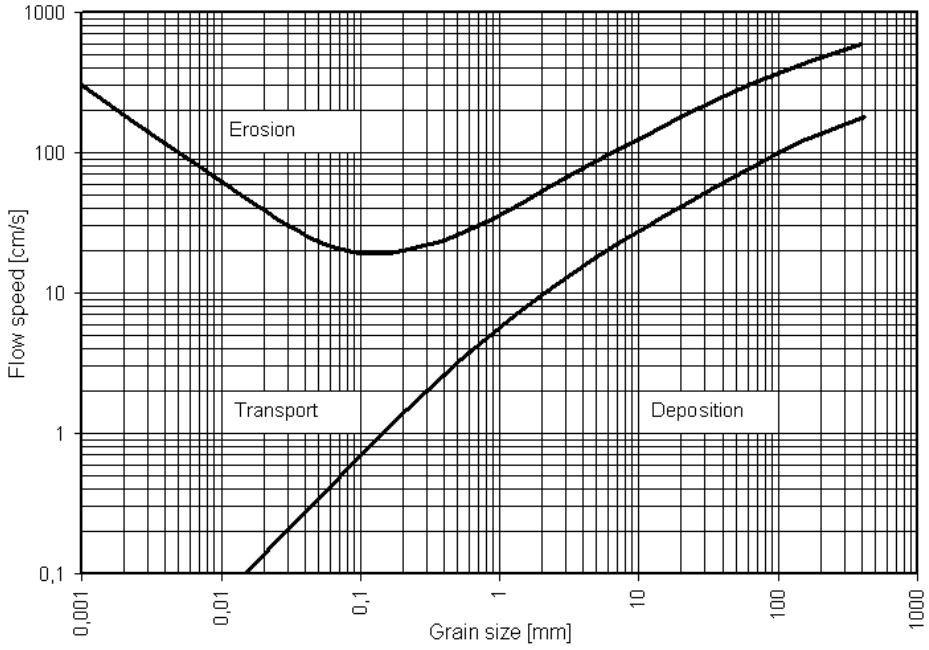

FIGURE 2.1: Hjulström diagram showing the dependency between the sediment grain-size and the (critical) velocity required for its erosion, transport or deposition. Source Wikipedia, licensed with CC-by-SA-3.0, GFDL.

Among the formulae valid for sediment mixtures (i.e. mixed grain-size sediments) Gvelesiani (1970) proposes a relation of the mean threshold velocity depending on particles' weight, a function of particles' submergence h/d, and a proxy for sediments uniformity d_{95}/d, where d_{95} is the 95^{th} percentile of the grain-size distribution, with 95% of grains finer

$$U_{cr} = 1.41 \cdot \frac{\log \frac{8.8h}{d}}{\log(\frac{12d_{95}}{d} + 1)} \sqrt{\frac{2g\,\Delta\,d}{2.8}} \tag{2.11}$$

valid for gravel-beds with representative diameter $d > 1.5$ mm.
Again for gravel-bed, with a slightly easier formulation still relating the mean threshold velocity

to a function of particles submergence Neill, 1967 proposed the following empirical formula:

$$U_{cr} = 1.41\sqrt{g\ \Delta\ d}\left(\frac{h}{d}\right)^{\frac{1}{6}} \tag{2.12}$$

An early Zanke (1977) proposed a relation for mean threshold velocity depending on cohesion of the sediments and viscous near-bed influence for fine material in the form

$$U_{cr} = 2.8 \cdot c_{c,s}\left(\sqrt{\frac{\rho_s}{\rho} g\ d} + 5.25\frac{\nu}{d}\right) \tag{2.13}$$

where ν is the kinematic viscosity coefficient of water and $c_{c,s}$ is a coefficient for cohesivity of the bed sediments, spanning from 1 for cohesionless to 0.1 for cohesive sediments.
The relationships reported above were chosen among many available for their relevance for the present Thesis in two terms: the range of diameters for which the formula is proposed valid includes values relevant for microplastics studies, and the researchers investigated incipient motion not only for homogeneous sediments, but also for graded mixtures.

Threshold discharge

The definition of a threshold discharge presents many advantages, and was adopted by e.g. Bettess (1984) for gravel-bed streams (with grain-size greater than 2.5 mm). By calculating a dimensionless equation for threshold unit discharge

$$q_s = \frac{V_p d}{\sqrt{[g\ \Delta\ d^3]}} \tag{2.14}$$

and using Shields' curve as a basis (see Section 2.2.2.3), he derived the following relation, valid for natural sediments with relative density ρ_s/ρ =2.65, and depending merely on the critical specific discharge q_{cr}

$$q_{cr} = \frac{0.104\ \sqrt{g\ \Delta\ d^3}}{S_b} \cdot \log(\frac{1.211}{S_b}) \tag{2.15}$$

where S_b is bed slope of the stream.
Bathurst and colleagues (1987) in the same years found a similar relationship for steep channels with coarse, nonuniform bed material (and consequent low relative depths, $h/d < 10$) in the form

$$q_{cr} = \frac{0.15\ \sqrt{g\ d^3}}{S_b} \tag{2.16}$$

The use of threshold discharge has not been particularly popular in incipient motion studies, still, some applications appear, mostly for gravel-bed rivers (P. Carling, 1988), and the two formulations reported here are valid for a range of diameters which can overlap that of microplastics present in rivers.

Threshold stream power

Related to the concept of discharge, Bagnold (1954) proposed to relate erosion processes to a quantity he names *"stream power"*, encapsulating mean flow discharge Q, S_e representing the slope of the energy grade line (or depending on uniform flow assumption S_B, bed slope), density ρ and gravity constant g, as follows

$$\Omega = \rho g Q S_e \tag{2.17}$$

From Equation 2.17, the stream power per unit bed area can be estimated as

$$\omega = \rho g U S_e = \tau U \tag{2.18}$$

Strictly valid only for natural sediment ($\rho_s \approx 2600\ kg/m^3$), threshold conditions can be obtained by substituting threshold values for bed shear stress and shear velocity.

Threshold bed shear stress

A parameter more closely related to the near-bed hydrodynamics is the bed shear stress, which informs on the force exerted by the flowing water at the bed surface and on the bed particles. Empirical equations have been proposed to estimate the critical bed shear stress at the inception of motion, and here some are reported.

The first proposed equation dates back to 110 years ago, proposed by Schoklitsch (1914), and links the threshold bed shear stress (computed in $[kg/m^2]$) to particles' parameters (density, representative diameter, and shape through a shape factor CSF)

$$\tau_{0,cr} = 0.448 \cdot \rho g \sqrt{CSF \cdot \Delta d^3} \tag{2.19}$$

where CSF is Corey shape factor (Corey, 1949) computed as the ratio between the shortest particles' axis a_3 and the square root of the product of the two longest dimensions a_1, a_2 ($CSF = a_3/\sqrt{a_1 a_2}$), and d is a representative dimension of the particle.

A few years later another author (Krey, 1925), suggested a formulation depending on only particle density and the representative grain-size d:

$$\tau_{0,cr} = \begin{cases} 0.076 \cdot (\rho_S - \rho) g d, & d \geq 6mm \\ 0.000285 \cdot (\rho_S - \rho) g d, & 0.0001mm < d < 6mm \end{cases} \tag{2.20}$$

where $\tau_{0,cr}$ was estimated in $[kg/m^2]$.

Kramer (1935), proposed yet another relationship, linking the same particles' characteristics to the threshold bed shear stress (computed this time in $[g/m^2]$) in the form

$$\tau_{0,cr} = 29 \sqrt{\frac{(\rho_S - \rho) g d}{KUP}} \tag{2.21}$$

where KUP is Kramer's uniformity parameter describing the sediment mixture (KUP = 1 for uniform sediment and KUP < 1 for non-uniform sediment). Equation 2.21 is valid in the range $d \in [0.24, 6.52]$ mm and $KUP \in [0.265, 1]$.
Only one year later,in 1936, USWES recommended another formula for the estimation of the critical bed shear stress modifying Kramers' one:

$$\tau_{0,cr} = 0.258 \sqrt{\frac{\Delta d}{KUP}} \tag{2.22}$$

with $d \in [0.205, 4.077]$ mm and $KUP \in [0.28, 0.643]$.

Turbulence-oriented thresholds

As early as 1940, White proposed to incorporate the effects of turbulence through a *turbulence coefficient* (see Equation 2.25) to account for instantaneous bed shear stress versus time-averaged bed shear stress on single particles getting mobilised from a flat bed. Later, it was the seminal work by Einstein (1942), highlighting the stochastic nature of bedload transport, that allowed for a more detailed description of near-bed hydrodynamics, including turbulence, to enter the characterisation of the onset of transport.
Following Einstein (1942), Sutherland (1967) describes the entrainment of particles as due to *"turbulent eddies disrupting the viscous sublayer and impinging directly onto the grain surface"*, stressing the key role of turbulence in the entrainment mechanism. Research into the characteristics of such eddies unveiled the role of specific flow events, linked to positive (greater than the mean) fluctuations of flow velocity in the longitudinal direction (Heathershaw and Thorne, 1985; Nelson et al., 1995), through quadrant analysis.
The concept of a distribution of bed shear stresses rather than a single value is the key in Grass' work (1970) to describe the onset of transport. By accurate laboratory measurements of grain instability and instantaneous longitudinal and vertical components of the flow velocity, he computed the local instantaneous bed shear stress and compared it to the distribution of critical shear stress depending on local bed topography and particle exposure. The result is a statistical formalisation of the problem, based on two probability distributions whose increasing overlapping increases the likelihood of the onset of motion (see Figure 2.5).
Questioning the concept of a threshold for motion, Lavelle and Mofjeld (1987) discussed the importance of turbulent fluctuations at the bed, as the key factor determining the incipient motion of single grains. They therefore refused the notion of *threshold*, arguing that single turbulent events are able to mobilise particles at mean bed shear stresses well below the Shields' curve.
Looking into the near-bed turbulence features with laser-Doppler velocimetry, Nelson et al. (1995) conclude that for developed boundary layer flows, although sweeps ($u' > 0$, $w' < 0$, where u' and w' are, respectively, the fluctuations of longitudinal and vertical components of the flow velocity from its time-averaged value, following Reynolds' decomposition) mobilise higher amounts of bed sediments than all other interactions, the duration of the events also plays a major role in

determining the bulk (time-averaged) sediment transport. The authors argue, instead, that for developing and transitional boundary layer flows, other features, like flow separation, have a major role in the mobilisation of bed sediments.
Zanke (2003) investigated the effects of fluctuations in the bed shear stress and turbulence-generated lift force on the entrainment threshold with respect to the *"smooth-wall" curve*. He found that the *turbulent bed shear stress* and lift combined reduce the "smooth wall" threshold, and his results find good agreement with previous experimental data (among others, Shields, 1936; White, 1940; Neill, 1967; Mantz, 1977; Yalin and Karahan, 1979).
Diplas et al. (2008) investigated the role of both the magnitude and the duration of turbulent fluctuations, highlighting the key role of the latter in the initiation of motion (as anticipated by Nelson et al., 1995), thus proposing the use of impulse at the particle's location to characterise incipient motion. Further, Celik et al. (2010) and Valyrakis et al. (2010) adopted such a framework, which allows for a *quasi-deterministic* characterisation of the onset of motion of individual particles, for different degrees of exposure.
Dwivedi et al. (2011) conducted experiments on single particle's motion, estimating hydrodynamic forces on variously exposed particles. Consistently with the work of Nelson et al. (1995) they found high-magnitude drag and lift forces induced by sweep (quadrant 4) events to be responsible for the entrainment of both shielded and exposed particles, and, consistently with Diplas et al. (2008) they stress the role of impulse on the onset of motion.

2.2.2.2 Particle-oriented descriptors

A second way to approach the incipient motion has been to focus on forces and torques at the particle level and derive the destabilising mechanism analytically. If we consider a single particle resting on the bed surface, the forces acting on such particle are reported in Figure 2.2. Friction represents the effects of all contact reactions between the chosen particle and the surrounding particles. Lift is the vertical component (normal to the bed for zero-slope) of the hydrodynamic force acting on the particle, and drag is the component in the main flow direction. Buoyancy depends on the fluid's density and displaced volume, while weight on the particle's relative density and volume.

Forces balance at the particle level
The drag and lift force acting on a particle can be expressed as a function of the near-bed velocity at the particle level u_p in the forms

$$F_D = \frac{1}{2}\rho C_D u_p^2 A_p \tag{2.23}$$

$$F_L = \frac{1}{2}\rho C_L f(u_p^2) A_p \tag{2.24}$$

where C_D and C_L are the particle drag and lift coefficient, respectively, depending on particle

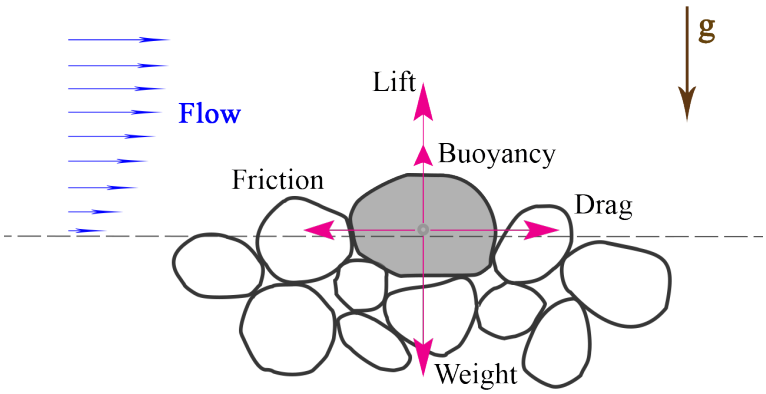

FIGURE 2.2: Schematic illustrations of various forces acting on a single grain for zero-sloped beds. (after Armanini, 2018).

shape, surface roughness and orientation, $f(u_p^2)$ is a function of the velocities at the particles' lowest and uppermost point and A_p is the area of the particle exposed to the flow (e.g. for an exposed sphere of diameter d it can be assumed equal to $\frac{\pi d^2}{4}$).
The approach by White (1940) balances forces around a particle assuming the effect of lift negligible. He divided his experiments into two categories, hydraulically smooth (which he names *low-speed cases*) with $Re^* \leq 3.5$ and hydraulically transitional to rough (*high-speed cases*) for $Re^* \geq 3.5$. By balancing friction and hydrodynamic forces at the particle level, and introducing a packing coefficient $c_{packing}$ and a coefficient for the near-bed turbulence c_{turb} corresponding to the ratio of instantaneous ($\tau_{0,t}$) vs mean ($< \tau_{0,t} >$) bed shear stress

$$c_{turb} = \frac{\tau_{0,t}}{< \tau_{0,t} >} \tag{2.25}$$

he obtained for smooth regime and spherical particles

$$\tau_{cr} \cong 0.18 \cdot g\Delta d \tan\phi \tag{2.26}$$

while, for transitional to rough flow regime, he found a reduction of up to 40% of the threshold bed shear stress τ_{cr} compared to smooth flow regime likely due to turbulent fluctuations in the turbulent boundary layer.
Einstein (1949) assumed that a particle moves when its submerged weight is exceeded by the instantaneous hydrodynamic lift force. By measuring lift fluctuations due to turbulence on hemispheres, they proposed to choose an elevation of $0.35d$ for the measurement of u_p. Based on these results, the threshold lift force $F_{L,cr}$ was related to the threshold bed shear stress simply, by the Task Committee on Preparation of Sedimentation Manual Committee on Sedimentation (1966)

$$F_{L,cr} \approx 2.5 \cdot \tau_{0,cr} \tag{2.27}$$

Wiberg and Smith (1987) proposed an equation, for a given grain-size and density, depending on the near-bed drag force, lift force to drag force ratio, and particle angle of repose. They expressed the lift force as

$$F_L = \frac{1}{2}\rho C_L A_p (u_{p,t}^2 - u_{p,b}^2) \tag{2.28}$$

where $u_{p,t}$ and $u_{p,b}$ are the instantaneous velocities at the top and bottom of the particle, and the drag force as

$$F_D = \frac{1}{2}\rho C_D u_{p,A}^2 A_p = \frac{1}{2}\rho C_D \tau_0 < f^2(z/z_0) > A_p \tag{2.29}$$

where $u_{p,A}$ is the velocity averaged over the particle cross-section and the function $< f^2(z/z_0) >$ indicates a dependency on the structure of the near-bed velocity profile. By analytically resolving the particle's equilibrium, they derived

$$\tau_{0,cr} = \frac{2}{C_{D_{cr}} C_{shape}} \frac{\tan\phi \cos S_{b,\alpha} - \sin S_{b,\alpha}}{< f^2(z/z_0) > \cdot [1 + (F_L/F_D)_{cr} \tan\phi]} \tag{2.30}$$

where C_{shape} is a parameter depending on particle's shape, $S_{b,\alpha}$ is the bed slope and ϕ is the particle's friction angle.
Kirchner et al. (1990) use the balance of forces at the threshold for motion for individual spherical particles, in the form

$$\frac{F_D}{\tan\phi} + F_L = \frac{\pi}{6}(\rho_S - \rho) g D^3 \tag{2.31}$$

assuming the validity of the logarithmic distribution of flow velocities up to the mean bed level. Following Wiberg and Smith (1987) in the formulation of drag and lift forces, and defining *protrusion* (see Section 2.2.2.4) as the particle height above the mean bed level, they derived the threshold bed shear stress based on local geometrical considerations

$$\tau_{0,cr} = (\rho_S - \rho) g \frac{\pi D^3}{6} \Big\{ \frac{1}{\tan\phi} \frac{C_D}{2\kappa^2} \cdot \int_{p-e}^{p} \sqrt{D^2 - [2z - (2p - D)]^2}\, f(z)^2 dz + \\ + \frac{\pi C_L}{8\kappa^2} D^2 [f(p)^2 - f(p - D)^2] \Big\}^{-1} \tag{2.32}$$

where the function $f(z)$ describes the distribution of near-bed velocities in the form

$$f(z) = \begin{cases} 0, & z \le 0 \\ ln\left(\frac{z+z_0}{z_0}\right), & z > 0 \end{cases} \tag{2.33}$$

and z_0 is the roughness length of the bed, which they set equal to $0.1 d_{84}$.

Torque balance at the particle level

Vollmer and Kleinhans (2007), define incipient motion for an individual grain by the torque equilibrium around a pivot point at the downstream contacting particle. By making use of the concepts of particle *exposure* and *protrusion* (see Section 2.2.2.4), geometrical considerations about the distance of the pivot point, and time-averaged parameters, they obtained a relationship for the threshold bed shear stress in dimensionless form as

$$\frac{\tau_{0,cr}}{g\,(\rho_S - \rho)\,D} = \frac{(\cos S_{b,\alpha} - \sin S_{b,\alpha} / \tan \alpha_{pivot}) \tan \alpha'_{pivot} k_{packing}}{\left(1 + \frac{F_L}{F_D} \tan \alpha'_{pivot} C_D f(\frac{z}{z_0})\right)} \tag{2.34}$$

where α_{pivot} and α'_{pivot} are angles between the pivot point and barycentre of the particle and the point where drag force is exerted (see for clarification the full paper by Vollmer and Kleinhans, 2007), $k_{packing}$ is the packing density parameter [m^2], depending on particle shape, size distribution and porosity. And $f(z/z_0)$ is a function accounting for the thickness of the viscous sub-layer, following the rationale in Wiberg and Smith (1987).

2.2.2.3 Shields' diagram

Shields' approach to the problem of particles' onset of transport was developed by means of laboratory experiments on homogeneous sediments of varying relative density in the range 1.04 - 4.4 (corresponding to 4 density classes for crushed amber, lignite, granite and barite) and has been widely used ever since.

Shields' formulation of the incipient motion problem sees the balance of the flow *tractive force*, or drag force, with the particle *resistive force*, i.e. friction force, proportional to all forces in the direction normal to the flow, in the form

$$F_D(u^*) = F_{fr} \tag{2.35}$$

This requires that, at the onset of motion, the friction coefficient c_{fr} equals the value of the tangent of the friction angle $c_{fr} = \tan \phi$ (Armanini, 2018). The forces involved, with reference to Figure 2.2, are the hydrodynamic drag and lift components (Equations 2.23 and 2.24, respectively) and the submerged weight equal to particle weight W subtracted of particle's buoyancy B

$$W_{sub} = W - B = g(\rho_S - \rho)\forall_p \tag{2.36}$$

By imposing equilibrium of forces in the flow direction, the threshold condition for the particle can be obtained as

$$\frac{u^{*2}}{g\Delta d} = f\left(\frac{\rho u^* d}{\nu}\right) \tag{2.37}$$

By defining the Shields' mobility parameter as

$$\theta = \frac{u^{*2}}{g\Delta d} = \frac{\tau_{0,cr}}{g(\rho_s - \rho)d} \tag{2.38}$$

a dimensionless relation for the incipient transport conditions of bed particles can be therefore written as (Niño et al., 2003)

$$f_{cr}(Re^*, \tau_{0,cr}) = 0 \tag{2.39}$$

where Re^* is the particle Reynolds number and $\tau_{0,cr}$ is the mean bed shear stress at onset of motion, both estimated through the bed shear velocity u^*. The original Shields' diagram plots the particle Reynolds number vs his newly defined (Shields') parameter, separating mobility and non-mobility of particles through a shaded area where incipient transport was observed (see Figure 2.3).

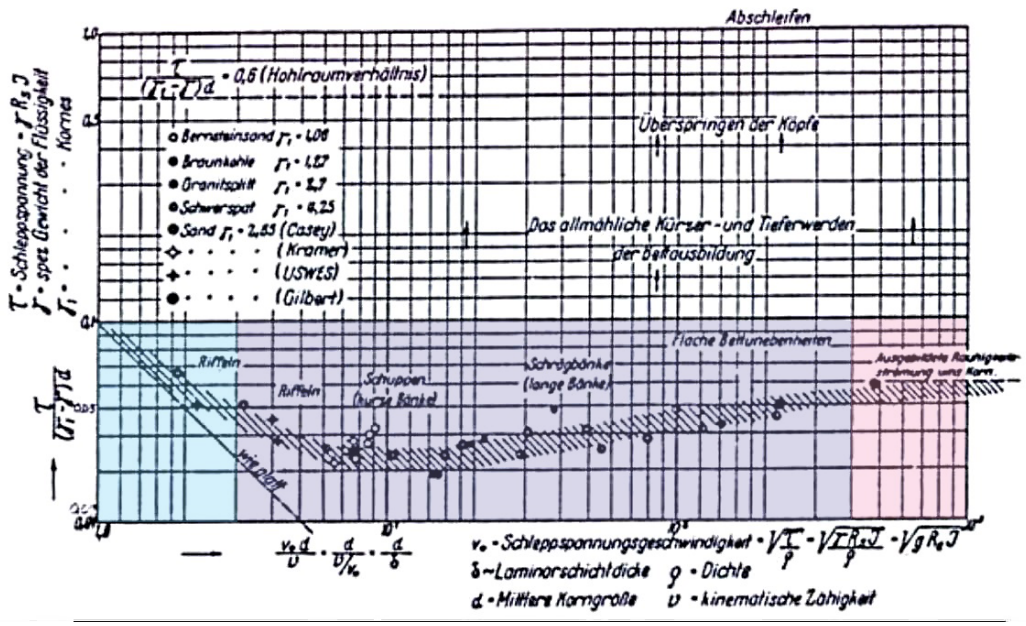

FIGURE 2.3: Original Shields' diagram, modified from Shields, 1936 PhD Thesis to highlight near-bed regimes, from left to right: in light blue smooth-wall, in violet transitional and in pink rough wall regime.

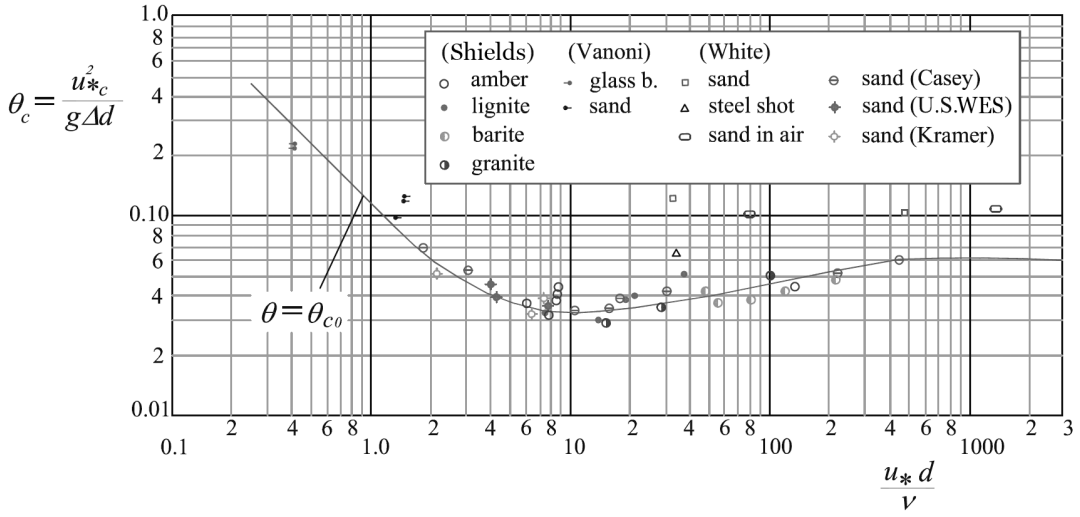

FIGURE 2.4: Higher resolved Shields' diagram, modified from Armanini, 2018 reporting the original dataset plotted by Shields'.

Shields' diagram has ever since been used, usually collapsing the shaded area into a single curve (Dey and Ali, 2019) which can be described by e.g. Paphitis (2001) valid for the range of $Re^* = (0.01 - 10^5)$

$$\theta_{cr} = \frac{0.188}{1 + Re^*} + 0.0475(1 - 0.699\exp^{-0.015Re^*}) \tag{2.40}$$

and upper and lower limits to envelope the high scatter in experimental data from Equations 2.41, valid in the same range of Re^* as Equation 2.40

$$\begin{aligned} \theta_{cr,upper} &= \frac{0.075}{0.5 + Re^*} + 0.03(1 - 0.699\exp^{-0.015Re^*}) \\ \theta_{cr,lower} &= \frac{0.280}{1.2 + Re^*} + 0.075(1 - 0.699\exp^{-0.015Re^*}) \end{aligned} \tag{2.41}$$

Shields' diagram, due to the use of particle Reynolds number Re^* (which corresponds to the bed Reynolds number for the bed homogeneity in his experiments), has the advantage of considering the flow regime. It goes from smooth-bed for $Re^* \leq 2$ (light blue in Figure 2.3) where there is a linear trend in the bi-logaritmic graph between Re^* and θ, to transitional for $Re^* = [2, 200]$ (purple shaded in the middle) where the relation follows a more complex dependency reaching a minimum value for θ at 0.03, to rough-bed for $Re^* \geq 200$ (magenta shaded area) where $\theta \cong 0.057$ is independent from Re^*.

One of the greatest disadvantages of Shields' formulation is that the abscissa and ordinate axes are interdependent through the bed shear velocity. For this reason, Yalin (1972) and later Miller (1977) proposed the use of a dimensionless particle diameter D^* in the form

$$D^* = d_{50}\left(\frac{g\Delta}{\nu^2}\right)^{1/3} \tag{2.42}$$

which results in a threshold curve for θ_{cr} vs D^* (Van Rijn, 1984)

$$\theta_{cr} = \begin{cases} 0.24{D^*}^{-1} & \text{for } D^* \leq 4 \\ 0.14{D^*}^{-0.64} & \text{for } 4 < D^* \leq 10 \\ 0.04{D^*}^{-0.1} & \text{for } 10 < D^* \leq 20 \\ 0.013{D^*}^{0.29} & \text{for } 20 < D^* \leq 150 \\ 0.055 & \text{for } D^* > 150 \end{cases} \tag{2.43}$$

The Shields' criterion has been thoroughly discussed (as visible in the reviews by Buffington and Montgomery, 1997 and Dey and Ali, 2019). Among the critics to Shields' criterion validity, the scatter of data around the empirical curve takes the most space. Such scatter depends on numerous variables, among which the local structure of the bed (including packing, exposure and porosity), the local structure of the flow (accounting not only for mean values but also for turbulent fluctuations) and finally the methodological definition of incipient motion defined either as finite small transport (e.g. Yalin, 1963; Vanoni, 1964), or from observation of moving grains (like in the pioneering work of Francis, 1973; Drake et al., 1988; and Keshavarzy and Ball, 1999). Considering a wide range of conditions, spanning from incipient motion to sediment resuspension, A. J. Sutherland (1967) refused to use the concept of threshold, and by experimental work looking into turbulent eddies relate the onset of motion to turbulent events disturbing the viscous sublayer, for both flat-bed and beds with bedforms.

Among researchers criticising Shields' criterion, Lavelle and Mofjeld (1987), argued that the concept of threshold is not needed, basing their argument on the scatter of literature data and on observed turbulence at the particle level. They propose, following Shields' (1936) considerations on particle arrangement as a distribution of values, and based on turbulence fluctuation around mean bed shear velocity, to disregard the deterministic notion of *Shields' curve*, to the advantage of a more nuanced concept, where particle's motion can occur at any mean bed shear velocity provided turbulent fluctuations are strong enough to overcome particle inertia.

2.2.2.4 Graded sediments: geometric and hydrodynamic effects

The presence of a graded sediment mixture at the bed affects the incipient motion and remobilisation of particles, in that: (i) the exposure of the fractions to near-bed flow is not even and depends on the local upstream topography, and (ii) the roughness itself cannot be summarised by one value (e.g. Nikuradse's bed roughness height e_s, 1933). The former entails that particles can be shielded and protected from upstream larger grains (as firstly confirmed experimentally by Fenton and Abbott, 1977). The latter means that the structure of the near-bed flow field changes, when compared to uniform sediment beds, and the thickness of the viscous sublayer may not always contain bed particles, thus exposing particles of different sizes to different velocities. A first approach to tackle the mobilisation of different fractions in a graded mixture looks at the local topographical effect, via the concept of *protrusion* and *exposure*. Following Kirchner et al. (1990): (i) protrusion p indicates the elevation of the target grain from the mean bed level, while (ii) exposure e is defined as the elevation of the target grain above the crest of its closest upstream grain. Both *exposure* and *protrusion* are geometric indicators of the bed topography at the grain level, and can be used to describe the mobility of different fractions of a mixture as hereby summarised.
Starting from Einstein (1950) and later Egiazaroff (1965), a functional relationship was proposed linking the Shields' mobility threshold θ_{cr} (for a definition see Section 2.2.2.3) of a fraction vs mixture, to the ratio between the diameter of the moving fraction vs a diameter describing the mixture, in the form

$$\frac{\theta_{cr,i}}{\theta_{cr,m}} = f\left(\frac{d_i}{d_m}\right) \tag{2.44}$$

where $\theta_{cr,i}$, is the threshold Shields' parameter for size fraction i, $\theta_{cr,m}$ is Shields' parameter for the m-th grain-size fraction, d_i is the diameter of the i-th fraction and d_m is the diameter of the m-th fraction.
Many authors chose to refer to either the median (m = 50), or the mean diameter of the sediment mixture (e.g. Egiazaroff, 1965; Wiberg and Smith, 1987). Equations similar to Eq. 2.44 are called *hiding/exposure functions* and are used to estimate the mobility of different fractions in sediment mixtures. The first hiding/exposure function is the formulation proposed by Egiazaroff (1965) in the form

$$\frac{\theta_{cr,i}}{\theta_{cr,m}} = \left(\frac{\log_{10} 19}{\log_{10} 19\frac{d_i}{d_m}}\right)^2 \tag{2.45}$$

where d_m is the mean diameter of the mixture.
More generally, hiding/exposure functions are expressed in the form

$$\xi_i = a_1 \cdot \left(\frac{d_i}{d_m}\right)^{-a_2} + a_3 \tag{2.46}$$

where ξ_i denoted the hiding/exposure function for the i-th fraction having a diameter d_i and a_1 ad a_2 and a_3 are coefficients to be empirically determined.
Wilcock and Southard (1988) validated, through laboratory experiments and literature data, the relation in Equation 2.46 for sediments homogeneous in density, with grain-size distributions differing in sorting but not in the representative d_{50}. Their results show that the choice of the parameter d_i/d_{50} is convenient and adequate to model incipient motion of different size fractions in a mixture.
More recently, Yager et al. (2018) estimated the contribution to grain resistance of grain submerged weight, partial burial (*protrusion*) and intergranular friction. They found out that the role of *protrusion* and intergranular friction is major for estimating correctly θ_{cr} and sediment fluxes.
Hodge and Buechel (2022) investigated the effect of exposure/protrusion on threshold conditions of bed sediments in bedrock channels. By accurate bed surface characterisation and applying Kirchner's modelling approach (1990) to estimate threshold bed shear stress for the mobile grains, they proposed the use of a functional relationship to model threshold bed shear stress on bedrock rivers in the form

$$\theta_{cr} = \frac{D}{\sigma_z} \tag{2.47}$$

where D is the representative diameter of the moving grains and σ_z is the standard deviation of the elevations of the bed surface.

A second approach to the mobility of fractions in a sediment mixture is to look at near-bed hydrodynamics, having the means, and investigate the role of the viscous sublayer on the mobilisation of different fractions (Einstein, 1950). A recent contribution by Hassan et al., (2024) stresses the importance of viscosity in the near-bed region when considering the mobilisation of the coarse fraction of a mixture. By using two mixtures with the same coarse-to-fine diameter ratio (with fines being sand and 2-mm gravel for the two cases), they show that the transport of the coarse fraction is enhanced in the case of sand addition, but not for 2-mm gravel addition. This reflects a non-geometric effect (not depending only on hiding/exposure processes linked to local topography) which the authors explain as a variation in the thickness of the viscous sublayer (δ), due to a smoothing of the bed. When such a variation reduces δ the exposure of grains to turbulence and turbulent fluctuations becomes more important, and the coarse fraction becomes more mobile, being subject to a wider range of instantaneous velocities. Hassan et al. (2024) propose, following Parker et al. (2024), to summarise the effect of the viscous sublayer(and the increased mobility of grains generally coarser than the bed material) through a threshold on the dimensionless grain-size D^* occurring at $D^* = 51$. The authors argue that for $D^* > 51$ the viscous effect should be negligible, while for $D^* < 51$ the combination of viscous and geometric effects increases the mobility of the coarser fraction.

2.2.3 Incipient motion of sediments in flowing waters: a classification of approaches

By digression over the available literature, a shallow classification can be drawn for the various approaches developed to study the beginning of motion of cohesionless grains in open channel flows. The different categories read as follows:

- deterministic vs stochastic methods
- particle-oriented vs bed-oriented (or cross-section oriented)
- Lagrangian (particles observation-based) vs Eulerian (solid transport, weighing-based) methods

Under those categories, further refinement includes the consideration of diverse variables to describe this grain instability phenomenon (shear stresses, shear velocity, turbulence descriptors, and forces oriented), as well as the consideration of different flow conditions, relative to the range of Reynolds numbers used in the studies. For the sake of simplicity, we neglect incipient motion studies in the presence of wavy motion, focussing instead on open channel turbulent uniform flow.

2.2.3.1 Deterministic vs stochastic methods

Since the first studies, it has been acknowledged how the process of onset of transport of particles from a loose bed is highly stochastic in nature, and how the transition from no-motion to motion of single grains needs statistical descriptors (e.g. the pioneering work of Shields, 1936) before it being generalised to the whole bed. In its classical form, the simplest deterministic approach sees a unique value below which no significant transport occurs, and above which sediment transport can be expected. The unique value is usually derived from a time-space averaging of flow variables (e.g. Nikora et al., 2013). On the other hand, a full stochastic characterisation of incipient motion/transport requires the full probability distribution of both flow and bed properties: to be summarised in at least velocity (and turbulent fluctuations) or shear velocity, or bed shear stresses for the flow, and a proxy of solid transport (e.g. number of particles dislodged or mass/volumes transported). While for the statistics of the flow, a lot of work has been done (e.g. Yalin and Karahan, 1979; Diplas et al., 2008; Cecchetto et al., 2018; Keshavarzi and Ball, 2011 and Roseberry et al., 2012 among others), the statistic characterisation of bed topography has been devoted to much less detailed studies, and among those, only rarely have researchers focussed on the conditions for the onset of motion (a few examples are Chin and Chiew, 1993; Hodge and Buechel, 2022; Rebai et al., 2024). Probabilistic approaches for the estimation of incipient motion have built upon Einstein's theory (1942 and 1950), which defines the probability of motion of a grain as a function of flow intensity exerted on the bed, triggering (dimensionless) sediment transport. Among deterministic approaches, early contributions date back to White (1940), with an analysis of forces on a single grain resting on the bed (see Section 2.2.2.2).

Paintal (1971) carried out experiments with extremely low still measurable bedload transport rates for which the Shields numbers (see Equation 2.38) were well below the threshold values predicted by the Shields curve. They did not identify a unique critical bed shear stress for the onset of motion, and therefore proposed the selection of very small bedload transport rates to compute a critical value for the bed shear stress.
Lavelle and Mofjeld (1987) following Shields' (1936) considerations on particle arrangement as a distribution of values, and based on turbulence fluctuation around mean bed shear velocity they propose to disregard the deterministic notion of *Shields' curve*, to the advantage of a more nuanced concept, where particle's motion can occur at any mean bed shear velocity provided turbulent fluctuations are strong enough to overcome particle inertia.

2.2.3.2 Particle-oriented vs bed-oriented

To overcome the difficulties inherent to the stochastic nature of grains motion, starting from the 1980s' a number of researchers started focusing on single particles' motion, involving rather sophisticated measurements of single grains parameters (Section 2.2.2.2). As complementary approach is the consideration of the river bed as one entity, and the description of the onset of motion and transport via a lumped characterisation of such a system. Both views entail a refined degree of complexity, and most recent studies have taken advantage of the increase in hardware and software capabilities (Wohl, 2013).
Particle-oriented descriptions resolve analytically forces or torque equilibrium at the grain-scale, to estimate a threshold value of either bed shear stress τ_B or bed shear velocity u^* linked to the destabilisation of the studied particle. Among more complex formulations, Lee and Balachandar (2012) applied force and torque balance to predict the critical bed shear stress for exposed particles, accounting also for turbulent fluctuations. Such approaches require the knowledge of many parameters, not only for the description of near-bed flow, but also for the geometry of the bed in the vicinity of the particle, information which, usually is not available.
Conversely, bed-oriented descriptions estimate incipient motion and onset of transport from areal averaged quantities (if from visual estimation) or transport measurements. Such descriptions need double averaged information on the near-bed flow field (like mean bed shear velocity or stress), and do not require a detailed description of the bed. Relevant formulations in this terms are Shvidchenko and Pender (2000) and Keshavarzy and Ball (1999), from which part of the methodology applied in this Thesis derives.

2.2.3.3 Lagrangian vs Eulerian approaches

While the experimental setup can reflect the focus of the study, in the same setup two philosophies can coexist for what the methodology is concerned, and those dictate the way the system is described.
When a Lagrangian approach is used, the focus is on particle kinematics and detailed description of trajectories and resting times are reported (Campagnol et al., 2015; Radice et al., 2017; Rebai et

al., 2024). Lagrangian approaches, through statistics over a high number of particles' trajectories (both particle- and time- dependent), allow for obtaining detailed information on the average travel time of particles, resting periods (Hosseini-Sadabadi et al., 2019), and oscillations before motion (Rebai et al., 2024).
On the other side, Eulerian approaches allow a description of flow and particle dynamics in mean terms, for quantifying e.g. bedload fluxes within a defined volume. Statistics in Eulerian terms involve time-dependent quantities (Ballio et al., 2018).

2.2.4 Incipient motion measurements: weighted vs visual estimation

When looking at the many points added to the canonical Shield's diagram, the sparsity of the experimental results is evident, spanning two orders of magnitude (Ockelford and Yager, 2022). This can be ascribed not only to the stochasticity of the remobilisation process but also to the wide variety of approaches stemming from the specific discipline and applications of the sought threshold value and to the availability of instruments and technological constraints. Thus we see, that, for approximately the first 50 years of research, most of the contributions in the direction of a *threshold for transport* included weighting the transported grains at a control section (i.e., the control volume in the Eulerian approach). This approach offers areal, if not volumetric, averages of moving bed particles transiting a section in a given time, as measured quantity, and generally brings about estimates of threshold conditions which are linked to hydrodynamic parameters averaged over both time and space.
From the 1970s, with the advent of cheaper visual techniques and later digital photography, a shift towards *threshold for motion* allowed visual estimates of moving particles to enter Shields' diagram (Grass, 1970; Francis, 1973; Drake et al., 1988). Such estimates build upon a count of the individual grains (i.e., the Lagrangian approach) moving in the interrogation area and only part of such literature estimated solid fluxes exiting such an area (e.g., Campagnol et al., 2012). Threshold curves derived from the particle-counting type of measurements are generally lower than the transport-derived ones (Ockelford and Yager, 2022), and results originating from different techniques (and flux assumptions) are therefore hardly comparable (Ballio et al., 2018).

2.2.5 Microplastics remobilisation and incipient motion studies: an overview

With the history of incipient motion studies so rich in results, and the advent of a new candidate-sedimentary material, i.e. microplastics, a few studies to date addressed the onset of motion for such material, with the aim to propose and modify present formulations for wider applications in MPs research and microplastics budgeting. A recent review by Rohais and colleagues, (2024) stresses the need for more evidence to develop in-depth knowledge about MPs erosion behaviour. In the still limited literature available, we can list Waldschläger and Schüttrumpf (2019b) and Goral et al. (2023a), who conducted experiments in an annular flume and measured the motion of single isolated MPs. Their results, using the classical Shields' framework for mobility of

sediments, show an apparent higher mobility for the MPs tested, compared to the clastic sediments' mobility. According to the observations reported in Chapter 5, this peculiar behaviour can be attributed to two factors: i) different material characteristics for clastic and plastic sediments and ii) MPs bed availability. The latter has, to date, not been investigated in MPs threshold for motion research, and, according to the author, plays an important role in defining such threshold, as later outlined (see Chapter 5).

Another relevant source for this section is the work by Yu and colleagues (Yu et al., 2022) who performed incipient motion tests for transversely aligned MPs in a linear flume. Their study investigates the role of bed roughness on the incipient motion threshold for a range of MPs differing in polymer composition (and therefore density), shape and size. They propose a criterion to adapt the classical Shields' parameter θ_c (Shields, 1936), and movability number formulation u^*_{cr}/w_s (Paphitis, 2001, modified according to Beheshti and Ataie-Ashtiani, 2008) to the MPs case, by accounting for the three parameters relevant for such materials (e.g. density, shape and size). A more recent paper by the same authors (Yu et al., 2023), revising the rationale of Waldschläger and Schüttrumpf (2019b), looked into the sheltering effect of the bed surface roughness in the quantification of MPs' threshold of motion. There, the authors propose another formula for the estimation of the classical Shields' parameter θ_c, based on the density and equivalent diameter of both MPs and bed surface roughness.

Although the body of evidence for MPs remobilisation and incipient motion assessment is limited, general agreement exists on MPs' erosional behaviour differing from natural clastic sediments. This is mostly explained, by the researchers cited above, with the high variability of the three parameters (i.e. density, shape and size) describing MPs, vs. the rather limited variability shown when dealing with clastic sediments (especially for what density and shape are concerned). Indeed the diversity of particles' characteristics of MPs appears to hamper a unified formulation of threshold conditions with classical approaches borrowed from sedimentary research. Still knowledge of systems with a reduced degree of complexity, e.g. considering each characteristic separately to assess its importance in defining the erosional threshold, is paramount to a more systematic formulation of such a relationship.

Within this work, an attempt is made to simplify the variability of MPs characteristics, by considering only compact-shaped MPs, with similar dimensions, thus trying to distinguish the effect of the specific density of the plastic sediment class.

2.2.6 On the many, different definitions for incipient motion

Usually, sediment threshold is defined in terms of hydrodynamic parameters, the most used of which is bed shear stress. Sediment threshold can be defined "as the mean bed shear stress that produces a certain minimal amount of sediment flux" weighted or visualised. Common threshold are assumed as 10^{-6} - 10^{-4} [kg $s^{-1}m^{-1}$] (e.g. Yalin and Karahan, 1979; Shvidchenko et al., 2001 and Radice et al., 2008).

To date, no agreement has been reached, as to which parameter can be mostly representative of

the sediments threshold, and we have, as outlined in Section 2.2.3, either motion-based estimates which count the particles moving, or transport-based measurement where the solid flux is collected and its volume or weight measured (Yager et al., 2018; Ockelford and Yager, 2022).
In this Thesis, motion estimates through particles' counts are used and related to observed conditions of bed-shear velocity, from which bed-shear stresses are later computed. This allows to discuss the use of Shields' approach for microplastics' remobilisation studies.

2.3 A semi-probabilistic definition of threshold conditions for mobilisation

Incipient motion can be treated either deterministically by resolving individual grains equilibrium, or via a probabilistic approach for bed-averaged estimates. The first mode uses a Lagrangian framework, looking at particle-level forces and kinematics. The second, treats mobility as a bed-dependent parameter, lumping local stochastic effects (such as e.g. microtopography, particles' orientations and exposure) into one, reach-averaged quantity. The present work revolves around this latter approach, proposing a simplified method to assess the movability of plastic particles on different types of bed substrates under unidirectional flows stemming from near-bed velocity data and information about bed surface changes.
In Shields' approach, the scatter in the values of the Shields' movability number is due, among others, to the local heterogeneities of the bed substrate such as bed surface structure and texture (microtopography and roughness), giving rise to (i) hiding/exposure effects, (ii) differences in protrusion and pivot angle and interactions among grains (Ferreira et al., 2015), (iii) difference in local turbulence. The viable way to account for this variability is to treat the problem of incipient motion and motion threshold in probabilistic terms, evaluating the variability in time and space of relevant hydrodynamic and bed cover parameters.
Building upon what literature can offer us (see Section 2.2), the variables for the hydrodynamic description of the problem are linked to the near-bed velocity field, with bed shear velocity and shear stress most often regarded as the key parameters governing particles' mobilisation (Buffington and Montgomery, 1997; Dey and Papanicolaou, 2008; Dey and Ali, 2019; Shvidchenko, 2000).
If one chooses bed shear stress as the parameter governing bed particles' remobilisation, active and resisting stresses on individual particles can be represented via probabilistic distributions, both in space and time. Figure 2.5 shows a proxy for the instantaneous probability distribution of bed shear stresses for individual particles.
While the estimation of bed shear stresses can be derived from information on the near-bed flow field, the estimation of grains resisting stress is highly complex, depending on grain-scale interaction and forces/moment balance. Indeed, for the bed grains instability (causing incipient motion), balance approaches at the grain scale have been used, and the Shields' formulation itself can be derived from forces balance (Armanini, 2018, see Section 2.2.2.3). A fully probabilistic approach is therefore very hardly achievable, and requires attentive estimation of particles' resistance (Witz

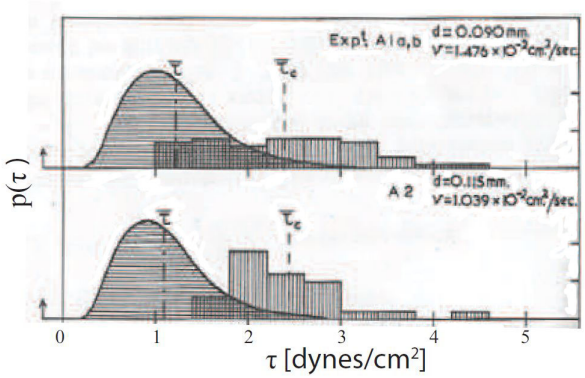

FIGURE 2.5: Probability distributions for the particle resisting shear stress (discontinuous probability function) and the ambient fluid shear stress (continuous probability function) acting on bed particles. The probabilities of instantaneous bed shear stress due to flow turbulence $\bar{\tau}$ and shear stress needed to dislodge the particles $\bar{\tau}_C$ are determining the sensitivity of grains to mobilisation (original from Grass, 1970, as reported in Cecchetto, 2017).

et al., 2019).

In the present work, both near-bed hydrodynamics and bed grains' mobility are treated through their probabilistic distribution, both in space and in time. With a fixed time step, the time average of the cross-sectional integrated distribution of finely space-resolved velocity measurement, as well as areal bed changes, are computed and analysed as outlined in Chapter 3.3.

Chapter 3

Methodology

"Nel prodotto finito, nelle scienze come in poesia, non c'è traccia della fatica del processo creativo e dei dubbi e delle esitazioni che lo accompagnano."
"In the final product, in science like in poetry, no trace remains of the efforts of the creative process and the doubts and hesitations accompanying it."

Giorgio Parisi, 2022

3.1 Experimental programme and experiments' design

The experimental work to investigate incipient motion and mobilisation of compact plastic particles was performed at the Hydrodynamic Models Laboratory (*HML*) at the Institute of Geophysics, Polish Academy of Sciences. The experimental facility together with the experimental design and instrumentation are hereby described. The experimental programme was designed to investigate the remobilisation of compact microplastic particles in simplified reference conditions, resulting in two sets of experiments, as listed below:
i) incipient motion of plastic particles from a loose plastic bed, homogeneous bed experiments
ii) remobilisation of compact microplastics from a natural clastic bed, clastic bed experiments
The first set of experiments with the two types of plastic particles constituting the mobile bed under steady, quasi-uniform flow conditions aimed to provide *baseline conditions* for the onset of motion of plastic grains. Homogeneous mobile bed experiments, like those carried out by Shields (1936) for natural sediments, are the easiest to perform and the parameterisation of incipient motion conditions for the bed grains requires simply the estimation of grains' density and diameter (e.g. Shvidchenko and Pender, 2000; Lee and Balachandar, 2012; Roušar et al., 2016). Near-bed hydrodynamics were measured with Ultrasonic Velocity Profiler (UVP), and bed particles motion was recorded through videos.

Experiments on the remobilisation of microplastics from a flat, clastic bed were also carried out at the *HML* facility. This second set of experiments aimed to study whether differences in the bed surface content of microplastics had any effect on the conditions for the onset of motion. Therefore, a range of surface concentrations of MPs (spanning from 0.05 % to 1% surface cover) was scattered over the clastic bed. The hydrodynamics characterisation and bed surface changes were recorded again with UVP (a different model from homogeneous bed) and videos.
For all experiments, other measured variables were bed slope, water discharge, bed elevation and flow depth at relevant cross-sections and water temperature.
In this Chapter a description of the flume and apparatus used is provided, as well as key aspects of the methodology adopted. For details on the experimental protocol for flat bed tests at *HML*, please refer to Appendix C.

3.1.1 Measuring apparatus

The near-bed hydrodynamic conditions were measured with UVP for all experiments. Two UVP devices were used: the UB-Lab P model by Ubertone, in its alpha version for testing for the homogeneous bed tests and the DOP model by Signal Processing provided by the University of Bologna Hydraulic Laboratory for the mixed bed tests. From UVP velocity measurements, shear velocities were estimated by fitting the near-bed velocities to the logarithmic law.
The bed movements were recorded with cameras and ad-hoc image analysis algorithms were used to estimate the amount of surface plastic grains detached from the loose bed. The derived threshold conditions for the onset of motion on the plastic grains are strictly valid only for this particular setup, i.e. plastic grains moving on a loose bed made up of the same plastic grains. Indeed we claim (as in 1.3) the term *incipient motion* is to be properly used specifically for grains moving on a substrate composed of the same material.
The slope was measured with a digital leveller with an accuracy of 0.02°, and was kept constant at a value of 0.01 mm/m for all experiments (both homogeneous and mixed bed).

3.1.2 Materials

Ellipsoidal plastic grains, differing only in material composition, namely polyamide 6 (PA6) and polyoxymethylene (POM) with a grain-size of around 3 mm were used in all experiments as movable sediments. The sieve analysis for the two materials is shown in Table 3.1. As both PA6 and POM particles are ellipsoidal, the median diameter resulting from sieve analysis (d_{50}) is a measure of the minor of the ellipsoid axes (Kennedy et al., 1985). The measured d_{50} is 2.4 mm for PA6 and 2.9 mm for POM, and it was not further used, to comply with microplastics studies, (with the standard set in Waldschläger and Schüttrumpf, 2019a), preferring the use of an equivalent diameter (see Equation 3.1).
Following the procedure outlined, among others by Waldschläger and Schüttrumpf (2019a) and Yu et al. (2022), the equivalent diameter for the two materials was estimated. The areal equivalent

TABLE 3.1: Results from the sieve analysis for the two microplastics used

PA6	**mesh size** [*mm*]	<1,18	1.7	2.36	2.8	3.35
	percentage passing [%]	0.0	0.58	6.03	51.74	89.08
POM	**mesh size** [*mm*]	<1,18	1.7	2.36	2.8	3.35
	percentage passing [%]	0.0	0.0	0.0	6.06	95.12

diameter d_{eq} was computed as the diameter of a circle with the same area of the plastic ellipse, following the formula 3.1.

$$d_{eq} = \sqrt{a_1 \cdot a_2} \tag{3.1}$$

where a_1, a_2 are the major and minor axes of the particle approximating ellipse. Measurements of a_1 and a_2 were done manually using a calliper, on a small sample of 10 grains per material after visual inspection of the grains on millimetre paper. Equivalent diameter values for the two materials are 2.9 mm for PA6 and 3.1 mm for POM respectively, differing slightly from the values for spherical equivalent diameter given in Mrokowska and Krztoń-Maziopa (2024), corresponding of 2.88 mm for PA6 and 3.16 mm for POM. From here on, when referring to d_{MP}, we implicitly mean the equivalent circle area diameter of the microplastic particles, $d_{eq,MP}$.
For convenience, Table 3.2 reports the density and equivalent diameter values for the two microplastic particles used.

TABLE 3.2: Summary of microplastic particles' characteristics

MP type	ρ [kg/m^3]	d_{MP} [mm]
PA6	1100	2.9
POM	1410	3.1

The bed material for clastic bed experiments was natural sand and gravel. The grain-size distribution of the gravel bed sediments is reported in Table 3.3, uniformity coefficient $CU = d_{60}/d_{10}$ is 1.15. Due to the value of CU, the gravel was considered uniform (Miura et al., 1997), and d_{50} = 2.79 mm was chosen as representative diameter. Gravel particles' shape was angular and their density ρ_S was 2650 kg/m^3.

TABLE 3.3: Granulometric distribution of the chosen gravel for HML flat bed experiments. Data from the producer.

mesh size [*mm*]	<2,0	2.0	2.5	3.0	4.0
percentage passing [%]	0.5	9.5	62.0	25.0	3.0

The grain-size distribution of the sand used is reported in Table 3.4, and the resulting uniformity coefficient CU is 1.46. Due to the value of CU smaller than 2, the sand was considered uniform (following Miura et al., 1997), and d_{50} = 0.72 mm was chosen as representative diameter for the

sand mixture. Sand grains' shape was angular and their density was 2650 kg/m^3.

TABLE 3.4: Granulometric distribution of the chosen sand for HML flat bed experiments. Data from the producer.

mesh size [*mm*]	1.0	0.8	0.5	0.4	<0.4
percentage passing [%]	2.5	32.5	61.5	3.0	0.5

3.2 HML flume experiments: flat bed

The tilting flume at the Hydrodynamic Models Laboratory (HML) at the Institute of Geophysics, Warsaw, is 5.2 m long, 0.25 m wide, with walls 0.3 m high. The system operating the flume is closed, having two tanks (upstream and downstream) connected by pipes (see Figure 3.1). Three pumps are present to circulate water from the upstream tank to the flume inlet, and one additional pump in the downstream tank supports high-flow conditions. The flume can be operated for discharges spanning from 30 l/min to 160 l/min (0.5 l/s to 2.7 l/s), in quasi-steady, quasi-uniform flow. The regulation of discharge was operated by the manual opening of a valve located downstream of the loading tank (Figure 3.1). At the flume entrance, an array of rigid tubes serves as flow-stabiliser. The flume's cross-section is rectangular for 5.2 m and the maximal usable length spans 5.0 m. The water level can be controlled by a weir gate located at the flume outlet, after which free fall occurs. In the downstream tank, a sediment trap is located, with a mesh size of around 2.8 mm (this allowed to trap the chosen microplastic grains, as well as the gravel).

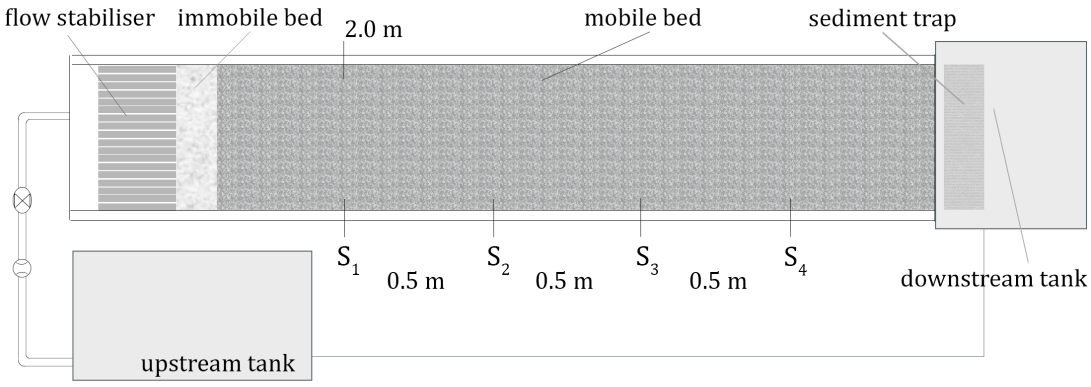

FIGURE 3.1: Sketch of the HML flume, planar view. Sections S_{1-4} starting from a distance of 2.0 m from the inlet, where measurements were taken. At the outlet, a sediment trap was located, collecting transported particles.

Homogeneous bed tests and mixed bed tests were performed with discharges spanning respectively from 115 l/min to 140 l/min (1.9 l/s to 2.1 l/s), and from 115 l/min to 160 l/min (1.9 l/s to 2.7 l/s) in steady quasi-uniform flow conditions. In homogeneous bed experiments, local scour at the

flume inlet was prevented with a 0.4 m long area of marble cobbles, see Figure 3.1. This created an immobile bed, and after the initial transient during filling, no scouring was observed.
Experiments were performed in flat-bed conditions, and the bed was stable (neither localised erosion nor changes in the bed morphology occurred) for the whole experiments' duration. Such conditions were attained, not only for the natural beds, namely gravel and sand, sediments for which the mobility threshold exceeded the one searched for (of the microplastic grains), but also in the case of microplastic bedded experiments. The absence of bed rearrangements during the experimental tests was key to ensuring that the observed conditions were neither local nor flow-driven changes in the bed morphology. Indeed, such changes directly affect areal patterns of sediment motion, in that they generate areas where dominant aggradation/degradation form, thus invalidating the assumption of ergodicity of the observed process.

3.2.1 Plastics homogeneous bed experiments

Experimental work on sediment transport has been using artificial sediments as a proxy for natural clastic ones for more than half a century, see Section 2.1.2, and numerous results from literature (Ippen and Verma, 1955; Graf and Pazis, 1977; Komar and Clemens, 1986) highlight how, for uniform bed material, the mobilisation threshold follows the classical Shields' threshold curve pattern (Buffington and Montgomery, 1997; Lee and Balachandar, 2012).
The need to derive the threshold values for the chosen materials (PA6 and POM 3-mm ellipsoidal grains) required us to carry out a first batch of experiments, to validate this literature-proven hypothesis under the experimental conditions we could model. Herein a short description of the experimental procedure is reported, which complies with other plastic-bedded experiments by e.g. Radice et al. (2017).

3.2.1.1 Short protocol

Plastic incipient motion experiments were performed at three different flow conditions, with discharge steps of 5 l/min, and measurements of the flow field and bed changes. Velocity was measured at three consecutive cross-sections for both PA6 and POM plastic grains, and three repetitions were made of each condition. A summary of the hydraulic conditions is reported in Table 3.5. As visible from Table 3.5, the ranges of both discharge and depth were different for the two types of plastics. This choice was due to the characteristics of the flume, the discharge regulation apparatus and the operation of the weir gate at the flume end, as well as the difference in density of the two materials.
On bed preparation.
The bed arrangement was as follows: high-porosity gum mats filled with the chosen plastic granules (either PA6 or POM) covered the full length of the flume. The thickness of the bed layer was around 3 - 3.5 cm, allowing it to cover the mats, with 2-cm-thick loose bed (corresponding to around six times a grain diameter). The total experimental area covered around 1.5 m in length and the whole flume width where measurements were carried out at three to four cross-sections.

TABLE 3.5: General ranges for the hydraulic conditions in the plastic bed experiments. Discharge Q, water depth y, bed elevation from the flume rigid bottom Z_{Bed}, water surface elevation from the flume rigid bottom h

MP type	**Q** [*l/s*]	**y** [*mm*]	$\mathbf{Z_{Bed}}$ [*mm*]	**h** [*mm*]
PA6	1.92 - 2.08	59 - 64	25 - 28	82 - 89
POM	2.33 - 2.50	40 - 46	20 - 24	62 - 68

The first cross-section was located 2.0 m downstream of the inlet, see Figure 3.1, and the following sections had a distance of 0.5 m from one another.

On flow measurements.

The discharge value per each test was determined using an ultrasonic flowmeter built into the inlet pipe. Tested discharges were in the range 1.9 - 2.1 $\cdot$ 10^{-3} m^3/s and 2.3 - 2.5 $\cdot$ 10^{-3} m^3/s for PA6 and POM bed tests respectively. The mean water depth was around 6 cm and 4.5 cm for PA6 and POM bed respectively, and it was not constant along the flume, with an average increase of around 2-3 mm along a 1.5 m-long stretch. The bed slope was <0.0001. The bed layer was levelled manually, with the aid of an ad-hoc built leveller operated from the wall top.

On velocity measurements.

Two UVP transducers were placed on the external wall upstream and downstream pointing, at the flume centre with angles of ±70°, respectively. The reason for the external positioning of the transducers is linked to the type of sediments used: at the chosen flow depths (spanning from 4.5 for POM to 6.5 cm for PA6), small perturbations of the water surface were triggering motion of the light microplastic particles, in their vicinity, and the perturbations generated by the 3 MHz transducers in use with the UB-Lab P were disturbing the observed phenomenon significantly. The possibility to measure the flow without disturbances (thanks to the presence of polycarbonate walls) was therefore exploited, and transversal measurements of longitudinal velocity were performed. The transducers' position was manually regulated and adjusted, starting from 0.5 cm up to 3.5 cm and 2 cm from the bed surface, meaning 5 or 4 transversal profiles were recorded, respectively for the PA6- and POM-bed tests. The transversal profiles of velocity were measured at fixed distances from the bed surface, i.e., at 0.5, 0.8, 1, 2 and 3.5 cm above the mean bed level. The measured velocities across the flume are later used to derive the longitudinal velocity, from which the shear velocity was estimated, as outlined in Section 3.3.1.

On identification of grain motion: camera measurements.

All tests were performed in steady, quasi-uniform flow conditions. The first flow condition tested was set by visual observation of grains' motion, which occurred all along the flume length, and was labelled simply by a discharge value, since bed layer thickness and water level were constant for all tests. From this, successive step-wise increases of flow rate by 5 l/min resulted in three slightly different flow conditions triggering increasing grains' mobilisation.

The plastic sediments' detachments from the bed were recorded by videos. The camera was located above the flume, and its field of view comprised the whole width, observing the flume from the top. Single particles' detachments were identified from the video frames in small time

intervals as outlined in Section 3.3.2. The result of the image analysis algorithms is the count of detected motions in all consecutive time windows for the duration of the experiment.

3.2.1.2 Hydrodynamic measurements

Measurements of the flow field were carried out via the use of a UVP mounted on the side wall of the flume (Figure 3.2). This particular choice is justified by the need to avoid disturbances of the water surface and its perturbations, because of the relatively low depths adopted. The mean hydraulic conditions are outlined in Table 3.5. The range of depths y is due to measurements performed at different equispaced cross-sections (Figure 3.1), in steady, quasi-uniform flow conditions. Per each flow conditions the range of flow depths varied by a maximum of 3 mm along a 1.5 m-long stretch. The bed elevation Z_{Bed} and the water surface elevation h were measured from the rigid bottom of the flume.

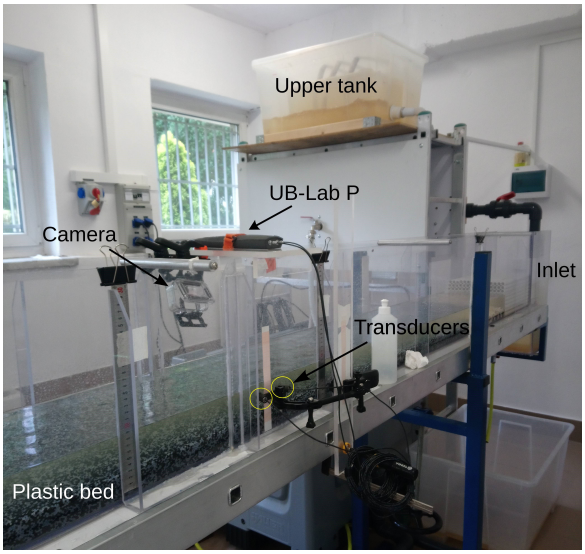

FIGURE 3.2: Experimental setup during PA6 experiments, the transducers for velocity measurements are placed at an intermediate vertical position in the first available cross-section.

Figure 3.2 shows all components of the experimental setup. The UVP transducers mounted at the wall had an angle of ±70°, with their beams meeting approximately at the flume centre. Measurements were performed sequentially per each test, starting from the upstream cross-section and moving downstream, starting from the closest to the bottom transect and moving upward. The resulting velocity measurements cover 4/5 of the flume width (because of a particular deficiency in the adopted transducers, provided together with the UB-Lab P beta version for testing, which was not able to detect anything in the first 5 cm). The cell size for each measurement was 0.91 mm long, allowing to resolve both PA6 and POM grains, having a dimension of around 3 mm (Table 3.2).

Two components UVP measurements from the wall (i.e., along 70° sloped beams) and the homogeneity assumption within beam axes (max longitudinal distance of ≈ 12.5 cm) allowed mapping of the longitudinal and transversal velocities across each section, providing information

on the spatial distribution.

Figure 3.3 reports an example of the obtained data. The mapped area is the central part of the flume, spanning 0.15 m in width in total. As visible, the flow is quasi-uniform across the section, with velocities slightly increasing (around 15 - 20%) close to the right wall. This asymmetry was likely due to a combination of the geometry of the flume inlet and bed roughness effects because it was consistent for all the tests, with lower velocities at the left wall compared to the right side.

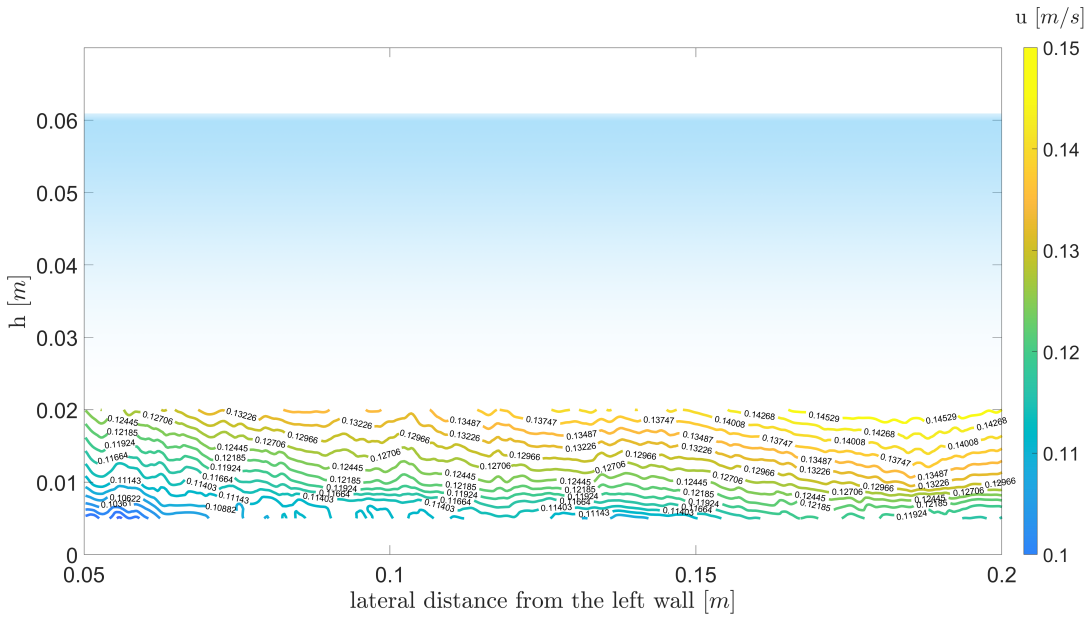

FIGURE 3.3: Isolines of near-bed UVP-measured longitudinal velocities for PA6 experiments. The water depth (highlighted in light blue) was around 60 mm.

The mean flow velocity for the test reported in Figure 3.3 was around 0.14 m/s (PA6 bed at fixed discharge Q = 1.92 l/s) and it is visible that it corresponds to the range of highest values measured close to the bed (covering about 30% of water depth). Therefore, we assumed that the measured data provide good information about the flow field in the near-bed region and we fitted the data to the law of the wall as later outlined in Section 4.3.1.

3.2.1.3 Bed movements measurements

The measuring apparatus for bed movements consisted of one down-looking camera, recording videos of the bed surface. The positioning of the camera, with lens parallel to the bed surface and elevation above the water surface around 0.10 - 0.15 m, resulted in recording all water surface perturbations, which, consequently, led to methodological choices briefly outlined hereon (see Section 3.3). The pre-processing of collected data required a time-averaging procedure, the temporal scale of which was dictated by the image signal characteristics. Details on the definition of such scale have been provided in Section 3.3.2. The measurements from videography resulted in a time series of bed changes, which, coupled with near-bed velocity data, offers some insight into the understanding of compact MPs' incipient motion dynamics.

3.2.2 Natural bed experiments: microplastics on a clastic bed

Sparse is research on bed sediments significantly different from the mobile material at the bed, with few examples in the transport of heavy minerals and gold particles (among others Slingerland, 1977; Kuhnle and Southard, 1990; Komar, 2007; P. A. Carling and Breakspear, 2006); or biogenic sediments and shells (Allen, 1984; Weill et al., 2010; Rieux et al., 2019).
The presence of plastic fragments and debris requires a better understanding of the role of sediment density on the onset of transport processes. Besides, the availability of mobile material on the bed may also play a role in the onset of transport, as when only a few grains are mobile, those exposed to favourable (local) conditions for mobility are even less. We argue that the definition of a threshold condition should consider the availability of movable sediments, and for this reason, not only the two materials presented in the homogeneous tests were used on two clastic sediment beds differing for mean grain-size, but also the amount of MPs on the bed was varied, with values as from Table 3.6.

TABLE 3.6: Tested MPs surface concentrations **c1** - **c5** (in percentage of area covered by MPs) on clastic beds.

c1	**c2**	**c3**	**c4**	**c5**
0.05%	0.1%	0.2%	0.5%	1.0%

3.2.2.1 Clastic bed experiments: gravel

Adding a first degree of complexity to the system, the second group of experiments saw a combination of gravel composing the bed and the plastic grains used in the homogeneous bed experiments as mobile material (Section 3.1.2, characteristics reported in Table 3.1).
The tests were performed in steady flow conditions starting from a discharge of 115 l/min (1.96 10^{-3} m^3/s) and 150 l/min (2.5 10^{-3} m^3/s) for PA6 and POM respectively, determined by visually observing when grains tended to move. Three different steady flow conditions were produced consecutively, with increments of 5 l/min for five diverse surface concentrations of plastic grains corresponding to a range of 0.05 - 1.0 % surface area. In all tests, velocity measurements were done via UVP and plastic grains movements were recorded via videos.

Short protocol

The gravel bed experiments were run at five fixed discharge conditions, increasing the concentration of the surface plastic grains in the range 0.05% - 1.0% (every time repeating the seeding conditions and reducing the discharge to seeding value Q_{seed}). After each condition had been run, a visual check on the number of particles mobilised and which exited the area allowed eventually to adjust the quantity of the next seeding to comply with chosen values (0.05%, 0.1%, 0.2%, 0.5%, 1%). The duration of each experiment (at fixed flow conditions) was around 5-6 h.

TABLE 3.7: General ranges for the hydraulic conditions in the gravel bed experiments. Discharge Q, water depth y, bed elevation from the flume rigid bottom Z_{Bed}, water surface elevation from the flume rigid bottom h.

MP type	**Q** [*l/s*]	**y** [*mm*]	$\mathbf{Z_{Bed}}$ [*mm*]	**h** [*mm*]
PA6	1.75 - 2.08	46 - 48	33 - 34	78 - 81
POM	2.33 - 2.67	44 - 48	33 - 35	81 - 84

On bed preparation.
The HML flume was set to a quasi-zero slope, and the bed was prepared by pouring gravel, with a d_{50} of 2.8 mm, over a plastic film covering the flume surface, up to a thickness of around 20 mm. Then, the film was folded on the gravel base layer, and another 10-15 mm of gravel were poured. The levelling of the bed was done manually, with an ad-hoc leveller, which allowed for partially compacting the bed as well. A weir gate at the outlet of the flume was positioned, at a height of 65 mm from the rigid bed. The flume was filled with a discharge of 30 - 40 l/min (0.5 - 0.7 10^{-3} m^3/s) up to a water depth of around 70 mm, then the discharge was increased to 60 - 70 l/min (1.0 - 1.2 10^{-3} m^3/s) and let flow for 10 minutes to obtain a (partially) water-worked bed. On top of the so-formed horizontally levelled bed, different concentrations of microplastic particles were randomly distributed, and the changes in their incipient motion conditions were measured, starting from reference data we collected previously (see Chapter 4), referring to the motion of microplastics on a bed composed of microplastics. None of the tested conditions triggered the motion of the gravel grains composing the bed, therefore the clastic bed is considered hydraulically immobile.
On seeding.
Seeding was done at a discharge Q_{seed} of 90 l/min (1.5 10^{-3} m^3/s) and 120 l/min (2.0 10^{-3} m^3/s) for the PA6 and POM grains respectively, which was observed to be sufficient to allow the plastic grains to deposit in an area approximately 0.10 - 0.15 m downstream from the seeding point. The seeding points were located in 5 sections, covering 1.5 m around the interrogation area. Seeding was done manually, by dropping wet grains in the flowing water at around 2 - 3 cm distance from the bed. The manual seeding distribution followed the scheme reported in Figure C.3 (see Appendix C.2 for more detailed explanation). The distribution of the plastic grains was as randomly scattered as possible, and after seeding the bed looked like Figure 3.4 (where it is visible a larger area around the measured section).

3.2.2.2 Clastic bed experiments: sand

Adding a second degree of complexity to the system, the third group of experiments consisted of a sandy bed and the same plastic grains used before, as mobile material (for the characteristics of mobile sediments and bed sediments see Section Section 3.1.2).
As for the previous gravel tests, three different steady flow conditions were produced consecutively, with flow rates spanning the range 75 - 85 l/min (1.2 - 1.4 10^{-3} m^3/s) for PA6 and 130 - 140 l/min

FIGURE 3.4: Example of gravel bed covered by PA6 grains at 1% surface cover. It is visible how the MPs are distributed randomly and uniformly over the bed. The image was not used for further processing.

(2.1 - 2.3 10^{-3} m^3/s) for POM, again with increments of 5 l/min. The five surface concentrations of plastic grains were in the range of 0.05 - 1.0 % surface area. Again, velocity measurements were performed via UVP and plastic grains' movements on the sandy bed were recorded through videos.

Short protocol

The sandy bed experiments were run at three fixed flow conditions, increasing, as for the gravel bed tests, the concentration of plastic grains at the bed surface in the range 0.05% - 1%, and repeating the seeding at a fixed seeding discharge value Q_{seed} different from the one used for gravel. The surface concentration of plastic grains was adjusted after each run, and the duration of one experiment was around 3 - 4 h. Table 3.8 summarised the hydraulic conditions tested.

TABLE 3.8: General ranges for the hydraulic conditions in the sand bed experiments. Discharge Q, water depth y, bed elevation from the flume rigid bottom Z_{Bed}, water surface elevation from the flume rigid bottom h.

MP type	**Q** [l/s]	**y** [mm]	$\mathbf{Z_{Bed}}$ [mm]	**h** [mm]
PA6	1.25 - 1.41	64 - 69	35 - 36	95 - 104
POM	2.16 - 2.33	71 - 75	36 - 37	103 - 110

On bed preparation.

The *HML* flume was set to quasi-zero slope and the bed base layer was prepared in the same way as for the gravel bed experiments (see Section 3.2.2.1). Above the base layer, 1 - 2 cm of sand with a d_{50} of 0.8 mm was poured and manually levelled with an ad-hoc leveller along the whole flume length. At the outlet of the flume, a weir gate was positioned, with the same weir crest level as for gravel bed experiments, corresponding to 65 mm above the flume rigid bottom.

The flume was then filled with a discharge of 20 - 30 l/min (0.3 - 0.5 10^{-3} m^3/s) up to a water depth of around 20 - 30 mm: this step was needed to remove air bubbles trapped in the sand surficial layer and ensure all sand was wet. Then the discharge was increased to 60 l/min (1.0 10^{-3} m^3/s) and was let flow for 15/20 minutes to have a water-worked bed. None of the tested conditions triggered the motion of the sand grains composing the bed, therefore it is considered hydraulically immobile.

On seeding.

Seeding was done manually at a discharge of 75 l/min (1.2 10^{-3} m^3/s) and 100 l/min (1.7 10^{-3} m^3/s) for the PA6 and POM grains respectively, which was observed to be sufficient to allow the plastic grains to deposit in an area approximately 10 cm downstream from the seeding point. The seeding procedure is the same as outlined in Subsection 3.2.2.1.

3.2.2.3 Hydrodynamic measurements

Measurements of the flow field were carried out with the use of UVP instrumentation, placing one 3 MHz transducer in the water at an angle of 70° facing upstream (see Appendix C.2, Figure **??**). The velocity measurements were performed at two symmetrical locations at 7 cm from the side walls in three consecutive cross sections. Measured time-averaged vertical profiles were used to derive bed shear velocity (as outlined in Section 3.3.1).

3.2.2.4 Bed movements measurements

Remobilisation of MPs grains was measured by means of a camera, mounted facing the bed. Videos were recorded in three consecutive cross-sections, and grain motion was derived by analysing the central half (Region of Interest, ROI) of the camera Field of View (FOV) in the videos (see Figure 3.5).

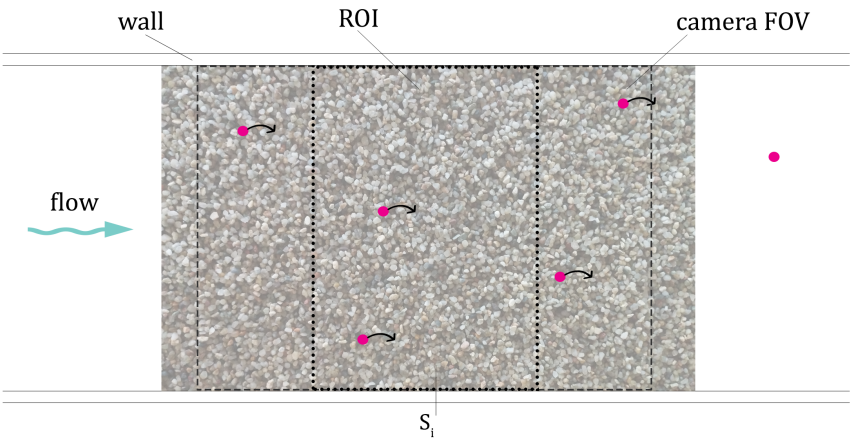

FIGURE 3.5: Camera field of view over the region of interest (ROI) for detecting the mobilisation of microplastics on a gravel bed.

Videos were recorded in the same locations of velocity profiles, to map plastic grains' cover movements in the region of interest. The GoPro 9 camera capture setting was set to linear at a 60 fps. Notably, due to the low water depths, the camera was located 0.15 m above the water surface, and we chose to record the flume bed as it was, with water surface perturbations (without the use of transparent panels, which would have disturbed the near-bed flow field). This meant a rather extensive pre-processing of raw frames, to get rid of the noise created by perturbation of the water surface as outlined in in the following Section 3.2.2.4.
Image analysis methods were used, to identify single particles' motion from video sequences. The analysis of the image sequence involved preprocessing the raw images to remove the water surface perturbations (as in Section 3.2.1.2), and increase the visibility of areas where particles had moved. The analytical steps were the same as for the homogeneous bed experiments, with the only difference in the choice of the threshold for the identification of changes, which depended on the bed cover characteristics and colour-filtering adopted in the preprocessing steps.

3.3 Data analysis fundamentals

The following subsection provides an overview of the analysis of data collected for the various experiments carried out in the *HML* facility. It is divided according to the different types of data, and reports the key hypotheses applied to the studied process, as well as an overview of both UVP and image processing/analysis methods.

3.3.1 Analysis of velocity data

In the tests with homogeneous bed, the UVP signals, resolved into transects, were collated resulting in a time series of the velocity field in each section, lasting approximately 3 min, at a sampling rate of 1.6 Hz and 1.75 Hz for PA6 and POM respectively. Such time series was then resampled at 0.2 Hz to derive a coarser time series of time-averaged 2D velocities in three cross sections starting from S2, (Figure 3.1), 2.5 m downstream of the inlet. The amplitude of the resampled time window was defined following the time resolution for which the number of detachments was derived in the following Subsection 3.3.2. This step was needed to harmonise the data.
In the tests with clastic beds, UVP measurements were performed at two locations, distant 7 cm from the walls, symmetrically. The signal consisted therefore of two vertical profiles, with a spatial resolution over the transducers' axis of 0.91 mm, allowing for the identification of the boundary layer region from measured data. The sampling rate for this second group of experiments was higher, from 10 Hz (for PA6 on sand) to 15 Hz (for POM on gravel). Again, resampling was performed at 0.2 Hz for the three cross-sections where measurements were recorded. The amplitude of the resampled time window was imposed by the noise in the image data.
The UVP datasets were analysed in terms of the vertical distribution of longitudinal velocity, to

derive the shear velocity for the various flat-bed cases. The analysis of velocity data was based on the following hypotheses:

a) quasi-uniform flow along the flume allowing us to model the velocity distribution and the related shear velocity and shear stress through a single value for each cross-section;

b) steady flow, allowing the subdivision of the time series of velocity data considering each time-averaged velocity value as an independent;

c) validity of the logarithmic velocity distribution in the near-wall region.

From the measured velocities the near-wall region was identified. In the case of homogeneous bed, it corresponded to the measured transects up to half the water depth. In the case of clastic bed, the near-bed region was identified as the last centimetre before the echo peaked at the bed. By fitting the data to Equation 3.2, the shear velocity u^* was derived.

$$u(z) = \frac{u^*}{\kappa} \ln z + (-\frac{u^*}{\kappa}) \ln z_0 = C_1 \ln z + C_2 \tag{3.2}$$

Where $u(z)$ is the time-averaged velocity at each point along the transect, u^* is the space-resolved shear velocity, z is the elevation above the bed of the measured transect, z_0 is the hydrodynamic roughness length and κ is the Von Kármán constant, set at 0.41 since the relative submergence y/d_{MP} in the tests exceeded the threshold value (corresponding to $y/d_{MP} = 15$) set by Gaudio et al. (2010).

The fitting to the law of the wall was performed for time-averaged velocities over both the whole experiment duration (around 3 min) and a time window of 5 s (consistent with choices dictated by videography, see Section 3.3.2) in which we assume steady, uniform flow conditions to be valid. The resulting distribution is the basis of the semi-probabilistic approach hereby adopted to solve the time-averaged properties.

It is worth recalling that other methods exist to estimate the bed-shear velocity, as outlined by Pokrajac et al. (2006). Among the main limitations of our chosen method is its applicability to very shallow flows, where the near-bed velocity distribution can deviate significantly from the logarithmic approximation (Detert, 2008).

3.3.2 Analysis of videos for particles' detachments

Recorded videos were divided into frames for further processing. Pre-processing of images consisted of:

(p.i) selecting the image portion to analyse: for homogeneous bed experiments, the central third of the image was chosen, while for mixed bed experiments, the central half was chosen, to cover more MP particles and be more representative. In the two cases, the processed images covered approximately 13 and 19 cm in the longitudinal direction and the full flume width in the transversal direction.

(p.ii) resampling the full resolution (corresponding to 0.1 mm/px) to 1/5 of its value. The rationale behind such a choice was to analyse a more manageable dataset, for the whole video duration (around 3 min).

(p.iii) converting to appropriate colour scale: greyscale and blue channel (out of the three RGB) were chosen for PA6 and POM homogeneous bed tests, while a combination of colour thresholding in the CIELAB colour-space and greyscale conversion were selected for MPs on gravel and sand respectively (see Figure 3.6).

(p.iv) in 5 out of 6 datasets, the RGB information was relevant (only PA6 homogeneous tests had black and white grains). When selecting the colour scale, some adjustments were needed to the images: contrast enhancement was applied before colour filtering and thresholding.

(p.v) only in the case of clastic bed, the last step was masking of the immobile part of the bed, to save computational time and reduce noise.

The outlined preprocessing of images was very computationally intensive, and was strictly due to our need to reduce the effect of surface perturbations. Indeed, surface perturbations altered the refraction angle of light, thus causing noise in the bed surface recorded in the pictures. To reduce such noise, temporal averaging in time windows was applied (see later *a.1*), and the definition of the duration of the TW required the convergence of the cumulative average of pixel (colour) values (Ermilov et al., 2022). Especially for clastic bed experiments, when colour information was linked to the presence of plastic grains, the identification of the colour threshold and consecutive colour-thresholding step of the time series of images took most of the computational time.
The image analysis procedure, on the other hand, included the following steps:

(a.i) identification of the minimum time-interval (i.e. Time Window, TW) to have a stable value of the pixel-wise mean,

(a.ii) computation of the first-order moments of each pixel,

(a.iii) identifying a function for colour-intensity thresholding and set a threshold,

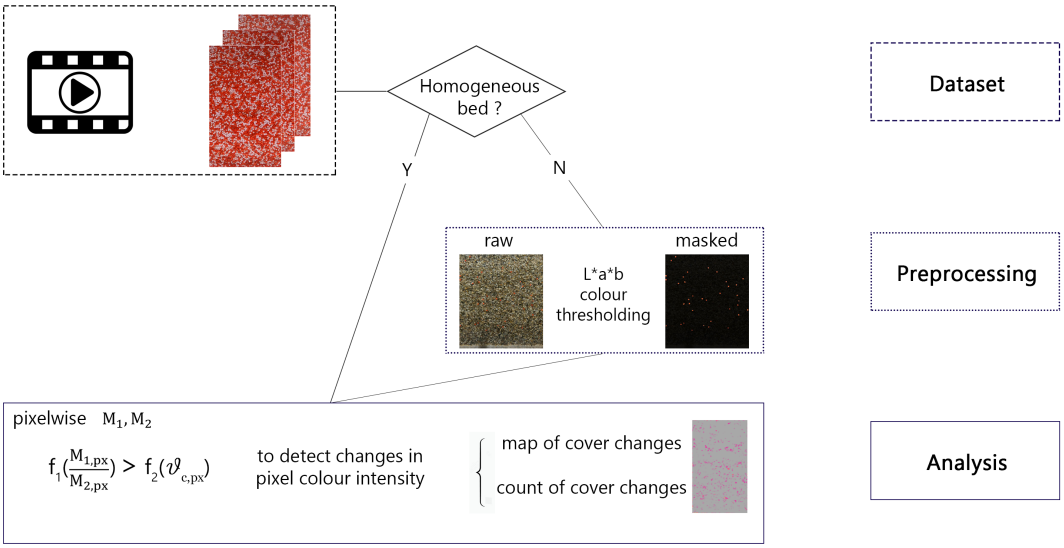

FIGURE 3.6: Workflow from dataset selection to image analysis. If the image has more than two colours, preprocessing is needed, and colour thresholding is done in the CieLAB colour space. The analysis sees the computation of pixel-wise mean $M_{1,px}$ and standard deviation $M_{2,px}$ that are later used to identify areas where significant change in the colour intensity occurred. Once filtered by size, these areas correspond to particle-sized cover changes.

(a.iv) from the thresholded image, identify particle-sized areas where changes of bed cover occurred (the thresholded portion) and count them (see Figure 3.6, Analysis).

The time interval, see (a.i), depends on the need to denoise image data: high-frequency oscillations linked to water surface perturbations were filtered out, thus retaining bed-cover relevant information. The identification of such and interval was obtained when the cumulative mean pixel values, in different pixels, converge to an asymptote. The use of first-order moments, (a.ii), allows a simple way of detecting changes. The mean $M_{1,px}$ and standard deviation $M_{2,px}$ in each time interval were computed for all pixels, and a function of their ratio was used to identify areas where bed cover change occurred (see Figure 3.6), where ϑ is the threshold for change identification.

$$e^{M_{2,px}/M_{1,px}} > \vartheta e^{1} \tag{3.3}$$

This method allows to just detect the necessary information regarding whether a given pixel in the bed cover changed in the chosen time window TW, and was used in all experiments for the detection of changes in the bed cover. The assumption inherent to this method is that wherever a change in bed cover occurred, a particle either deposited or detached, and due to the local equilibrium hypothesis, both are considered proxies of motion. Sample results to illustrate the data derived from the TW-averaging are reported in Figure 3.7 as the cumulative detected bed changes over time.

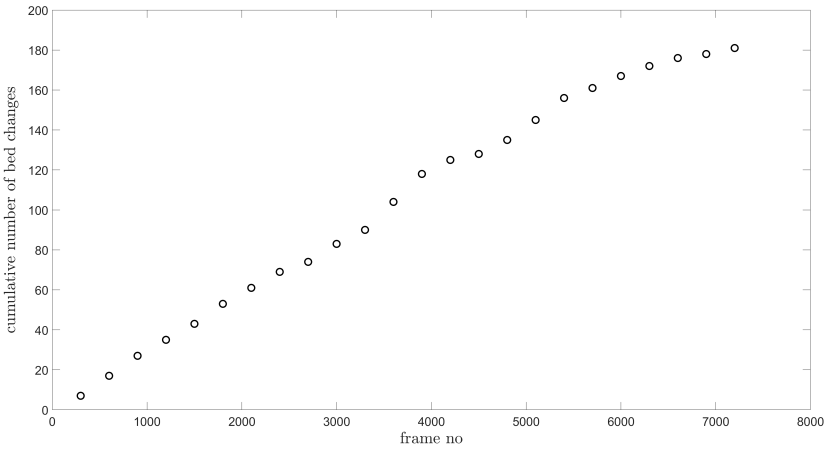

FIGURE 3.7: Cumulative sum of bed changes detected at each time-window (for the dataset PA6_Q2t3).

The algorithm for the detection of areas of change depends on the input image sequence properties such as image brightness and colours. In each time series (in each video) the threshold ϑ for detection is therefore different, and was manually adjusted. The algorithm can be very easily applied to red and white mixtures, while a mixture of white and coloured particles, especially red (RAL 3000 colour, with RGB values [169, 66, 63]), needs attention in the colour thresholding step. Accuracy depends on the chosen threshold, and on the time interval over which the bed changes are to be estimated (in our experiments it was chosen as 5 s).

For homogeneous bed tests, the initial choice of the threshold was visual, by comparing detected vs. visually counted changes. Then, the value resulting in the lowest difference among the two counts in 8 consecutive time intervals was chosen. Visual assessment of the validity of such threshold was carried out for 20 - 25 % of the homogeneous bed dataset, in randomly chosen time intervals. For PA6 data, errors in detection account to a maximum of 10 % of detected bed changes, while for POM data they are higher, amounting to 10 - 15 % of total bed change detections. The given values for detection errors refer to cumulative changes in the longer time interval (lasting 40 s, which is approximately 1/3 of the total experiment duration).

For clastic bed experiments, the initial visually estimated threshold was adjusted manually resulting in different accuracy of change detection for the two materials, on the two clastic beds, after visual assessment of approximately 10 - 15 % of the dataset. Again, for PA6 data, errors in bed change detection account for a maximum of 10 %, while for POM data they reach 20 % of bed change detections. The given values refer to each time window of 5 s.

Image resolution also has a role (not investigated in our study), indeed local statistics change when the resolution changes and this reflects in the ratio of the second to the first moment $M_{2,px}/M_{1,px}$ of the pixel-wise colour intensity distribution.

A further step, if one wants to compare differently resolved images, is to understand the dependency of the detection algorithm upon the image resolution. The rationale behind the chosen

compromise for spatial/temporal resolution is outlined in the following. Spatial resampling was chosen to allow rather fast computation on the domain, without losing too much detail, it involved downscaling from 30 px per particle's mean equivalent diameter to 6 px per diameter. This resolution allows still for some flexibility in the detection, requiring computational efforts which are 10x lower than for fully-resolved images. The choice of the temporal resolution is, instead, dictated by parameters related to the single video sequences: the smallest value at which pixel-wise cumulative averages converge is chosen. For our data, this corresponds to 5 s.

Chapter 4

Plastic grains over a plastic bed

"Zwiemy je ziarnkiem piasku.
A ono siebie
ani ziarnkiem, ani piasku.
Obywa się bez nazwy
ogólnej, szczególnej,
przelotnej, trwałej,
mylnej czy właściwej."

"Lo chiamiamo granello di sabbia.
Ma lui non chiama se stesso
né granello, né sabbia.
Fa a meno di nome
generale, individuale,
instabile, stabile,
scorretto o corretto."

W. Szymborska, 1996

4.1 Introduction

Many natural environments see a fluid flow over a loose granular boundary, and the interactions and reciprocal feedback among them have shaped landforms at any viable scale: from soil microtopography to rills, ditches, rivers and landscapes. For our purpose, we focus on what can be referred to as fluvial transport and mobilisation, occurring at the bed and boundary of watercourses and rivers. The beginning of movement and transport has a crucial role for modellers, since, when a threshold between immobility and motion can be identified, an equilibrium model can be developed and applied for any value above such threshold. The binary nature of threshold conditions makes their study an "evergreen" priority in sedimentary research, and, as outlined in Chapter 2, state-of-art frameworks, methods and techniques have been diversely applied to handle the subject. For a thorough discussion on the parameterisation of the incipient motion problems and on the possible frameworks to approach it, please refer to Sections 2.2.2 and 2.2.3. The simplest model for incipient motion and transport sees a flat bed, of homogeneous cohesionless sediments, (potentially) mobilised by a steady, uniform flow discharge. Mobility, for a cohesionless bed of homogeneous grains, is highly stochastic in nature (Grass, 1970; Lavelle and Mofjeld, 1987), since every single grain is exposed to the flow in a slightly different manner, and

the flow's feedback to the particles' exposure manifests in a range of conditions depending on local microtopography (namely, at the grain scale).
In the experiments discussed in this chapter, the flat bed conditions are assumed to distribute potential grain mobility due to microtopography effects uniformly over the bed plane.
Two sets of experiments on the incipient motion of plastic particles are described here, and the results are presented and discussed. The chosen plastic materials reflect a density higher than the ambient fluid (water), corresponding to $\rho_{MP} = 1100\ kg/m^3$ for PA6 and $\rho_{MP} = 1410\ kg/m^3$ for POM grains respectively. The type of microplastics studied is referred to as nurdles (Figure 4.1), classified as primary microplastics, spilt into the environment from containers through transport for secondary processing into products. The choice of the plastics, both for shape (compact ellipsoids) and density parameters, is due to the need to have a material with characteristics comparable with sediments (compact shape, density greater than water, for which descriptors as reported in Section 2.2.2 are equivalent to those used for sediments) but stressing out the density effect in the mobilisation process. The "plastics on plastics experiments" here reported aim to set a baseline for the definition of incipient motion conditions for the two types of plastics, a baseline which will be later compared to the more complex cases of remobilisation of deposited microplastics from a clastic sediment bed (see Chapter 5).
We define compact-shaped plastic grains as plastic particles without cavities or holes, for which the distance of any point laying on the grain surface from the barycentre of the grain does not vary significantly. As outlined in Section 2.1.1, we assume that the plastic particles chosen for our experiments can be treated as classical sedimentary material. Indeed, when the density range allows, the compact plastic grains are able to deposit given appropriate flow conditions, and later get into motion, as other (natural) sedimentary material. This is reflected in the large use of plastic granules in physically-scaled models, Section 2.1.2, as well as in process-oriented models for incipient motion characterisation (collected in a survey by Bettess, 1990).

4.2 Experiments

The experiments were conducted in the HML flume at the Institute of Geophysics, Polish Academy of Sciences, in Warsaw. Details on the experimental procedure are reported in Chapter 3 and Appendix C. The bed was uniformly covered with a layer of plastic particles (the used plastics are visible in Figure 4.1), levelled to a flat-bed topography. The plastic bed thickness was 8 - 10 MPs diameters to ensure uniform roughness conditions (no bed frictional regime, Armanini, 2013). The general flow conditions are reported in Table 3.5 while more detailed information on the hydraulic and hydrodynamic conditions can be found in Appendix B.

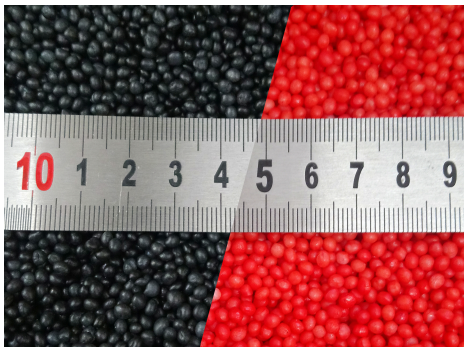

FIGURE 4.1: PA6 (black) and POM (red) particles chosen for the experiments.

4.2.1 Experimental conditions

Experiments of MPs moving from a homogeneous sediment bed composed of microplastic involved three flow conditions tested per type of plastic bed, with three repetitions for each test to ensure repeatability, and measurements of flow velocities and bed changes in three consecutive cross-sections.

Table 4.1 summarises the flow conditions for all experiments with PA6 and POM in cross-section S_3 (see Figure 3.1). The range of Reynolds number is proper for turbulent flow and the near-wall regime was transitional in all experiments with both plastics. This is reflected by flow Reynolds' $Re^* > 7500$ for all tests, and particle Reynolds' number in the range $Re^* \approx 5$ - 70, between smooth and rough wall, with the turbulent boundary layer not fully developed. The flow was subcritical, with Froude number around 0.2 and 0.3 in PA6 and POM experiments, respectively. The estimation of bed shear velocity is discussed later and results are reported in Section 4.3.1.

The dataset consists of UVP transect measurements with two 3 MHz transducers, sampling at 1.6 Hz, and videos of bed changes recorded at 4K and 60 fps. The total number of combinations amounts to 27 for each material, with spatial resolution for the velocity data of 1.1 - 1.5 mm (equal to approximately half on the plastic grain-size, 0.5 d_{MP}) across the section depending on acoustic parameters (see Appendix **??**), and raw spatial resolution for bed changes of approximately 0.1 mm depending on camera parameters. Due to the high spatio-temporal resolution of the videos, subsampling was applied, both in space and time. The spatial subsampling was applied by reducing the raw image resolution to 1/5 of the original, obtaining a grain mapped in areas of

6x6 pixels instead of 30x30, and making the whole image processing procedure to derive bed changes manageable within a commercial PC storage capacity. Temporal subsampling, on the other hand, was applied, to obtain bed changes every 5 s, for later processing and comparison to other bed conditions.

TABLE 4.1: Discharge-wise ranges for the hydraulic conditions in the plastic bed experiments for PA6 and POM particles at Section 3: discharge Q, water depth y, flow Reynolds' number Re, time-averaged bed shear velocity U^*, particle Reynolds' number Re^* and Froude number Fr. For other conditions see Appendix B.1

test	**Q** [*l/s*]	**y** [*mm*]	**Re** [-]	**U*** [*mm/s*]	**Re*** [-]	**Fr** [-]
PA6_Q1t1	1.9 ±0.02	60 ±1.0	7667	9.6	28.84	0.17
PA6_Q1t2	1.9 ±0.02	60 ±1.0	7667	10.2	30.66	0.17
PA6_Q1t3	1.9 ±0.02	60 ±1.0	7667	9.3	27.85	0.17
PA6_Q2t1	2.0 ±0.02	59 ±1.0	8000	8.7	26.24	0.18
PA6_Q2t2	2.0 ±0.02	60 ±1.0	8000	11.6	34.90	0.17
PA6_Q2t3	2.0 ±0.02	60 ±1.0	8000	10.1	30.30	0.17
PA6_Q3t1	2.1 ±0.02	61 ±1.0	8333	9.5	28.54	0.18
PA6_Q3t2	2.1 ±0.02	61 ±1.0	8333	9.3	37.81	0.18
PA6_Q3t3	2.1 ±0.02	61 ±1.0	8333	9.7	29.23	0.18
POM_Q1t1	2.3 ±0.03	45 ±1.0	9333	17.1	51.31	0.31
POM_Q1t2	2.3 ±0.03	45 ±1.0	9333	19.2	57.52	0.31
POM_Q1t3	2.3 ±0.03	45 ±1.0	9333	19.0	56.95	0.31
POM_Q2t1	2.4 ±0.03	45 ±1.0	9667	17.1	51.28	0.32
POM_Q2t2	2.4 ±0.03	45 ±1.0	9667	19.2	57.54	0.32
POM_Q2t3	2.4 ±0.03	45 ±1.0	9667	18.4	55.19	0.32
POM_Q3t1	2.5 ±0.03	45 ±1.0	10000	16.7	50.17	0.33
POM_Q3t2	2.5 ±0.03	46 ±1.0	10000	15.9	47.69	0.32
POM_Q3t3	2.5 ±0.03	44 ±1.0	10000	15.9	47.75	0.35

4.3 Experimental results

4.3.1 Bed shear velocities

To derive the near-bed flow field, the velocity data transects were measured in the lower half of the water depth, see Figure 3.3. Local shear velocities were computed from the measured transects at each data point, by fitting the vertical available measurements to the logarithmic law for near-wall velocity distribution, as from Equation 3.2.

To verify the consistency of the logarithmic velocity distribution hypothesis, we checked, for each cross-sectional time-averaged value, whether they lie in the wall region, where the log-law is considered valid (e.g. see Nezu and Rodi, 1986). For this purpose, dimensionless mean velocity U+ and elevation coordinate $Z+$ were computed by scaling the time-averaged velocity U and transects elevation z by the characteristic scales for velocity and length in the wall region (i.e. the

time-averaged shear velocity U^* and the viscous length ν/U^*).
From Figure 4.2 we can verify that our data lie in the region $Z^+ > 30$. Nezu and Rodi, 1986 indicate that the wall region, where the log-law is valid, is $30 < Z^+ < 0.2\frac{U^* y}{\nu}$. This allows us to apply the log-law assumption, with the data following a linear trend (Figure 4.2).

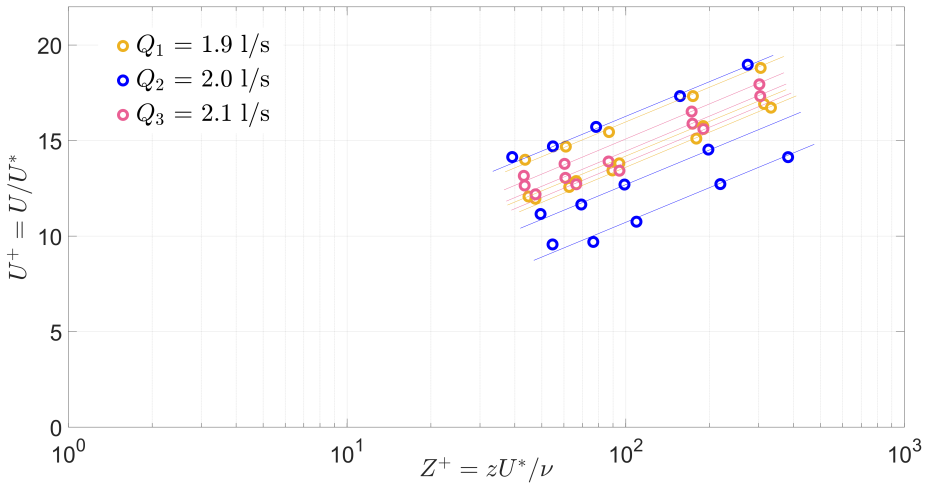

FIGURE 4.2: Distribution of mean flow velocities measured via UVP at increasing elevations from the mean bed for Section 3 in PA6 experiments (lighter plastic grains).

The estimation of the bed shear velocity was therefore carried out by fitting the data points over the available transects (5 points for PA6 and 4 points in POM bedded experiments in the direction normal to the mean bed level) to the logarithmic profile (Equation3.2). This resulted in a dense space-resolved (1 data point every 1.1 mm in the transverse direction) estimation of local shear velocities u^*, which can be used as a proxy for their probabilistic (spatial) distribution across the cross-section. Following the need for time-averaging of bed-changes data (see Section 3.3.2, definition of the Time Window - TW), velocity profiles were obtained both for the whole experiment duration, and for 5-s intervals covering the whole experiment. The former were used in most of the analysis outlined in this Chapter, while the latter served two purposes: (i) assessing that the flow was steady throughout the experiment (and therefore the temporal distribution of estimated bed shear velocity for each experimental condition followed a Gaussian curve), (ii) later comparing with clastic bed data (Chapter 5). For the first purpose, the Kolmogorov-Smirnov test for normality at significance level p = 0.05 was carried out on all plastic bed experiments, and the computed temporal bed shear velocities every 5 s resulted normally distributed.

4.3.2 Bed changes

Changes in the bed cover were mapped from images of the bed in an area covering the full flume width, extended around 0.15 m in the longitudinal direction and centred where the UVP transect was located (for a detailed methodology description refer to Chapter 3.2.1). Bed changes were estimated in time intervals corresponding to 5 s, and a series of bed changes maps was created,

including an estimate for the number of changes and their location.
The bed changes maps show an increase in mobilised particles following increasing discharge value (Figure 4.3), while the time-averaged local bed shear velocities do not seem to be a good choice for the estimation of particles' mobilisation. Indeed, as visible from Figure 4.3, variations of the same order of magnitude of the local time-averaged bed shear velocities u^* generate different responses in the bed cover changes. Such variability can be likely ascribed to near-bed turbulence, at frequencies much higher than 0.2 Hz (5 s sampling intervals).

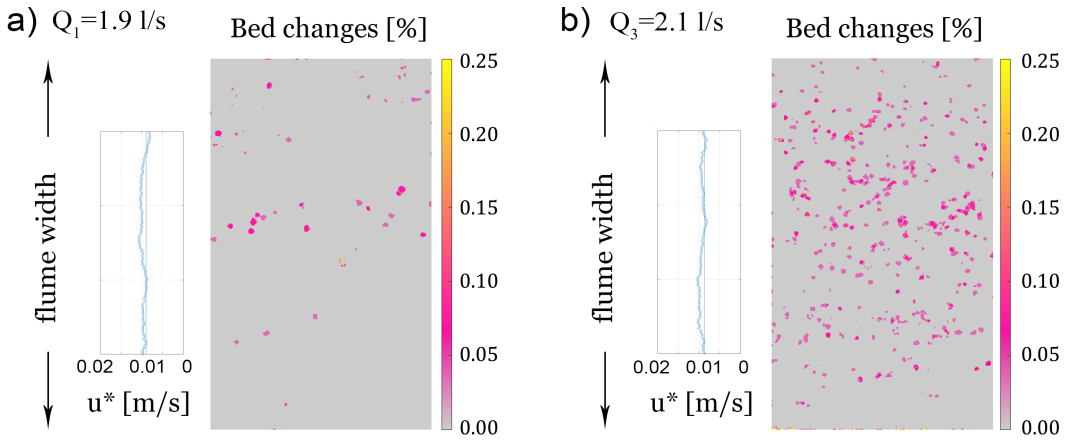

FIGURE 4.3: Example of time-averaged bed shear velocities computed from UVP measurements and cumulative bed changes for the minimum (a) and maximum (b) discharges tested on PA6 bed. The scale indicates how long in the time intervals single particles were not in their initial position (light grey meaning unchanged bed cover and yellow meaning sheet-flow occurring throughout the whole experiment).

From estimates of bed change measurements, the *bed changes frequency* can be expressed as the number of dislodged particles per unit time $\dot{n}$, vs. the total number of particles virtually available for displacement (the number of particles on the bed surface layer) N_{Tot}. This results in the expression

$$\frac{\dot{n}}{N_{Tot}} = \frac{n}{t\,N_{Tot}} \tag{4.1}$$

where n is the number of displaced particles in a time window, with $\dot{n}$ its temporal derivative, N_{Tot} is the total number of particles, which in the case of homogeneous bed amounts to 100% of the bed cover, and t is the duration of the time window in seconds.
The estimation of N_{Tot} considers the area covered in the analysed footage A (the total area of the Region of Interest ROI), and treats the bed surface particles as spheres, accounting also for a surface packing density, $\phi = 0.75$, indicating how much of the imaged area is covered by particles directly exposed to the flow. The total surface packing density ϕ was estimated as an average of five values obtained in sub-areas measuring 8 by 8 particles (approximately 50px x 50px in

reduced resolution). This gives an expression for N_{Tot} in the form

$$N_{Tot} = \frac{A \cdot \phi}{\frac{\pi}{4} d_{MP}^2} \tag{4.2}$$

The same formulation for bed changes estimation was used by Shvidchenko (2000 and 2000) and named *intensity of sediment motion,* $\boldsymbol{I}$ to characterise his incipient motion regime, and we adopt the same threshold he set at $\dot{n}/N = 10^{-4} s^{-1}$.

4.3.3 Threshold conditions

In the experimental runs, the intensity of bedload transport was rather small, lower than 0.01 particles/s in the observed area, and we assume that the highest discharge tested corresponds to conditions of *weak motion* as defined by Chiew and Parker (1994). Following the classical approach devised by Shields (1936), the observed conditions of the PA6 (orange) and POM (pink) tests are plotted (Figure 4.6). For both plastics a linear pattern is identifiable, as the time-cross-sectional averaged Shields' number and particle (MP) Reynolds number are both derived from velocity measurements, as was done in the plotted literature results (Wolman and Brush, 1961; Neill, 1967; Everts, 1973; Petit, 1994; Keshavarzy and Ball, 1999). When looking at the local values (densely, 1.1 mm, space-resolved across the flume width, with u^* computed every 5 s), they span a very wide range for Shields' numbers $\theta_i = 10^{-9} - 4 \cdot 10^{-2}$, with the highest values corresponding to approximately the maximum u^* observed for time-cross-sectional averaged value (reported in Figure 4.4 for both MPs).

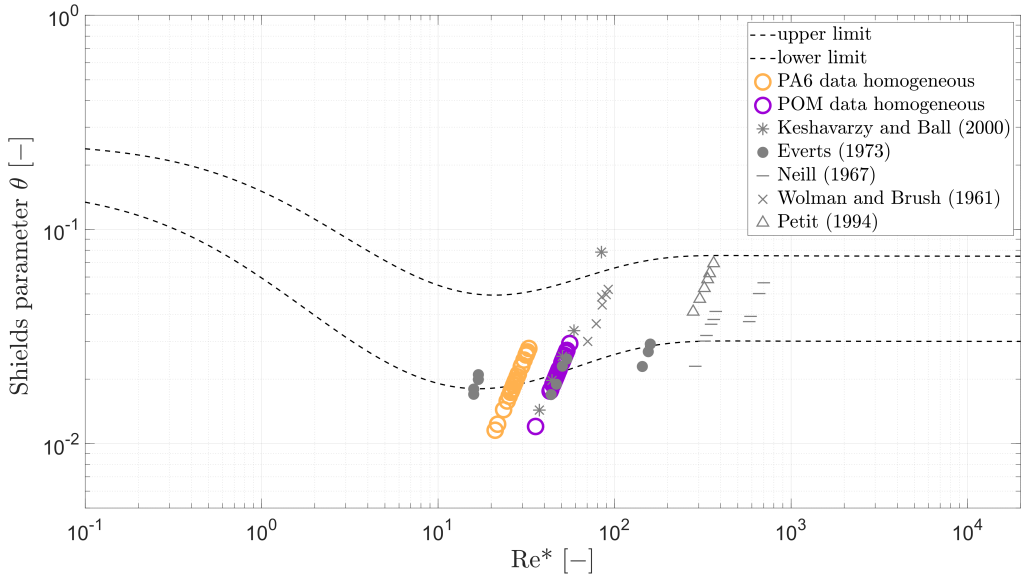

FIGURE 4.4: Experimental data points for PA6 (orange) and POM (pink) bedded tests versus literature data derived with similar methodology. The Shields' curve range (dashed) follows the relation proposed by Paphitis, 2001.

The higher density of POM appears to shift the experimental results to the right, towards higher particle Reynolds' numbers, while the variability among tests for the time-space averaged values of the Shields' parameter does not appear to be significantly affected. Notably, in our specific case, the diameter d_{MP} and density ρ_{MP} of the two materials are related (see Table 3.2), in that for each material (and density) we have one diameter value, and this has a role in the POM shift to higher particle's Reynolds number. To resolve this relation, we discuss the mobility threshold of particles' with reference to their submerged weight, in that higher bed shear velocities are needed to set into motion heavier particles, conditions which hold for the transitional regime ($Re^* \approx 20$ – 70) we conducted the tests (see Figure 4.5).

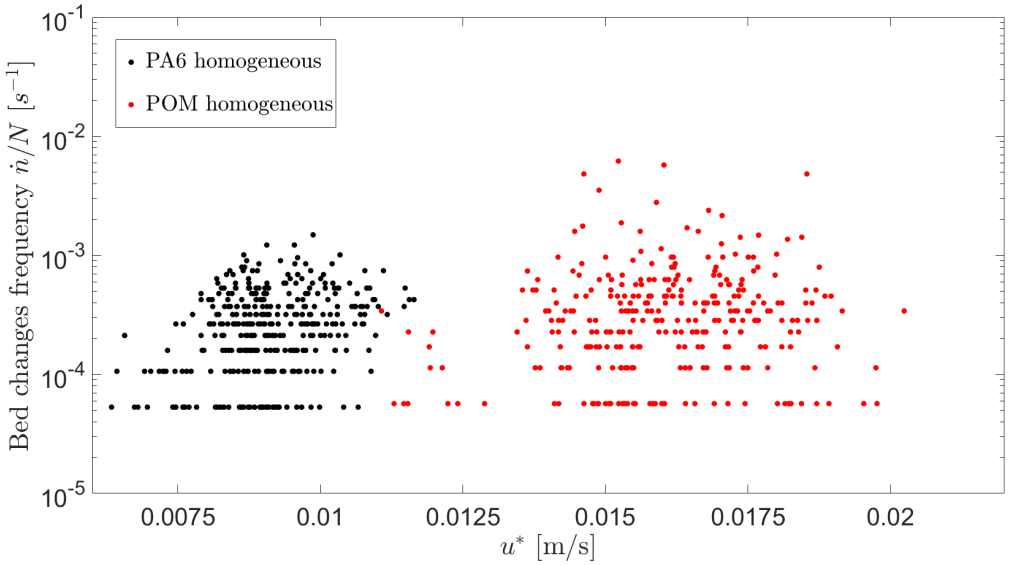

FIGURE 4.5: Proxy distribution of experimental data points for PA6 (black) and POM (red) bed changes frequency $\dot{n}/N$ vs bed shear velocities u^*, computed for time intervals of 5 s for all experiments. The variability of bed shear velocities is evident for both plastic materials.

Adapting a methodology widely used in structural engineering for the identification of limit states (*EN-1990:2002 Eurocode 0, Basis of Structural Design.* 2001), the proposed derivation of the threshold conditions for the two plastics is based on the measured quantities, i.e. bed shear velocity and bed changes. *Limit states* are defined, in structural engineering, as conditions at which the behaviour of an element of the structure change: i.e. the element behaviour shifts from (i) elastic to plastic, showing irreversible deformation, (ii) plastic to failure, when it breaks creeps or breaks showing severe cracks and permanent damage. Translating this concept to sediment transport, possible limit states are: (i) the onset of motion, at which a bed behaviour under the hydrodynamic forcing changes from fixed to mobile, with few particles moving as bedload, (ii) the onset of entrainment (into suspended load), at which bedload particles are detaching more and more from the near-bed region, and getting transported as suspended load, (iii) the onset of bed creeping, when the bed uppermost layer, interacting with the flow, gets mobilised en-masse,

and moves as a granular fluid.
A *limit state* requires the identification of a threshold, which for our purposes was chosen at bed changes frequency $\dot{n}/N = 10^{-4}s^{-1}$, for which the corresponding shear stress is derived from a sufficiently large number of tests. It is referred to as *semi-probabilistic approach*, since the *limit state* value is not defined in probabilistic terms, but the stress corresponding to it is.
In our *semi-probabilistic* method, the chosen value of threshold bed changes frequency ($10^{-4}s^{-1}$) was used to identify the associated *threshold probability* in the measured distribution ($P_{cr}|_{\frac{\dot{n}}{N}=10^{-4}}$). Such probability was then adopted to compute the associated threshold bed shear velocities ($u^*|_{P_{cr}}$) from the measured bed shear velocities distribution.
The results are reported in Table 4.3, where, considering the probabilities associated with the chosen threshold for bed changes frequency, we can see that approximately $1/4$ of our measurements for both bed materials are below such threshold. This represents around 100 data points for each homogeneous bed (as can be also seen from Figure 4.5).

TABLE 4.2: PA6 and POM threshold conditions on homogeneous bed: $\frac{\dot{n}}{N}|_{cr}$ is the chosen (threshold) for bed changes frequency, $P_{cr}|_{\dot{n}/N}$ is its associated probability of occurrence, u^*_{cr} corresponds to $u^*|P_{cr}$ identified by the chosen threshold for frequency of bed changes $P_{cr}|_{\dot{n}/N}$, and $\tau_{0,cr}$ was computed for the obtained values of threshold bed shear velocities u^*_{cr}. For completeness, also the particle's Reynolds' number Re^* and threshold Shields' parameters θ_{cr} are shown.

MP type	$\frac{\dot{\mathbf{n}}}{\mathbf{N}}\|_{\mathbf{cr}}$ $[s^{-1}]$	$\mathbf{P_{cr}}\|_{\dot{\mathbf{n}}/\mathbf{N}}$	$\mathbf{u^*_{cr}} = \mathbf{u^*}\|_{\mathbf{P_{cr}}}$ $[m/s]$	$\tau_{\mathbf{0,cr}}$ $[Pa]$	$\mathbf{Re}^*$ [-]	$\theta_{\mathbf{cr}}$ [-]
PA6	10^{-4}	0.264	0.0086	0.0737	24.90	0.0173
POM	10^{-4}	0.256	0.0150	0.2253	45.03	0.0170

4.4 Discussion

The linear trend in the Shields' diagram for measured data (Figure 4.4) is mostly evident and strictly linked, as already discussed, to the measurement method adopted, in which measured velocities are used to compute both particles' Reynolds number and Shields' mobility number. The shift for the heavier microplastic grains to higher particles' Reynolds number is assumed to be directly linked to the different specific weights (and density, since both particles have approximately the same dimensions), leading to heavier particles being more stable than lighter ones on beds with similar geometric roughness. The influence of grains' weight translates, for natural sediments, in the Rouse profile (Rouse, 1940). Grains weight also causes *selective transport* for a clastic sediment mixture, where lighter/finer fractions are more easily transported than heavier/coarser ones.
Looking at Figure 4.5, we have a wide variability of bed shear velocities, for each *bed changes frequency* observed. The *semi-probabilistic approach* adopted allows us to overcome the "overlapping problem", and identify a threshold linked to the probability of occurrence of the chosen *bed change frequency*. The threshold identified lies below the Shields' curve limit identified by Paphitis 2001 (see Figure 4.6, which is consistent with other visual-based estimations of incipient

motion conditions on homogeneous beds (Ockelford and Yager, 2022). Moreover, the threshold was not extrapolated from observations, since it lies within our data range, and the assumption of *weak movement* (as described by Kramer, 1935 and Chiew and Parker, 1994), is considered correct.

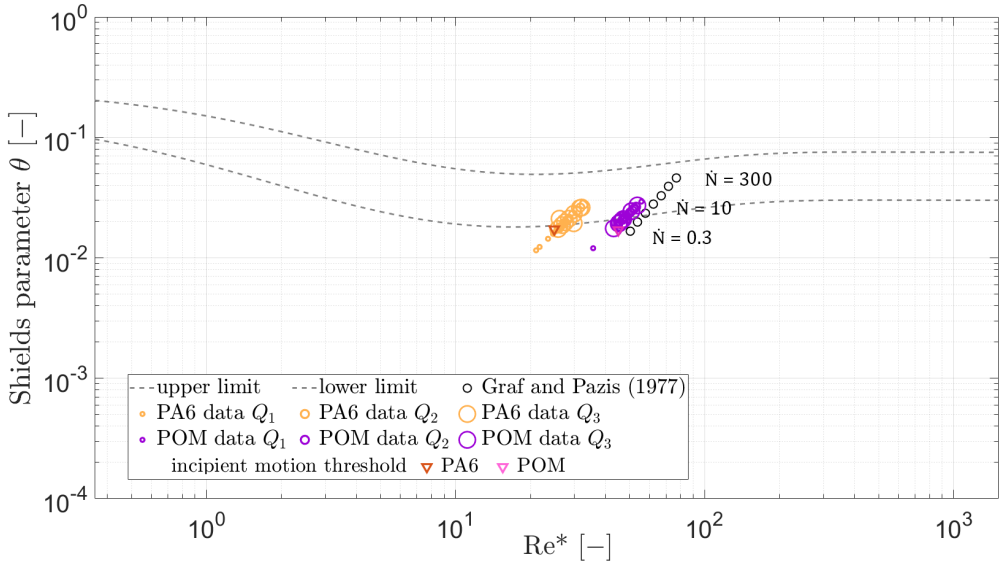

FIGURE 4.6: Experimental data points for PA6 and POM bedded tests versus Graf and Pazis, 1977 data for other plastics homogeneous bed tests. The Shields' curve range (dashed) follows the relations by Paphitis, 2001. The particle Reynolds number and Shields' number calculated for all tests for the two plastics are sorted by discharge (size of symbols). Downward triangles indicate the incipient motion threshold identified with the *semi-probabilistic approach* proposed.

Figure 4.6 shows our measured Shields and particle's Reynolds' number vs. literature data by Graf and Pazis (1977) derived for lightweight (plastic) particles with similar density to POM and similar diameter (ρ_s = 1.41 kg/m^3 and d_s = 3.02 mm), where the increasing values for critical Shields' and Reynolds' numbers correspond to an increase in the number of mobilised particles per unit time $\dot{N}$, in the range 0.3 - 300 particles/s. Our data, differently from Graf and Pazis, 1977, are much more overlapped, and the identification of conditions for the different *bed changes frequencies* is not straightforward from mean flow conditions. This can be ascribed to two factors: (i) the Graf and Pazis's counting method (1977) looked at transects, while the here proposed $\dot{n}$ is estimated over an area, (ii) the time resolution of our measurements (5 s averages) is much higher than Graf and Pazis. Both choices generate a more variable signal, for which no unique value is identifiable for the different *bed changes frequencies*. As for the shift towards higher values of Re^* for literature data versus our heavier particles (POM characteristics are comparable to those of the plastic sediments in Graf and Pazis, 1977), this is likely due to the different submergence the plastics had. Indeed for the literature data, the flow depth was around 45 cm, while in our case, POM experiments had a depth one order of magnitude smaller.

TABLE 4.3: Plastic sediments data, and experimantal conditions, from Graf and Pazis, 1977.

ρ_s $[g\ cm^{-1}]$	**d** $[mm]$	**U** $[m/s]$	**y** $[cm]$
1.41	3.02	13.4	38 - 54

4.5 Summary

Incipient motion patterns for microplastic grains detaching from a homogeneous bed are aligned, as expected and anticipated in Section 2.1.2 with past research on incipient motion for natural (and artificial) granular materials. The variability of incipient motion conditions for our experiments reflects the variability of past experiments around incipient motion. The conditions for this first set of experiments correspond to homogeneous bed conditions, for which literature provides a plethora of references. Still, given the vicinity to Shields' curve limit, we can see how Shields' diagram is a valid approximation for baseline conditions for microplastics motion, where by baseline we mean "homogeneous bed conditions".

We observed that the range of estimated local time-averaged bed shear velocities across the section does not directly correlate with increasing flow conditions (Figure 4.3), which instead seem to have an influence on the percentage of bed changes. This might be related to the lower density of the particles, which makes them more sensitive to deviations from the mean bed shear velocity. To solve this, the analysis was carried out at a higher temporal resolution, computing every 5 s time-averaged bed changes and bed shear velocities, which were used for the estimation of threshold conditions for the two types of homogeneous beds via a *semi-probabilistic approach*. The proposed methodology relies on only two measured quantities, namely bed changes per unit time and bed shear velocities, and does not require synchronisation of measurements, which might be problematic and costly.

Chapter 5

Remobilisation of plastic particles from a clastic bed

"In every outthrust headland, in every curving beach,
in every grain of sand there is the story of the earth."

Rachel Carson, 1950

5.1 Introduction

Natural sedimentary material constituting the solid boundary of rivers and streams consists predominantly of siliciclastic particles, with quartz among the most abundant minerals (the average specific density of quartz grains being 2.65 g/cm^3). Therefore, the river bed composition has been described mostly in terms of the granulometric distribution of the (clastic) sediments composing its uppermost layer. Variations in density and shape are not usually addressed when approaching the problem of sediment mobilisation and transport, thus leading to a parameterisation of sedimentary processes based solely on the grain characteristic grain-size (see Sections 2.2.2.3 and 2.2.2.4). As outlined by Viparelli et al. (2015), experiments on the effect of relative particle size outnumber by a few orders of magnitude those for the effect of the relative density of particles. Indeed, the dominant parameter for the erosion and deposition of natural clastic grains has traditionally been considered the dimension, usually synthesised either into representative classes or into a representative diameter: e.g. median (d_{50}) or equivalent (d_{eq}) diameter.
Transport models are built upon the governing equations of fluid motions (conservation of mass, momentum and/or energy) coupled with sediment continuity in the *active layer* (the bed surface layer from which particles are mobilised and redeposited). The sediment continuity equation (Exner equation) describes the feedback between variations in bed sediment flux and bed degradation/aggradation in time, related to erosional (Φ_E) and depositional (Φ_D) processes, and takes

the form

$$\Phi_E - \Phi_D = \frac{\partial q_S}{\partial x} = -\frac{\partial z_b}{\partial t} \tag{5.1}$$

where q_S is the solid discharge per unit width and z_b is the bed surface elevation. It resolves the mass balance within the control volume (i.e. a portion of the riverbed) and the fluxes at its boundary, with the latter calculated by erosion/deposition rates (to be converted into mass flux, i.e., namely the sediment transport formula) mostly and uniquely linked to bed shear stress values. The estimation of mass flux q_S takes the form of sediment transport formulae, which, in many instances, adopt the concept of threshold to distinguish between no-transport and transport (e.g. Meyer-Peter and Müller, 1948; Yalin, 1963 and Parker et al., 1982). This general (deterministic) approach stems from the pioneering investigations of Shields (1936) which set a way to identify a threshold condition. Therefore, a good estimate of the threshold values triggering transport is essential for any estimation of transport, sediment budgeting, or, more generally, fluvial engineering application.

The presence of new sedimentary material (i.e. plastic particles) has the potential to shuffle this well-sorted (and widely tested) deck of tools. Moving one step farther from the homogeneous bed model, in this Chapter we address the remobilisation behaviour of plastic grains on two natural (clastic) sediment bed configurations, uniform gravel and uniform sand, moving closer to real conditions.

Variations in the coarse content of the *active layer*, the bed uppermost layer interacting with the flow by sediment transport, occur naturally in rivers due to *selective transport* processes, i.e. the transport of different size fractions, where finer particles have higher mobility than coarser ones. When the content of fines in the bed decreases due to a (temporary) increase in the *transport capacity* (or decrease in fine *sediment supply*), a coarsening of the bed surface layer occurs, which is named *armouring*. The *armoured layer* protects the lower layers from erosion, (temporally) reducing the exchange of solid fluxes between bed and current (Armanini, 2018).

By contrast, the higher the geometric roughness of the (*armoured*) bed surface, the more single particles can fit depressions, being, then, less exposed to the flow-induced shear. At the same time, higher bed roughness modifies the near-bed velocity field shifting the turbulent regime towards rough wall conditions, and exposing particles to near-wall turbulence.

The density, affecting the grains' weight, plays a role in the equilibrium of single particles: gravity force is considered as stabilising, and the lower the density, the lower its contribution to single grains' stability. Gravity force is also scaling the magnitude of the other stabilising contribution, the inter-gain friction exerted at the boundary. Under the same hydrodynamic forcing, the lower the density, the less stable a single grain is.

In natural conditions, the material transported as bedload is the same as the bed-forming material, for continuous exchange happens at the bed interface. When we consider plastics entering this delicate balance, a lot of new questions arise regarding the process of remobilisation and entrainment, as well as transport dynamics. The *sediment analogy* framework has been used, in a

first instance, to model MPs behaviour. This framework models the microplastic remobilisation with the same model and approaches used in sediment transport research, treating the microplastics as sediments, combining into calibration/adaptation parameters (e.g. a *hiding/exposure coefficient*) the variability due to MPs' various shapes. The advantages of using the same formulation for both plastic and natural clastic sediments are evident, as a direct translation means not only faster progress in building knowledge around MPs, but also a potential improvement in the robustness of the well-established models for sediment transport.
Making therefore the *sediment analogy* framework a standard in MPs transport research, the two most relevant studies on remobilisation of MPs used one-particle observation to derive the critical threshold (Waldschläger and Schüttrumpf, 2019b and Goral et al., 2023a). Yu et al. (2022 and 2023), instead, observed remobilisation in a row of particles oriented transversely to the main flow direction. They identify the threshold conditions when 50% of the material is moved. These studies used an extremely controlled positioning of particles, which is very far from what occurs in natural conditions.
As for the transport dynamics, Lofty et al. (2023) investigated saltation and trajectories of MPs moving as bedload, and did not find significant differences between clastic and plastic sediments' saltation kinematics. Notably, the particles chosen by the authors had mostly compact, spherical shape, for which no effect of the reorientation during jumps can be observed.
A key aspect to take into account when dealing with microplastics on the riverbed, is their availability (which might be linked to a "plastic *sediment supply*"). In the case of natural sediments, indeed, Bong et al. (2016), observed an increased critical velocity for thin sediment deposits whereas the effect vanished by increasing the thickness of the mobile sediment layer. Notably, their proposed relation applies to both fixed and loosed bed cases. While the conditions in Bong et al. (2016) are unlikely to occur for *plastic sediments* in fluvial environments, the presence of sparsely distributed particles and fragments on a streambed is (unfortunately) not unusual, and the amount of plastic mobile material might have an impact on the threshold conditions for its mobilisation. Therefore, after investigating the case of a homogeneous bed at the onset of motion, a second set of experiments aimed to investigate the role of inhomogeneity between bed and mobile particles. The definition of a remobilisation threshold for this second case needs a modification, compared to the one provided in Chapter 4, as, in this case, we assume a major role of bed surface-available MPs on their mobility.

5.2 Experiments

The experiments were performed with a slightly different setup from the one adopted for homogeneous bed tests (see Section 3.2.2 and Appendix C.2). The clastic sediment layer was prepared with the aid of non-slip gum mats to reduce the volume of clastic sediments needed (see Section 3.2.2.1). The gravel and sandy bed were levelled manually up to a thickness of around 3 - 4 cm, and the flume was filled with water up to the needed depth. The particles

were seeded manually, in diagonal lines with an oscillatory motion, spreading evenly on the bed surface (see Figure C.3) and allowed to deposit at low flow (see Section 3.2.2). Experiments on clastic bed differ in measuring apparatus, since another UVP device was used, projecting the acoustic beam from the water surface (instead of the wall) to eventually characterise the vertical profile of the flow velocity with finer resolution (i.e. smaller cell size). The experiments were performed at fixed discharge and increasing concentrations (see Chapter 3, Table 3.6), resulting in a dataset consisting of videos of bed changes and UVP measurements in the same cross-section.

FIGURE 5.1: Example of plastic PA6 particles on flat gravel (left) and sand (right) bed.

5.2.1 Experimental conditions

Experiments of microplastics moving on a clastic bed involved five increasing concentrations of MPs content in the uppermost bed layer, spanning from 0.5 - 1.0%. For each MPs surface concentration, three flow conditions were run, with discharges in the range 1.9 - 2.1 l/s (PA6) and 2.5 - 2.7 l/s (POM) for tests on gravel bed, and 1.2 - 1.4 l/s (PA6) and 2.1 - 2.3 l/s (POM) for tests on sandy bed. Tables 5.1 - 5.4 contain more detailed information about the flow conditions in the different tests. As in the homogeneous bed tests, the near-bed conditions were transitional between smooth and rough wall, and the flow was subcritical.

The velocity profiles were recorded at two verticals for each section, with transducers symmetrically placed at 7 cm from the wall and tilted 70° from the normal to the bed (for a side view of the setup, see C.4). The dataset consists of 2 UVP profiles measured with 4 MHz transducers, sampling at 16 Hz with a spatial resolution of 0.91 mm, and videos of bed cover changes in 4K at 60 fps.

The UVP data were used to estimate the bed shear velocity, by fitting the lower half of the measured profiles (up to approximately 1.5 - 2 cm distance from the mean bed, depending on the flow conditions) to the log-law (see Section 3.3.1 for further details). Image data, following the pre-processing steps outlined in Section 3.3.2, served to estimate the number of MPs mobilised. Again, both spatial and temporal averaging were applied, with the same values used for homogeneous bed (i.e. resolution reduced to 1/5 of original image resolution, and estimating bed changes in time windows of 5 s).

TABLE 5.1: Discharge-wise ranges for the hydraulic conditions in the gravel bed experiments for PA6 particles: discharge Q, water depth y, flow Reynolds' number Re, time-averaged bed shear velocity U^*, bed Reynolds' number Re^* and Froude number Fr. For other conditions see Appendix B.1

test	**Q** [*l/s*]	**y** [*mm*]	**Re** [-]	**U*** [*mm/s*]	**Re**$^*_{\mathbf{MP}}$ [-]	**Fr** [-]
PA6g_c1Q1t1	1.9 ±0.02	47 ±1.0	7667	8.4	25.26	0.24
PA6g_c1Q1t2	1.9 ±0.02	47 ±1.0	7667	6.2	18.28	0.24
PA6g_c1Q2t1	2.0 ±0.02	48 ±1.0	8000	7.8	23.40	0.25
PA6g_c1Q2t2	2.0 ±0.02	48 ±1.0	8000	8.7	25.95	0.25
PA6g_c1Q3t1	2.1 ±0.02	47 ±1.0	8333	7.8	23.43	0.26
PA6g_c1Q3t2	2.1 ±0.02	47 ±1.0	8333	7.8	23.38	0.26
PA6g_c2Q1t1	1.9 ±0.02	47 ±1.0	7667	8.8	26.31	0.24
PA6g_c2Q1t2	1.9 ±0.02	47 ±1.0	7667	8.1	24.19	0.24
PA6g_c2Q2t1	2.0 ±0.02	48 ±1.0	8000	7.5	22.47	0.25
PA6g_c2Q2t2	2.0 ±0.02	48 ±1.0	8000	7.0	20.80	0.25
PA6g_c2Q3t1	2.1 ±0.02	47 ±1.0	8333	8.2	24.55	0.26
PA6g_c2Q3t2	2.1 ±0.02	47 ±1.0	8333	8.6	25.46	0.26
PA6g_c3Q1t1	1.9 ±0.02	47 ±1.0	7667	7.9	23.60	0.24
PA6g_c3Q1t2	1.9 ±0.02	47 ±1.0	7667	7.8	23.25	0.24
PA6g_c3Q2t1	2.0 ±0.02	48 ±1.0	8000	7.3	21.93	0.25
PA6g_c3Q2t2	2.0 ±0.02	48 ±1.0	8000	6.9	20.60	0.25
PA6g_c3Q3t1	2.1 ±0.02	47 ±1.0	8333	7.2	21.59	0.26
PA6g_c3Q3t2	2.1 ±0.02	47 ±1.0	8333	6.6	19.63	0.26
PA6g_c4Q1t1	1.9 ±0.02	47 ±1.0	7667	8.0	23.96	0.24
PA6g_c4Q1t2	1.9 ±0.02	47 ±1.0	7667	6.9	20.82	0.24
PA6g_c4Q2t1	2.0 ±0.02	48 ±1.0	8000	5.8	17.29	0.25
PA6g_c4Q2t2	2.0 ±0.02	48 ±1.0	8000	6.4	19.28	0.25
PA6g_c4Q3t1	2.1 ±0.02	47 ±1.0	8333	7.3	21.63	0.26
PA6g_c4Q3t2	2.1 ±0.02	47 ±1.0	8333	6.5	19.65	0.26
PA6g_c5Q1t1	1.9 ±0.02	47 ±1.0	7667	7.1	21.07	0.24
PA6g_c5Q1t2	1.9 ±0.02	47 ±1.0	7667	6.2	18.48	0.24
PA6g_c5Q2t1	2.0 ±0.02	48 ±1.0	8000	8.8	26.45	0.25
PA6g_c5Q2t2	2.0 ±0.02	48 ±1.0	8000	7.1	21.20	0.25
PA6g_c5Q3t1	2.1 ±0.02	47 ±1.0	8333	9.2	27.53	0.26
PA6g_c5Q3t2	2.1 ±0.02	47 ±1.0	8333	8.6	25.73	0.26

TABLE 5.2: Discharge-wise ranges for the hydraulic conditions in the gravel bed experiments for POM particles: discharge Q, water depth y, flow Reynolds' number Re, time-averaged bed shear velocity U^*, bed Reynolds' number Re^* and Froude number Fr. For other conditions see Appendix B.1

test	**Q** [*l/s*]	**y** [*mm*]	**Re** [-]	**U*** [*mm/s*]	**Re**$^*_{\mathbf{MP}}$ [-]	**Fr** [-]
POMg_c1Q1t1	2.5 ±0.02	48 ±1.0	10000	8.3	24.88	0.31
POMg_c1Q1t2	2.5 ±0.02	48 ±1.0	10000	8.8	26.31	0.31
POMg_c1Q2t1	2.6 ±0.02	49 ±1.0	10333	10.7	32.09	0.30
POMg_c1Q2t2	2.6 ±0.02	49 ±1.0	10333	12.0	35.96	0.30
POMg_c1Q3t1	2.7 ±0.02	47 ±1.0	10667	11.8	35.38	0.33
POMg_c1Q3t2	2.7 ±0.02	47 ±1.0	10667	11.2	33.36	0.33
POMg_c2Q1t1	2.5 ±0.02	48 ±1.0	10000	8.5	25.42	0.31
POMg_c2Q1t2	2.5 ±0.02	48 ±1.0	10000	8.4	25.17	0.31
POMg_c2Q2t1	2.6 ±0.02	49 ±1.0	10333	11.3	33.76	0.30
POMg_c2Q2t2	2.6 ±0.02	49 ±1.0	10333	10.7	32.11	0.30
POMg_c2Q3t1	2.7 ±0.02	47 ±1.0	10667	11.5	34.36	0.33
POMg_c2Q3t2	2.7 ±0.02	47 ±1.0	10667	9.8	29.45	0.33
POMg_c3Q1t1	2.5 ±0.02	48 ±1.0	10000	9.0	26.94	0.31
POMg_c3Q1t2	2.5 ±0.02	48 ±1.0	10000	9.6	28.94	0.31
POMg_c3Q2t1	2.6 ±0.02	49 ±1.0	10333	11.0	33.07	0.30
POMg_c3Q2t2	2.6 ±0.02	49 ±1.0	10333	10.0	30.07	0.30
POMg_c3Q3t1	2.7 ±0.02	47 ±1.0	10667	10.8	32.50	0.33
POMg_c3Q3t2	2.7 ±0.02	47 ±1.0	10667	10.7	32.19	0.33
POMg_c4Q1t1	2.5 ±0.02	48 ±1.0	10000	8.9	26.71	0.31
POMg_c4Q1t2	2.5 ±0.02	48 ±1.0	10000	8.4	25.20	0.31
POMg_c4Q2t1	2.6 ±0.02	49 ±1.0	10333	9.7	29.22	0.30
POMg_c4Q2t2	2.6 ±0.02	49 ±1.0	10333	9.4	28.09	0.30
POMg_c4Q3t1	2.7 ±0.02	47 ±1.0	10667	12.3	36.98	0.33
POMg_c4Q3t2	2.7 ±0.02	47 ±1.0	10667	11.5	34.41	0.33
POMg_c5Q1t1	2.5 ±0.02	48 ±1.0	10000	7.7	23.23	0.31
POMg_c5Q1t2	2.5 ±0.02	48 ±1.0	10000	8.1	24.28	0.31
POMg_c5Q2t1	2.6 ±0.02	49 ±1.0	10333	10.4	31.05	0.30
POMg_c5Q2t2	2.6 ±0.02	49 ±1.0	10333	9.5	28.60	0.30
POMg_c5Q3t1	2.7 ±0.02	47 ±1.0	10667	11.1	33.36	0.33
POMg_c5Q3t2	2.7 ±0.02	47 ±1.0	10667	11.0	33.14	0.33

TABLE 5.3: Discharge-wise ranges for the hydraulic conditions in the sand bed experiments for PA6 particles: discharge Q, water depth y, flow Reynolds' number Re, time-averaged bed shear velocity U^*, bed Reynolds' number Re^* and Froude number Fr. For other conditions see Appendix B.1

test	**Q** [*l/s*]	**y** [*mm*]	**Re** [-]	**U*** [*mm/s*]	**Re**$^*_{\mathbf{MP}}$ [-]	**Fr** [-]
PA6s_c1Q1t1	1.2 ±0.02	65 ±1.0	5000	1.7	5.04	0.09
PA6s_c1Q1t2	1.2 ±0.02	65 ±1.0	5000	1.2	3.68	0.09
PA6s_c1Q2t1	1.3 ±0.02	66 ±1.0	5333	1.5	4.49	0.10
PA6s_c1Q2t2	1.3 ±0.02	66 ±1.0	5333	1.3	3.78	0.10
PA6s_c1Q3t1	1.4 ±0.02	67 ±1.0	5667	2.3	7.05	0.11
PA6s_c1Q3t2	1.4 ±0.02	67 ±1.0	5667	1.3	3.92	0.11
PA6s_c2Q1t1	1.2 ±0.02	65 ±1.0	5000	1.7	5.22	0.09
PA6s_c2Q1t2	1.2 ±0.02	65 ±1.0	5000	1.3	3.89	0.09
PA6s_c2Q2t1	1.3 ±0.02	66 ±1.0	5333	2.0	5.85	0.10
PA6s_c2Q2t2	1.3 ±0.02	66 ±1.0	5333	1.2	3.73	0.10
PA6s_c2Q3t1	1.4 ±0.02	67 ±1.0	5667	2.1	6.41	0.11
PA6s_c2Q3t2	1.4 ±0.02	67 ±1.0	5667	1.7	4.98	0.11
PA6s_c3Q1t1	1.2 ±0.02	65 ±1.0	5000	1.6	4.85	0.09
PA6s_c3Q1t2	1.2 ±0.02	65 ±1.0	5000	1.2	3.67	0.09
PA6s_c3Q2t1	1.3 ±0.02	66 ±1.0	5333	2.1	6.35	0.10
PA6s_c3Q2t2	1.3 ±0.02	66 ±1.0	5333	1.6	4.92	0.10
PA6s_c3Q3t1	1.4 ±0.02	67 ±1.0	5667	2.3	6.77	0.11
PA6s_c3Q3t2	1.4 ±0.02	67 ±1.0	5667	1.4	4.26	0.11
PA6s_c4Q1t1	1.2 ±0.02	65 ±1.0	5000	1.8	5.26	0.09
PA6s_c4Q1t2	1.2 ±0.02	65 ±1.0	5000	1.0	3.12	0.09
PA6s_c4Q2t1	1.3 ±0.02	66 ±1.0	5333	2.3	6.95	0.10
PA6s_c4Q2t2	1.3 ±0.02	66 ±1.0	5333	1.8	5.47	0.10
PA6s_c4Q3t1	1.4 ±0.02	67 ±1.0	5667	2.3	6.94	0.11
PA6s_c4Q3t2	1.4 ±0.02	67 ±1.0	5667	1.7	5.07	0.11
PA6s_c5Q1t1	1.2 ±0.02	65 ±1.0	5000	1.7	5.18	0.09
PA6s_c5Q1t2	1.2 ±0.02	65 ±1.0	5000	1.1	3.39	0.09
PA6s_c5Q2t1	1.3 ±0.02	66 ±1.0	5333	2.5	7.48	0.10
PA6s_c5Q2t2	1.3 ±0.02	66 ±1.0	5333	1.6	4.87	0.10
PA6s_c5Q3t1	1.4 ±0.02	67 ±1.0	5667	2.4	7.11	0.11
PA6s_c5Q3t2	1.4 ±0.02	67 ±1.0	5667	1.4	4.30	0.11

TABLE 5.4: Discharge-wise ranges for the hydraulic conditions in the sand bed experiments for POM particles: discharge Q, water depth y, flow Reynolds' number Re, time-averaged bed shear velocity U^*, bed Reynolds' number Re^* and Froude number Fr. For other conditions see Appendix B.1

test	**Q** [*l/s*]	**y** [*mm*]	**Re** [-]	**U*** [*mm/s*]	**Re**$^*_{\mathbf{MP}}$ [-]	**Fr** [-]
POMs_c1Q1t1	2.1 ±0.02	72 ±1.0	8667	6.2	18.67	0.14
POMs_c1Q1t2	2.1 ±0.02	72 ±1.0	8667	6.1	18.24	0.14
POMs_c1Q2t1	2.2 ±0.02	73 ±1.0	9000	6.2	18.51	0.15
POMs_c1Q2t2	2.2 ±0.02	73 ±1.0	9000	7.1	21.38	0.15
POMs_c1Q3t1	2.3 ±0.02	74 ±1.0	9333	5.9	17.74	0.15
POMs_c1Q3t2	2.3 ±0.02	74 ±1.0	9333	-	-	0.15
POMs_c2Q1t1	2.1 ±0.02	72 ±1.0	8667	6.4	19.16	0.14
POMs_c2Q1t2	2.1 ±0.02	72 ±1.0	8667	5.6	16.78	0.14
POMs_c2Q2t1	2.2 ±0.02	73 ±1.0	9000	7.1	21.30	0.15
POMs_c2Q2t2	2.2 ±0.02	73 ±1.0	9000	6.7	20.21	0.15
POMs_c2Q3t1	2.3 ±0.02	74 ±1.0	9333	6.1	18.37	0.15
POMs_c2Q3t2	2.3 ±0.02	74 ±1.0	9333	5.6	16.85	0.15
POMs_c3Q1t1	2.1 ±0.02	72 ±1.0	8667	6.2	18.49	0.14
POMs_c3Q1t2	2.1 ±0.02	72 ±1.0	8667	5.6	16.86	0.14
POMs_c3Q2t1	2.2 ±0.02	73 ±1.0	9000	6.5	19.38	0.15
POMs_c3Q2t2	2.2 ±0.02	73 ±1.0	9000	6.6	19.69	0.15
POMs_c3Q3t1	2.3 ±0.02	74 ±1.0	9333	5.7	17.08	0.15
POMs_c3Q3t2	2.3 ±0.02	74 ±1.0	9333	5.3	15.87	0.15
POMs_c4Q1t1	2.1 ±0.02	72 ±1.0	8667	6.0	17.85	0.14
POMs_c4Q1t2	2.1 ±0.02	72 ±1.0	8667	4.8	14.36	0.14
POMs_c4Q2t1	2.2 ±0.02	73 ±1.0	9000	7.1	21.35	0.15
POMs_c4Q2t2	2.2 ±0.02	73 ±1.0	9000	6.5	19.63	0.15
POMs_c4Q3t1	2.3 ±0.02	74 ±1.0	9333	6.0	17.90	0.15
POMs_c4Q3t2	2.3 ±0.02	74 ±1.0	9333	4.4	13.21	0.15
POMs_c5Q1t1	2.1 ±0.02	72 ±1.0	8667	6.3	19.00	0.14
POMs_c5Q1t2	2.1 ±0.02	72 ±1.0	8667	5.3	15.92	0.14
POMs_c5Q2t1	2.2 ±0.02	73 ±1.0	9000	6.8	20.45	0.15
POMs_c5Q2t2	2.2 ±0.02	73 ±1.0	9000	6.7	20.06	0.15
POMs_c5Q3t1	2.3 ±0.02	74 ±1.0	9333	5.8	17.41	0.15
POMs_c5Q3t2	2.3 ±0.02	74 ±1.0	9333	4.3	12.81	0.15

5.3 Experimental results

The mobilisation of PA6 and POM particles over the clastic bed was estimated with the same methodology adopted for homogeneous plastic bed (see Section 3.3). From the UVP measurements, bed shear velocities and bed shear stresses were computed, and from videos, bed changes' count was derived. The dataset consisted of 270 bed shear velocities and around 800 measurements of bed changes, for each combination of material and bed, in different conditions of flow rate Q and bed surface MP concentrations $\%C$. For each condition of Q and $\%C$, 20 bed shear velocities and around 30 counts of bed changes were available.
To compare our data with published literature, we plot on Shields' diagram (Figure 5.2) the observed Shields' mobility parameter, and as for the values for the abscissa we chose to use the mobile particle Reynolds' number Re^*_{MP} computed as

$$Re^*_{MP} = \frac{u^* d_{MP}}{\nu} \tag{5.2}$$

while other authors (Goral et al., 2023a) refer to the bed Reynolds' number Re^*_{Bed} computed as

$$Re^*_{Bed} = \frac{u^* d_{50,Bed}}{\nu} \tag{5.3}$$

where $d_{50,Bed}$ is the median diameter of the clastic sediments composing the bed.
In the estimation of the Shields' parameter θ, the grain-size d_{MP} refers to the mobile material as also the relative density Δ_{MP} computed as

$$\Delta_{MP} = \frac{\rho_{MP} - \rho}{\rho} \tag{5.4}$$

Figure 5.2 shows time-averaged conditions for the different combinations in the full dataset. Our data for homogeneous beds distribute on the Shields' curve (see Chapter 4), and have a variability comparable to other literature studies (e.g. Graf and Pazis, 1977). Plastic grains resting on a clastic bed (with median diameter $d_{50,Bed} < d_{MP}$) get remobilised at lower mean bed shear velocities, resulting in conditions (of motion) observed below the theoretical Shields' limit (consistently with Waldschläger and Schüttrumpf, 2019b and Yu et al., 2022). This is valid both for gravel bed tests and for sand bed tests, where the movement of grains was occurring at bed shear stresses one order of magnitude lower, approximately, than for homogeneous beds. By looking at Figure 5.2 the alignment among homogeneous and clastic bed measurements is evident. This alignment is also present in data provided by Waldschläger and Schüttrumpf (2019b), see later Figure 5.9, and Iuppa et al. (2024) for different morphotypes of MPs moving on beds of varying roughness, and is linked to the dimensionless mobile particle diameter d^*_{MP} depending only on particle's and ambient fluid characteristics (see later Equation 5.8, with reference to Meyering, 2012 and Garcia, 2008).

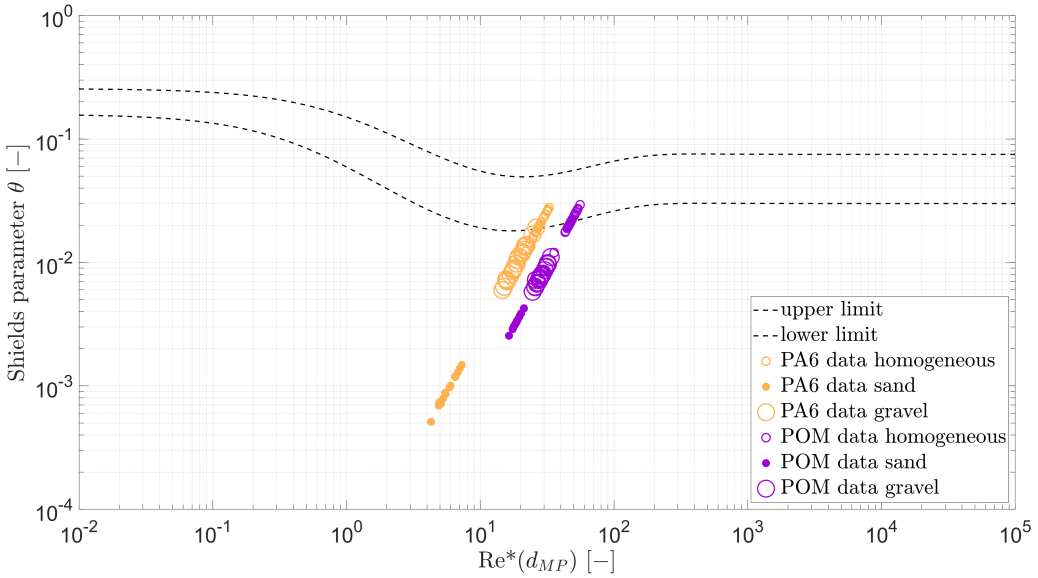

FIGURE 5.2: Experimental data points for PA6 (orange) and POM (pink) flat-bed tests versus homogeneous bed experiments (updated from Figure 4.4). Data on sand and gravel bed (full points and big circles) are visibly below the theoretical Shields' curve.

5.3.1 Bed shear velocities

The derivation of bed shear velocities was performed by fitting the time-averaged vertical profiles, in their near-bed portion (approximately 10 - 15 cells starting from the bed, see Section 3.2.2.3) to the logarithmic law (Equation 3.2). The spatial averaging across the section was done by computing the average of the two vertical profiles, thus obtaining one representative value per test. Time averaging was performed at two different resolutions: (i) a finer one every 5 s to be consistent with previous tests and image analysis data, (ii) a coarser one over the whole experiment (10 times larger than the finer one). The results of the finer were used to derive, similarly as in Section 4.3.3, the threshold conditions for the two beds, independently from the concentrations, as later explained in Section 5.3.4. For the sake of completeness, the goodness of fit parameters, for the fitted velocities on clastic beds, are summarised in Appendix B.
Figure 5.3 shows the measured distribution (from double-averaged velocity profiles in 5 s Time Windows) of bed shear velocities for the two types of plastic particles (PA6, lighter particles, in black/grey and POM, heavier particles in red). Observed shear velocities in the case of POM particles are higher than for PA6 particles, this is linked to our choice of observing similar mobility conditions for the two types of MPs. Moreover, moving along the x-axis, we have a decrease in bed-material grain-size and median diameter d_{50}, and our experimental conditions (both discharge Q and water level y, see Tables 5.1, 5.2, 5.3 and 5.4) adapted to it, resulting in decreasing observed bed shear velocities.

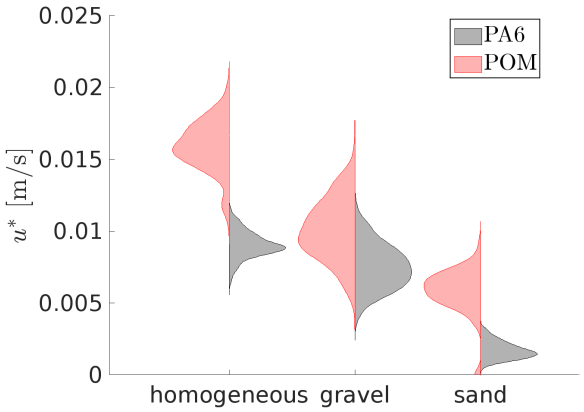

FIGURE 5.3: Violin plots showing the observed bed shear velocities u^* for PA6 (black, lower density) and POM (red, higher density) on the three different types of beds. The general trend with a decrease in observed u^* with decreasing geometric roughness (and grain-size) moving along the x-axis from homogeneous bed to gravel and sand bed is evident.

5.3.2 Microplastics' surface concentration changes

Changes in the MPs concentration on the clastic bed were derived from image data. For a detailed description of the methodology, see Section 3.3.2. As for the homogeneous bed experiments, a series of maps was created, from which the number of detached particles and their location were derived. The initial number of particles after seeding, N_{Tot}, was determined from the imposed percentage of surface covered in MPs as from Table 3.6. The estimation of changes in the MPs cover had a temporal resolution of 5 s, consistent with homogeneous bed tests (see Section 4.3.2). Figure 5.4 is an example of detected changes on gravel bed for the lighter MPs, PA6, for all surface concentrations in 20 consecutive time intervals (TW index).

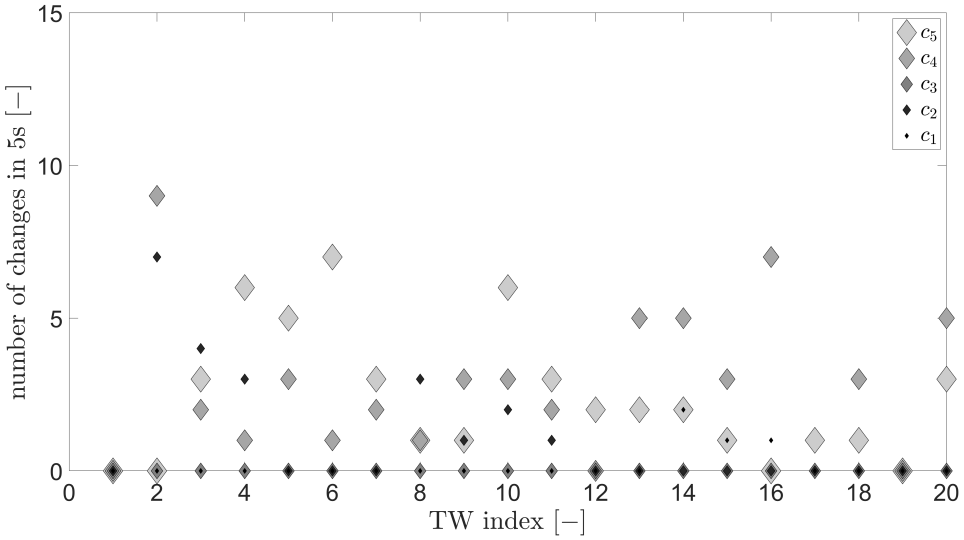

FIGURE 5.4: Detected number of changes for PA6 on gravel flat-bed tests sorted by MPs surface concentration at a discharge Q = 2 l/s.

5.3.3 Threshold conditions on clastic bed

From the full dataset presented at the beginning of Section 5.3 and in Figure 5.3, threshold conditions were obtained. The same methodology was used, as outlined in Section 4.3.3 for the homogeneous bed tests, with a modified $\dot{n}/N$ threshold value for the bed changes frequency, to account for the two orders of magnitude smaller amount of surface movable sediments. The *threshold bed changes frequency*, used to identify the threshold probability, and from it, to determine the associated threshold bed shear velocities, was set to a value $10^{-2}\ s^{-1}$. This value lied in the observed region for all conditions.

The derived threshold conditions are reported in Figure 5.5, as red and black markers. While for PA6 (black markers) the newly defined threshold is well within the time-averaged observed values, for POM on sand (red $*$) the threshold is at the border of the observation range. This was due to a constraint in the asset available, regarding the maximum discharge, which allowed only very rare (in time) and weak (in space) movement of the POM particles on the sandy bed. Differently, the PA6 on sand threshold was reached within the range of operability of the asset pumps. Notably, for PA6 particles on sand, the threshold is around $\theta_{cr} = 10^{-3}$, much lower than the one observed by other authors (e.g Waldschläger and Schüttrumpf, 2019b and Yu et al., 2022), as further discussed in Section 5.4.

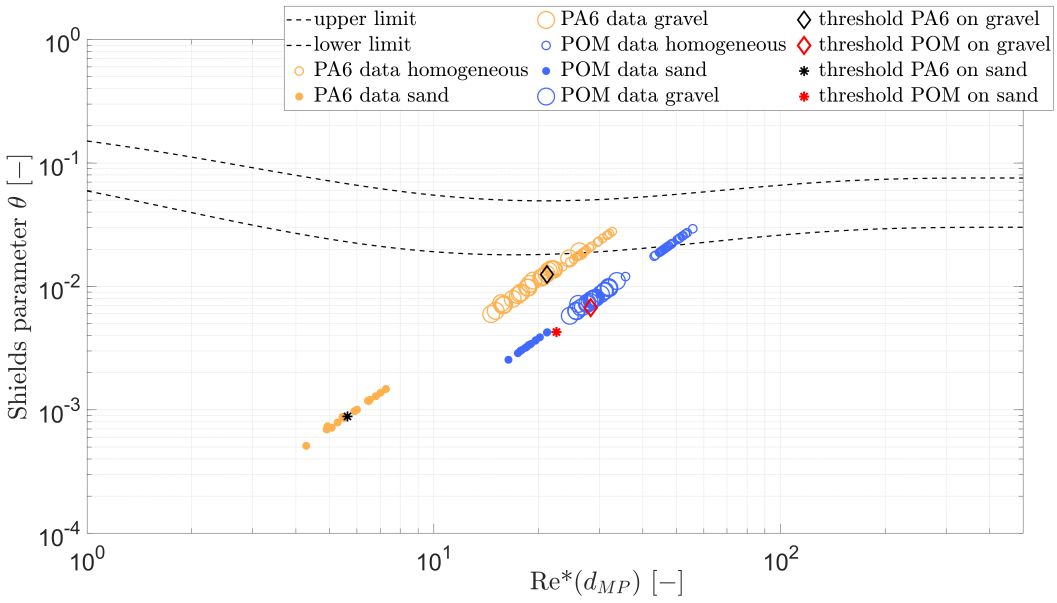

FIGURE 5.5: Modification of Figure 5.2 with threshold conditions derived from a fixed $\dot{n}/N = 10^{-2} s^{-1}$. Threshold for the chosen MPs on both sand ($*$) and gravel ($\diamond$) beds lies below the theoretical Shields' curve.

5.3.4 Microplastics mobility

Due to the different surface concentrations, the mobility of MPs was estimated as the relative number of mobilised MPs over the available ($\dot{n}/N_{Tot}$), where N_{Tot} took different values spanning from 7 - 8 particles for the lowest MPs concentration at the bed surface (0.05 %) to 130 - 150 for the highest tested (1 %). The effect of different concentrations (translating in different numbers of available MPs on the bed surface (N_{Tot}) is shown in Figure 5.6. There, what was anticipated in the Section 5.3.3 for experiments with POM on sand bed (4^{th} plot) becomes evident: the number of mobilised particles for these set of experiments is significantly lower than in all other cases, with a few exceptions. From this one can infer that observed conditions for POM on sand are more representative of lack of motion rather than motion. Indeed, in Figure 5.5 the threshold identified lies slightly above the maximum observed (derived from time averaging on the whole experimental length).

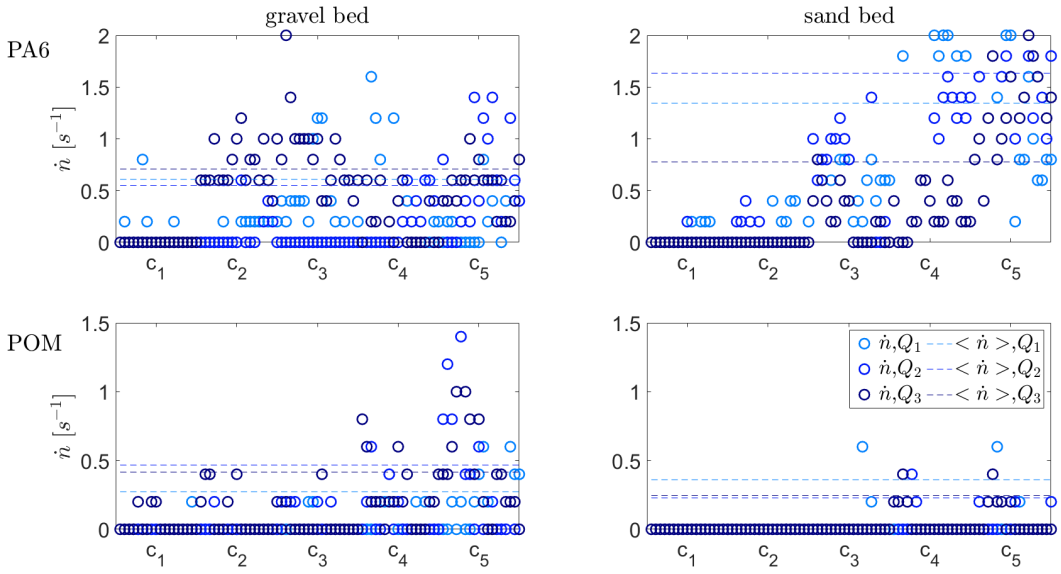

FIGURE 5.6: Detected frequency of particle motion $\dot{n}$ [s^{-1}] for PA6 (first row) and POM (second row) on gravel (first column) and sand (second column) beds. Data are sorted by discharge, where increasing darkness of blue means increasing discharge. On the x-axis the concentration increases from c_1 = 0.05% to c_5 = 1%.

5.3.5 Dimensional analysis and PCA

The effects of a hydrodynamically-immobile clastic bed on microplastic particles' mobilisation were investigated by dimensional analysis and Principal Component Analysis (PCA) to identify the strongest dependencies among measured parameters.

The dimensional analysis uses the Buckingham theorem (1914) to derive dimensionless groups from the dimensional parameters involved in a physical process. The choice of dimensionless groups is multiple, and it is left to the individual researcher's experience to select the relevant

ones, for it is not possible to identify *a priori* the groups which must be constructed (Longo, 2022). For our mixed sediment remobilisation problem, relevant parameters must describe the ambient fluid, the bed composition and the mobile material, while fundamental units for the sediment remobilisation process are mass [M], length [L] and time [T]. The list of relevant parameters is as follows (see also Chapter 3):

$$\begin{aligned} flow: &\quad Q \text{ or } U,\ y,\ \rho,\ \nu,\ g \\ bed\ sediments: &\quad S_B,\ \rho_S,\ d_S,\ CU,\ U^*,\ \tau^* \\ mobile\ sediments: &\quad \rho_{MP},\ d_{MP},\ CSF,\ n,\ N_{Tot},\ \%C \end{aligned}$$

where $\%C$ is the abundance of MPs on the bed surface.
By applying Buckingham theorem, the dimensional functional dependence of the above 17 variables, reduces to a non-dimensional functional dependence of 14 parameters. Classical parameters for natural sediment transport can be adapted to the case of two different granular materials composing the bed surface. This results in a set of dimensionless parameters which we assumed suitable for the mobilisation of MP (treated as sedimentary material) from a bed composed either of the same type of MPs (homogeneous bed case) or of clastic sediments (mixed bed case):

$$\begin{aligned} homogeneous\ bed: &\quad y/d_{MP}\ ,\ \rho_{MP}/\rho,\ Re,\ Re^*,\ Fr,\ Fr_S^*,\ \theta \\ mixed\ bed: &\quad d_{MP}/d_{50,Bed}\ ,\ Re^*_{Bed},\ Re^*_{MP},\ Re_{s,MP},\ d^*_{s,MP},\ \%C,\ \chi_B,\ \Delta,\ \Delta_{MP} \end{aligned} \tag{5.5}$$

In Equation 5.5, Fr_S^* is the (movable) particle densimetric Froude number (dimensionless), as from Aguirre-Pe et al. (2003), computed as

$$Fr_S^* = \frac{u^*}{\sqrt{g\ \Delta_{MP}\ d_{MP}}} \tag{5.6}$$

$Re_{s,MP}$ is the movable particle Reynolds number (dimensionless), representing the ratio between the weight of the mobile particles resting on the bed and the kinematic viscosity of the fluid and is computed as

$$Re_{s,MP} = \frac{\sqrt{g\ \Delta_{MP} d_{MP}^3}}{\nu} \tag{5.7}$$

while, the dimensionless diameter for the microplastics, as defined in Equation 2.42, results

$$d^*_{MP} = d_{MP} \cdot \left(\frac{g\ \Delta_{MP}}{\nu^2}\right)^{1/3} \tag{5.8}$$

the MPs surface concentration $\%C$, imposed as fixed values (see Table 3.6) when seeding, can, alternatively, be given by ratio of the portion of imaged area covered by MPs ($Area_{MPcover}$) and

the whole imaged area ($Area_{tot}$)

$$\%C = \frac{Area_{MPcover}}{Area_{tot}} \tag{5.9}$$

and the dimensionless degree of motion χ_B, comparable, in its form, to the dimensionless solid discharge per unit width by Ballio and Radice, 2007, is computed from the bed changes per unit time $\dot{n}$ as follows

$$\chi_B = \frac{\dot{n}\, Vol_{MP}}{N_{Tot} \cdot B \sqrt{g\, \Delta_{MP}\, d_{MP}^3}} \tag{5.10}$$

where Vol_{MP} is the volume of a single MP particle (approximated to a sphere), and B is the width of the flume.

The comparison of the possible parameters resulting from the Buckingham theorem and PCA allows us to select a (reduced) combination of dimensionless parameters which best describes the observed remobilisation of compact microplastics from both homogeneous and clastic bed (following Pektaş, 2015).

To clarify the interdependencies among the different dimensionless parameters, and their role in the estimation of the dimensionless degree of motion χ_B, a principal component analysis (PCA) was performed with each dimensionless parameter estimated from the 5 s-averaged values of the measured quantities. The PCA operates in the space of the chosen dimensionless parameters, and defines new parameters, as a linear combination of the initial ones, maximising the retained information. This is done by identifying eigenvectors and eigenvalues of the covariance matrix of the initial data, which have formerly been standardised to have zero mean and unit standard deviation. The new parameters (Principal Components), are linearly independent, and help determine the best lower-dimensional space, which derives from the terms corresponding to the largest eigenvalues of the covariance matrix of the data (Frascati and Lanzoni, 2009).

For the PC analysis, the dimensionless parameters in Equation 5.5 were set as input, with the exception of the flow Reynolds' number Re, since all experiments showed turbulent flow, which was substituted by stream power Ω (see Equation 2.17), as this parameter has been used for modelling incipient motion on rough, immobile beds (Ancey and Recking, 2023). The results are shown in Figure 5.7, which reports the most relevant parameters only.

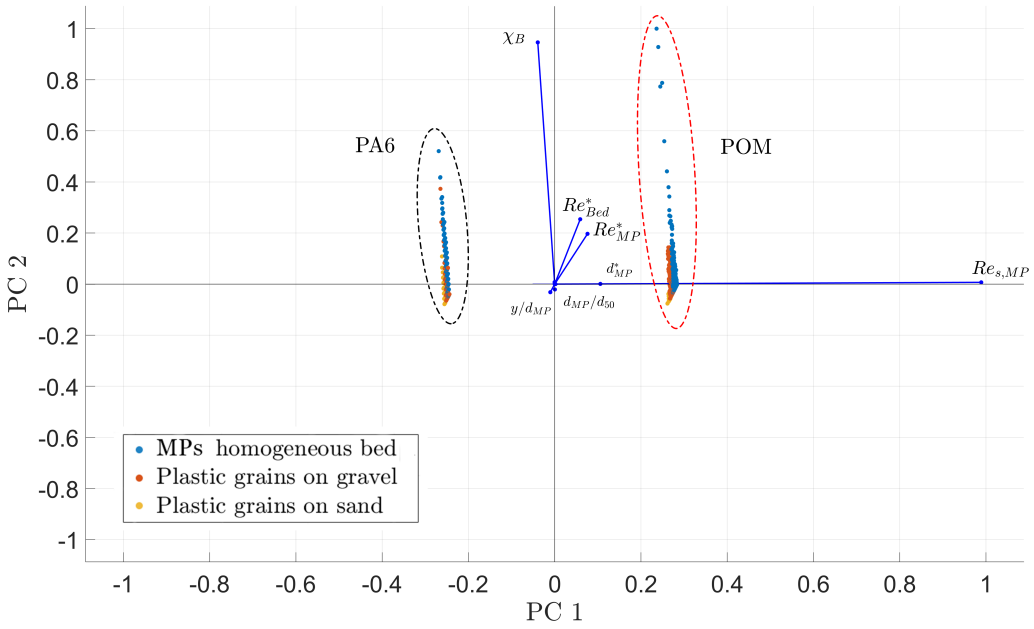

FIGURE 5.7: PC analysis of all experiments on homogeneous and clastic bed: first two principal components PC1 and PC2 on the x- and y-axis respectively. Dimensionless parameters used are from Equation 5.5 substituting the stream power Ω to Re. Only those with the highest relevance are shown.

The two axes show the orientation of the first and second Principal components (x- and y-axis respectively. The clusters indicate the material (PA6 or POM particles), and the colour (blue, orange and yellow) defines which bed type was used (homogeneous, gravel and sand respectively). The first PC is visibly aligned with the sedimentological Reynolds number of the mobile particle (microplastic) $Re_{s,MP}$, as well as the dimensionless MPs diameter d^*_{MP}, while most of the second PC component depends on the dimensionless degree of motion of the MPs (χ_B). The third principal component, not visible in 5.7, is connected to the mobile particle Reynolds' number Re^*_{MP} and to a lesser extent to the bed Reynolds' number Re^*_{bed}. The variability in the original data, explained by the first 3 PCs, is shown in Figure 5.8 and amounts to 99.9%.

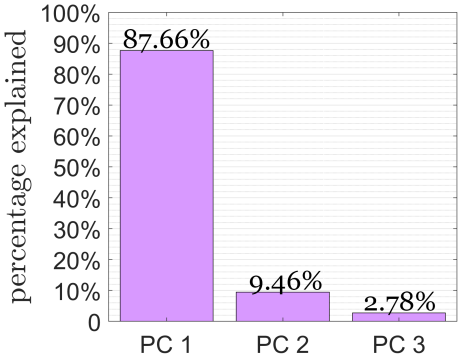

FIGURE 5.8: Percentage of variability in the data explained by the first 3 principal components.

5.4 Discussion

The use of Shields' mobility parameter (Equation 2.38) is well-established in sediment research, and a direct transfer of methods has been adopted to estimate plastic sediments onset of motion on natural beds (Waldschläger and Schüttrumpf, 2019b; Yu et al., 2022 and Goral et al., 2023a). Treating MPs as sediments (i.e. adopting a *sediment analogy* framework) implies assuming microplastics sedimentary processes are similar to those natural clastic sediments undergo. When comparing the present work's thresholds with literature data (by Waldschläger and Schüttrumpf, 2019b and Yu et al., 2022) the values for the tested particles lie in the same range as the one identified by both authors, with the exception of the PA6 (lighter plastic grains) on sand. The reason for this is likely the different submergence (y/d_{MP}) conditions of the light PA6 particles, which in the case of our tests was around 20 times the particle's diameter d_{MP}, while in both literature sources was greater than 100 d_{MP}. Indeed the water depth at which our experiments on sand were run (from Table 5.3), was approximately 6.5 cm, while for Waldschläger and Schüttrumpf it was 50 cm, and for Yu et al. it was 43 cm. The case of our lower water depth, combined with the density of PA6, results in very unstable particles resting on the sand bed. Indeed, in our case, the effect of the pressure head (due to the column of water on top of the MP particles) is approximately one order of magnitude lower than in both cited authors (it is directly proportional to the submergence), and this reflects in very low bed-shear velocities needed to set out PA6 ellipsoidal grains into motion on the sand bed.

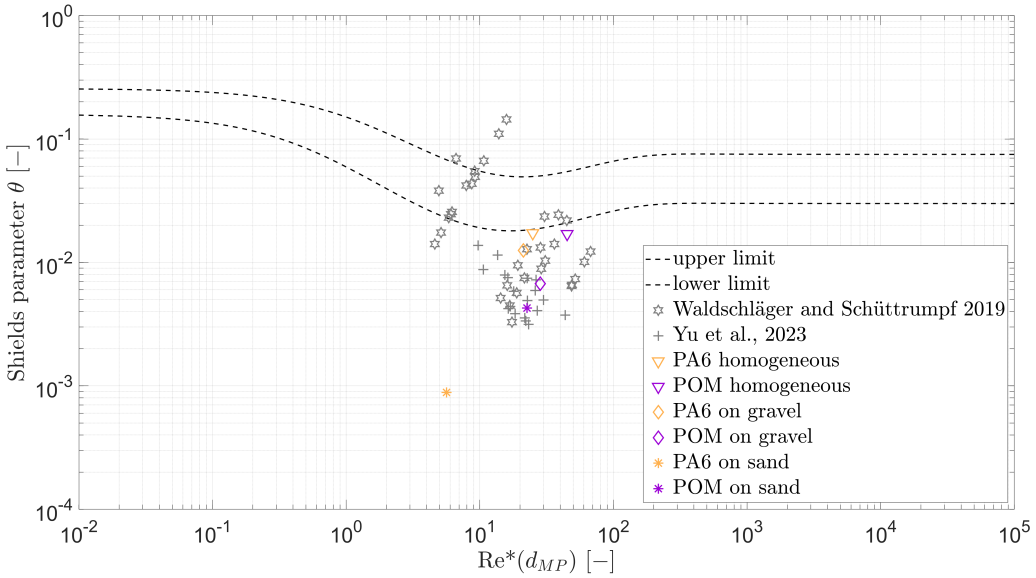

FIGURE 5.9: Threshold conditions for the PA6 (yellow) and POM (pink) particles determined in this work versus literature data (grey). Most of the values fall in the same region but PA6 on sand. The symbols show thresholds conditions on different bed, where literature data, and ▽, ◊ and ∗ represent our derived thresholds on homogeneous, gravel and sand bed respectively.

A striking difference from the experimental results by Shvidchenko and Pender (2000) with reference to the effect of relative submergence of the mobile particles can be observed. The authors observed (on homogeneous beds composed of natural clasts) higher bed-shear effects for shallower flows, with the most relevant increase for bed particles and their eddies comparable with the flow depth, behaviour late confirmed by, among others, Bolhassani et al. (2015). Unfortunately, the effect of relative submergence on the mobilisation of fractions from a mixed bed was not further investigated in later studies by the two groups. The effects of density of the mobile particle (still on homogeneous bed though) were, instead, included in the experimental study by Prancevic and Lamb (2015), who looked into the incipient motion at varying slopes and relative submergence for sediment beds with different densities (both clastic and acrylic grains characterised by values of Δ of 1.65 and 0.15 respectively). Even though the link of slope to relative submergence was present, they found that: (i) the "relative roughness was the key parameter controlling initial sediment motion in our experiments, not bed slope", and (ii) their observed threshold conditions for the acrylic bed were lower than the expected from available models. On our mixed bed, the combination of relative roughness effects, with low values of relative roughness (d_{50}/y) and low mobile particle submergence (y/d_{MP}) on sand, and low particle weight resulted in threshold conditions lower than other studies for the lighter MPs (PA6 grains). Looking with more detail at the distribution of the observed data, Figure 5.10 shows the measured relative mobility $\dot{n}/N$ versus the Shields' number θ for all experiments performed, including those on homogeneous bed (see Chapter 4).

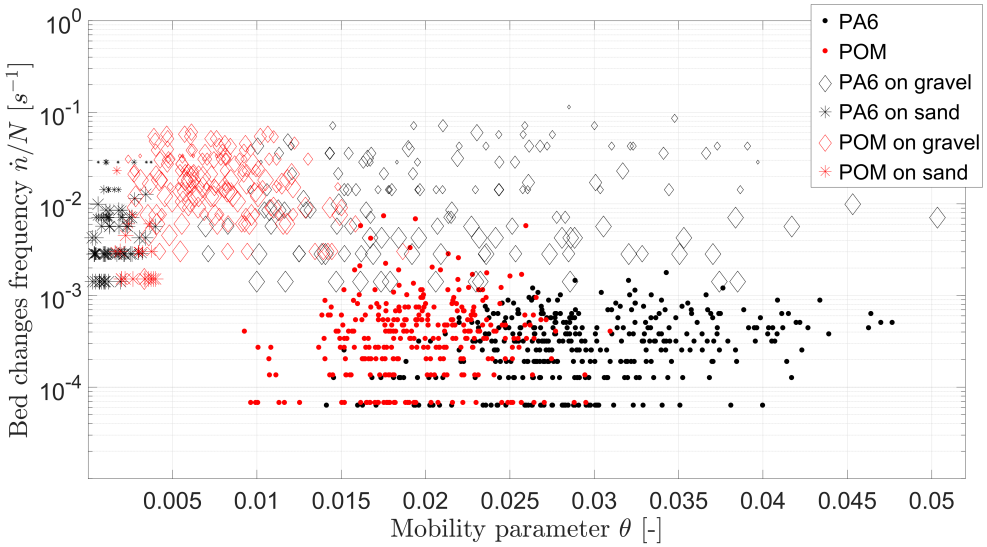

FIGURE 5.10: Experimental data points for PA6 (black) and POM (red) flat-bed tests for homogeneous bed (full ∘), plastics on gravel (◊) and plastics on sand (∗), the symbol size indicates the (increasing) surface concentration in the tests with values equal to 0.05%, 0.1%, 0.2%, 0.5%, 1%. Data on sand and gravel bed, due to the lower surface concentration, show a higher relative mobility (higher values of $\dot{n}/N$).

The fact that plastics are lighter than gravel, entails that their stability on gravel beds is on average

lower than that of a gravel particle. Indeed, the two components contributing to resistance, submerged particle weight and inter-particle friction, directly depend on the density. This is reflected in generally lower mean bed shear stresses required to set plastic particles into motion. From Figure 5.10, the variability of the Shields' parameter θ is generally higher for lighter plastic sediments (PA6) than for heavier ones (POM). Moreover, for the lighter PA6 grains, tests on gravel (◊) show higher Shields' numbers than those observed for the heavier POM on the same bed (◊). This can be related to the shape of the two particles, with PA6 grains being ellipsoidal, and POM grains being closer to spherical in shape. Although these results are far from conclusive, the density of the sediment plays a key role, when its value approaches that of the ambient fluid, which, on smoother beds (in our case sand beds) triggers particle motion at bed-shear stresses much lower than those expected by classical sediment transport theory (also accounting for a correction due to *hiding-exposure* effects).
For particles with a weight comparable with the ambient fluid, Shields' parameter θ enhances the effects of the near-bed velocity forcing. On the other hand, looking at the Shields' parameter for heavier particles does not provide such an insight, most likely due to the higher inertia of the grains. This implies that, while for natural clastic sediments and heavy minerals a threshold on Shields' parameter can be used to describe the onset of motion and transport of particles, for light sediments, having density comparable with the ambient fluid, such threshold cannot be uniquely identified, as the particles with low inertia are very sensitive to any fluctuation in the surrounding flow.

5.4.1 From analogy to analysis

The sediment analogy, i.e. using Shields' diagram to model microplastics inception of movement, has been adopted by all researchers dealing with the MPs onset of motion process (Waldschläger and Schüttrumpf, 2019a; Goral et al., 2023a; Yu et al., 2022 and 2023). While the adoption of a widely-accepted model is advantageous in many forms, the assumptions behind the model itself can hamper effective adoption, and generate confusion. The Shields' model, and its modifications, are undoubtedly useful in sedimentology, and represent an "averaged behaviour" of homogeneous bed material put into motion by unidirectional water currents. The averaging process implemented for obtaining the so looked-for curve operates at different levels and scales. It is a *temporal averaging*, implying (i) turbulence effects are overlooked in favour of a time-averaged indicators (the bed shear stress), (ii) local bed evolution is disregarded, and the roughness feedback on the near-bed flow does not vary. It is a *spatial averaging*, where (i) the variability of bed elevation/composition/sorting is averaged across the section leading to one elevation and roughness value, (ii) the local hydrodynamics are summarised into one single value for the volume considered (both cross-sectional and sometimes longitudinal averaging). It is a *particle-characteristics averaging*, implying that one bulk measure (of motion) including particles of different shapes is taken as representative. This "bulk measure" is a valid proxy when one considers natural materials, with their shapes varying almost continuously for compact-

morphotypes, but if one wants to focus on artificial materials, for which the variability in characteristics is limited to a finite number, a question arises regarding whether the same model can be applied.

While the first and second averaging dimensions (namely temporal and spatial) are a standard approach in treating hydrodynamics on rough beds (Nikora et al., 2007), the third averaging dimension (i.e. particle-characteristics) appeared significant only recently, as the *sediment analogy* framework has been applied to study microplastics transport processes (see the wide-ranging review by Waldschläger et al., 2022 and Russell et al., 2024).

Research on natural sediments resolves *particle-characteristics averaging* by considering a correction coefficient accounting for the grain-size variability, and the different conditions grains with different sizes undergo. Such a correction, which in the case of natural sediments is ascribed to differences in grain-size, was firstly proposed by Egiazaroff (1965) as a *hiding-exposure coefficient*, and further adapted. Latest applications (following Waldschläger and Schüttrumpf, 2019b) proposed to fit the hiding-exposure correction to represent also the microplastics threshold conditions on Shields' diagram.

From the results of the PC analysis (Section 5.3.5) we can see that the particle weight, through the dimensionless mobile particle diameter d^*_{MP} and more evidently the sedimentological Reynolds' number $Re_{s,MP}$, plays a key role in our dataset. This is due to the approach we chose, where conditions close to the incipient motion were observed in all experiments, and from those observations, the threshold was derived with a *semi-probabilistic approach*. The sediment transport rate for our test was purposely set to very low values, and therefore, the effect of the de-stabilising bed-shear stress on conditions close to *no transport* was hidden by the stabilising effect of particles' weight. When we remove from the PC analysis $Re_{s,MP}$, results are reported in Figure 5.11, where the first two components explain around 94.2% of the total observed variability in the data. The third component is almost parallel to the dimensionless diameter d^*_{MP}, and explains around 5% of the remaining variability.

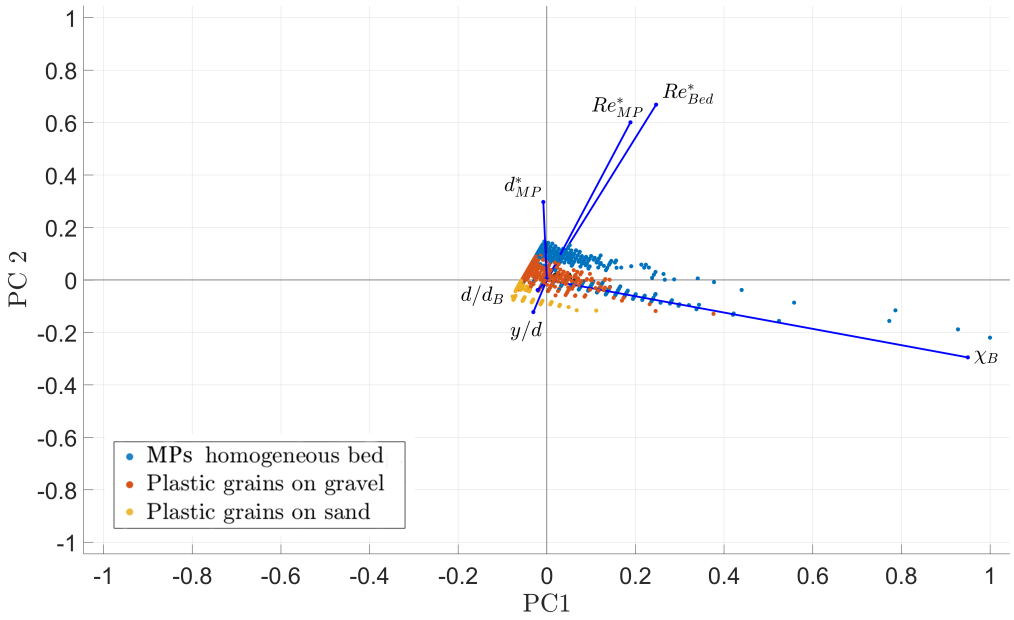

FIGURE 5.11: PC analysis of all experiments on homogeneous and clastic bed: first two principal components PC1 and PC2 on the x- and y-axis respectively. Dimensionless parameters used are the same as in 5.7 with the exclusion of $Re_{s,MP}$, only those with the highest relevance are shown.

5.5 Summary

The validity of our findings are limited to our simplified experimental system: homogeneous clastic bed with one type of microplastics (by density, size and morphotype) scattered on it, and rearranged by flow. The remobilisation conditions, defined in a similar fashion as incipient motion for the homogeneous bed tests, with a bulk correction due to the availability (see Section 5.3.3) appear to acceptably represent the onset of motion of the chosen MPs, when compared with other literature data. The identified threshold plots lower than the Shields' curve range for clastic sediments, as also observed by other authors. The application of *sediment analogy* framework allows to have initial assessment of the remobilisation conditions of microplastics on different beds, and was proven valid by past research (Waldschläger and Schüttrumpf, 2019b and Yu et al., 2023). The validity of such approach is still to be proven under mobile particle's submergence conditions differing from the ones for which it has been developed. The role of particle's submergence becomes important when considering floodplains, and their higher exposure to microplastic pollution linked mostly to recreational activities.

Chapter 6

Conclusions and further developments

"Tout est au mieux
dans le meilleur des mondes possibles"
"Everything goes to its best
in the best of all possible worlds"

Pangloss to Candide
Voltaire, 1759

6.1 Incipient motion of microplastics from homogeneous bed

The threshold condition for the onset of motion of microplastics on homogeneous bed was addressed by adopting the same methods (Shields' diagram) as for other homogeneous beds, composed of natural clastic sediments (**Q1.1**). We chose to use the widely-accepted Shields' diagram, and derived from experimental data of particles' motion and near-bed velocity measurements a threshold for the two types of microplastics, PA6 and POM grains. The derivation of a threshold relates particles' mobility to the near-bed hydrodynamic forcing, represented by bed-shear velocity from our measurements (**Q1.2**). This was done by setting a limit value for the *bed changes frequency* ($\dot{n}/N$), and relating it, through its probability of occurrence to observed bed-shear velocity u^* (characterised by the same probability). The threshold thus identified lies slightly beneath the range derived for natural sediments, consistently with other literature data. The *sediment analogy* framework, i.e. treating microplastics as sediments and translating methods from sedimentary research to derive their threshold conditions is valid in the case of MPs moving on a bed made of the same material. This similarity was also exploited in the past in scaled experiments of morphodynamic processes (see Section 2.1.2).

6.2 Remobilisation of plastic particles from a clastic bed

Experiments on the threshold conditions for the same type of MPs deposited on a mixed bed, see the adoption of the *sediment analogy framework* to study remobilisation. Adapting the methodology used for homogeneous bed to the mixed bed case, with a bulk correction on the *frequency of bed changes* limit to account for the lower availability of material, allows to derive threshold conditions for the lighter fraction (MPs). The threshold for remobilisation for MPs The threshold values for remobilisation, in all cases, are lower than those observed on a homogeneous bed, with the lowest values observed for the less rough beds. The methodological definition of threshold for a non-homogeneous bed was adapted, to take into account the lower availability of movable material, irrespective of the main bed composition (**Q2.1**). The MPs surface concentrations, spanning from 0.5% to 1%, did not appear to have an influence on the threshold for remobilisation definition (**Q2.2**), but it rather modified the probability of occurrence of motion, requiring a higher *frequency of bed changes* values to be set.

6.3 Are compact microplastics talking sedimentary processes' language?

Among all of microplastics morphotypes, those of compact shape resemble most natural clastic sediments. Their basic characterisation, when using the *sediment analogy framework* for transport processes, requires only information about their size and density, adding one degree of complexity (while is clear how for other morphotypes shape is key in determining the transport behaviour). The work presented in this thesis, especially those results of Chapter 5, highlight how, even for compact-shape MPs, the shape effect plays a role in the determination of a *bulk incipient motion threshold*. Indeed, for shapes deviating from spherical, the differences in the orientation of the MPs particles trigger remobilisation at different observed bed shear velocities, and the high variability in observed conditions for remobilisation for the PA6 more ellipsoidal particles reflects this. Although high variability in observed bed-shear stresses does not hamper *per se* the identification of a unique threshold, it has an effect on the range of uncertainty of any further estimation depending on such threshold, which usually takes the form of a solid discharge.

6.4 Further work

The study of microplastics sedimentary processes is slowly blossoming, and can be seen as an exciting "playground" (B. Sutherland, 2024, April 4) for widening our knowledge on transport of granular materials.
Many variations of the very simple system-model presented in this work are possible including:

- bed characteristics: slope (both longitudinal and lateral), bedform roughness
- bed material characteristics: uniformity in terms of size and density

- hydraulic characteristics: relative roughness, submergence variations
- bed layer characteristics: uniform or layered bed, density distribution
- mobile particle characteristics: morphotype (compact, flat or linear), density

There is a lot of room for experimental work, and research is slowly moving into more complex setups. Tackling only the first point in the list, an important step for improving the understanding of microplastic transport processes, is shifting from flat bed to perturbed bed with bedforms. The bedform roughness effect, and the size of the bedform interact with the plastic grains generating complex patterns of erosion and deposition which have just been scraped by recent work (Russell et al., 2023) in a rather qualitative way.
Among the biggest limitations, not only for our setting, but for general laboratory experiments on the transport of microplastics, is the fact that the studied particles are "frozen in a pristine state", and ageing and weathering dynamics are hard to capture at the laboratory scales of our investigations. Other researchers (Wang et al., 2024) carried out experiments on aged microplastic particles, and by increasing the ageing period found an increase in the incipient motion threshold, meaning that aged microplastics on fixed beds (as the one tested by the authors, and as do clastic bed behave at MPs incipient motion) have a motion threshold limit higher than pristine one, increasing the critical velocity. The road is still long before our understanding of plastics sedimentary processes reaches a satisfactory level, and in this "playground" the limits of what is physically reasonable are so loose that genuine curiosity and improvisation are still highly valuable.

Bibliography

Adam, V., Yang, T., & Nowack, B. (2019). Toward an ecotoxicological risk assessment of microplastics: Comparison of available hazard and exposure data in freshwaters. *Environmental Toxicology and Chemistry*, *38*(2), 436–447. https://doi.org/10.1002/etc.4323

Aguirre-Pe, J., Olivero, M. ı. a. L., & Moncada, A. T. (2003). Particle densimetric Froude number for estimating sediment transport. *Journal of Hydraulic Engineering*, *129*(6), 428–437. https://doi.org/10.1061/(ASCE)0733-9429(2003)129:6(428)

Akdogan, Z., & Guven, B. (2019). Microplastics in the environment: A critical review of current understanding and identification of future research needs. *Environmental pollution*, *254*, 113011. https://doi.org/10.1016/j.envpol.2019.113011

Alimi, O. S., Farner Budarz, J., Hernandez, L. M., & Tufenkji, N. (2018). Microplastics and nanoplastics in aquatic environments: Aggregation, deposition, and enhanced contaminant transport. *Environmental science & technology*, *52*(4), 1704–1724. https://doi.org/10.1021/acs.est.7b05559

Allen, J. (1984). Experiments on the settling, overturning and entrainment of bivalve shells and related models. *Sedimentology*, *31*(2), 227–250. https://doi.org/10.1111/j.1365-3091.1984.tb01961.x

Ancey, C., & Recking, A. (2023). Scaling behavior of bedload transport: what if Bagnold was right? *Earth-Science Reviews*, 104571. https://doi.org/10.1016/j.earscirev.2023.104571

Andrady, A., Barnes, P., Bornman, J., Gouin, T., Madronich, S., White, C., Zepp, R., & Jansen, M. (2022). Oxidation and fragmentation of plastics in a changing environment; from uv-radiation to biological degradation. *Science of The Total Environment*, *851*, 158022. https://doi.org/10.1016/j.scitotenv.2022.158022

Armanini, A. (2013). Granular flows driven by gravity. *Journal of Hydraulic Research*, *51*(2), 111–120. https://doi.org/10.1080/00221686.2013.788080

Armanini, A. (2018). *Principles of river hydraulics*. Springer. https://doi.org/10.1007/978-3-319-68101-6

Bagnold, R. A. (1954). Experiments on a gravity-free dispersion of large solid spheres in a newtonian fluid under shear. *Proceedings of the Royal Society of London. Series A. Mathematical and Physical Sciences*, *225*(1160), 49–63.

Bagnold, R. A. (1955). Some flume experiments on large grains but little denser than the transporting fluid, and their implications. *Proceedings of the Institution of Civil Engineers*, *4*(2), 174–205.

Bagnold, R. A. (1966). *An approach to the sediment transport problem from general physics*. US government printing office.

Bagnold, R. A. (1979). Sediment transport by wind and water. *Hydrology Research*, *10*(5), 309–322.

Ballio, F., Pokrajac, D., Radice, A., & Hosseini Sadabadi, S. A. (2018). Lagrangian and Eulerian description of bed load transport. *Journal of Geophysical Research: Earth Surface*, *123*(2), 384–408. https://doi.org/10.1002/2016JF004087

Ballio, F., & Radice, A. (2007). Grain kinematics in weak linear transport. *Archives of Hydro-Engineering and Environmental Mechanics*, *54*(3), 223–242. https://doi.org/10.1002/esp.4105

Bathurst, J. (1987). Bed load discharge equations for steep mountain rivers. *Sediment transport in gravel-bed rivers*, 453–491.

Beheshti, A. A., & Ataie-Ashtiani, B. (2008). Analysis of threshold and incipient conditions for sediment movement. *Coastal Engineering*, *55*(5), 423–430. https://doi.org/10.1016/j.coastaleng.2008.01.003

Berni, C., Michallet, H., & Barthélemy, E. (2017). Effects of horizontal pressure gradients on bed destabilization under waves. *Journal of Fluid Mechanics*, *812*, 721–751. https://doi.org/10.1017/jfm.2016.805

Bertling, J., Bertling, R., & Hamann, L. (2018). *Kunststoffe in der Umwelt: Mikro-und Makroplastik* (tech. rep.). Fraunhofer-Institut für Umwelts-, Sicherheits- und Energietechnik Umsicht.

Bettess, R. (1984). Initiation of sediment transport in gravel streams. *Proceedings of the Institution of Civil Engineers*, *77*(1), 79–88.

Bettess, R. (1990). Survey of lightweight sediments for use in mobile-bed physical models. *Movable bed physical models*, 115–123.

Bolhassani, R., Afzalimehr, H., & Dey, S. (2015). Effects of relative submergence and bed slope on sediment incipient motion under decelerating flows. *Journal of Hydrology and Hydromechanics*, *63*(4), 295–302. https://doi.org/10.1515/johh-2015-0039

Bong, C., Lau, T., Ab. Ghani, A., & Chan, N. (2016). Sediment deposit thickness and its effect on critical velocity for incipient motion. *Water Science and Technology*, *74*(8), 1876–1884. https://doi.org/10.2166/wst.2016.376

Boos, J.-P., Gilfedder, B. S., & Frei, S. (2021). Tracking microplastics across the streambed interface: Using laser-induced-fluorescence to quantitatively analyze microplastic transport in an experimental flume. *Water Resources Research*, *57*(12), e2021WR031064. https://doi.org/10.1029/2021WR031064

Brahms, A. (1754). *Anfangsgründe der Deich- und Wasser- Baukunst* (Vol. 2). Tapper.

Buckingham, E. (1914). On physically similar systems; illustrations of the use of dimensional equations. *Physical review*, *4*(4), 345.

Buffington, J. M., & Montgomery, D. R. (1997). A systematic analysis of eight decades of incipient motion studies, with special reference to gravel-bedded rivers. *Water Resources Research*, *33*(8), 1993–2029.

Campagnol, J., Radice, A., & Ballio, F. (2012). Scale-based statistical analysis of sediment fluxes. *Acta Geophysica*, *60*(6), 1744–1777. https://doi.org/10.2478/s11600-012-0028-6

Campagnol, J., Radice, A., Ballio, F., & Nikora, V. (2015). Particle motion and diffusion at weak bed load: Accounting for unsteadiness effects of entrainment and disentrainment. *Journal of Hydraulic Research*, *53*(5), 633–648. https://doi.org/10.1080/00221686.2015.1085920

Carling, P. (1988). The concept of dominant discharge applied to two gravel-bed streams in relation to channel stability thresholds. *Earth surface processes and landforms*, *13*(4), 355–367.

Carling, P. A., & Breakspear, R. M. (2006). Placer formation in gravel-bedded rivers: A review. *Ore Geology Reviews*, *28*(4), 377–401. https://doi.org/10.1016/j.oregeorev.2005.02.002

Carstens, M. R., Neilson, F. M., & Altinbilek, H. (1964). *An analytical and experimental study of bed ripples under water waves*. Engineering Experiment Station, Georgia Institute of Technology.

Cecchetto, M., Tregnaghi, M., Bottacin-Busolin, A., Tait, S., Cotterle, L., & Marion, A. (2018). Diffusive regimes of the motion of bed load particles in open channel flows at low transport stages. *Water Resources Research*, *54*(11), 8674–8691. https://doi.org/10.1029/2018WR022885

Cecchetto, M. (2017). *The development of stochastic based transport models to predict the advection and diffusion of bed-load sediment* [Doctoral dissertation, University of Sheffield].

Celik, A. O., Diplas, P., Dancey, C. L., & Valyrakis, M. (2010). Impulse and particle dislodgement under turbulent flow conditions. *Physics of Fluids*, *22*(4). https://doi.org/10.1063/1.3385433

Chiew, Y.-M., & Parker, G. (1994). Incipient sediment motion on non-horizontal slopes. *Journal of Hydraulic Research*, *32*(5), 649–660. https://doi.org/10.1080/00221689409498706

Chin, C., & Chiew, Y. (1993). Effect of bed surface structure on spherical particle stability. *Journal of waterway, port, coastal, and ocean engineering*, *119*(3), 231–242. https://doi.org/10.1061/(ASCE)0733-950X(1993)119:3(231)

Corey, A. (1949). *Influence of Shape on the Fall Velocity of Sand Grains (Master's thesis)* [Master's thesis, Colorado State College of Agriculture and Mechanic Arts].

Davis, W. M. (1909). The systematic description of land forms. *The Geographical Journal*, *34*(3), 300–318.

de Souza Machado, A. A., Kloas, W., Zarfl, C., Hempel, S., & Rillig, M. C. (2018). Microplastics as an emerging threat to terrestrial ecosystems. *Global change biology*, *24*(4), 1405–1416. https://doi.org/10.1111/gcb.14020

Detert, M. (2008). *Hydrodynamic processes at the water-sediment interface of streambeds* [Doctoral dissertation, Zugl.: Karlsruhe, Univ., Diss., 2008].

Dey, S. (2014). *Fluvial Hydrodynamics: Hydrodynamic and Sediment Transport Phenomena.* (Vol. GeoPlanet: Earth and Planetary Sciences). Springer. https://doi.org/10.1007/978-3-642-19062-9

Dey, S., & Ali, S. Z. (2019). Bed sediment entrainment by streamflow: State of the science. *Sedimentology*, *66*(5), 1449–1485. https://doi.org/10.1111/sed.12566

Dey, S., & Papanicolaou, A. (2008). Sediment threshold under stream flow: A state-of-the-art review. *KSCE Journal of Civil Engineering*, *12*, 45–60. https://doi.org/10.1007/s12205-008-8045-3

Diplas, P., Dancey, C. L., Celik, A. O., Valyrakis, M., Greer, K., & Akar, T. (2008). The role of impulse on the initiation of particle movement under turbulent flow conditions. *Science*, *322*(5902), 717–720. https://doi.org/10.1126/science.1158954

Drake, T. G., Shreve, R. L., Dietrich, W. E., Whiting, P. J., & Leopold, L. B. (1988). Bedload transport of fine gravel observed by motion-picture photography. *Journal of Fluid Mechanics*, *192*, 193–217. https://doi.org/10.1017/S0022112088001831

Dris, R., Imhof, H., Sanchez, W., Gasperi, J., Galgani, F., Tassin, B., & Laforsch, C. (2015). Beyond the ocean: Contamination of freshwater ecosystems with (micro-) plastic particles. *Environmental chemistry*, *12*(5), 539–550. https://doi.org/10.1071/EN14172

Drummond, J. D., Schneidewind, U., Li, A., Hoellein, T. J., Krause, S., & Packman, A. I. (2022). Microplastic accumulation in riverbed sediment via hyporheic exchange from headwaters to mainstems. *Science Advances*, *8*(2), eabi9305. https://doi.org/10.1126/sciadv.abi9305

Duong, T. T., Nguyen-Thuy, D., Phuong, N. N., Ngo, H. M., Doan, T. O., Le, T. P. Q., Bui, H. M., Nguyen-Van, H., Nguyen-Dinh, T., Nguyen, T. A. N., et al. (2023). Microplastics in sediments from urban and suburban rivers: Influence of sediment properties. *Science of the Total Environment*, *904*, 166330. https://doi.org/10.1016/j.scitotenv.2023.166330

Dwivedi, A., Melville, B. W., Shamseldin, A. Y., & Guha, T. K. (2011). Flow structures and hydrodynamic force during sediment entrainment. *Water resources research*, *47*(1). https://doi.org/10.1029/2010WR009089

Egiazaroff, I. (1965). Calculation of nonuniform sediment concentrations. *Journal of the Hydraulics Division*, *91*(4), 225–247.

Einstein, H. A. (1942). Formulas for the transportation of bed load. *Transactions of the American Society of civil Engineers*, *107*(1), 561–577.

Einstein, H. A. (1950). *The bed-load function for sediment transportation in open channel flows*. US Department of Agriculture.

Einstein, H. A., & El-Samni, E.-S. A. (1949). Hydrodynamic forces on a rough wall. *Reviews of modern physics*, *21*(3), 520. https://doi.org/10.1103/RevModPhys.21.520

EN-1990:2002 Eurocode 0, Basis of Structural Design. (2001). European Committee for Standardization, CEN, 36 B-1050, Brussels.

Ermilov, A. A., Fleit, G., Conevski, S., Guerrero, M., Baranya, S., & Rüther, N. (2022). Bedload transport analysis using image processing techniques. *Acta Geophysica*, *70*(5), 2341–2360. https://doi.org/10.1007/s11600-022-00791-x

Everts, C. H. (1973). Particle overpassing on flat granular boundaries. *Journal of the Waterways, Harbors and Coastal Engineering Division*, *99*(4), 425–438. https://doi.org/10.1061/AWHCAR.0000211

Fenton, J., & Abbott, J. (1977). Initial movement of grains on a stream bed: The effect of relative protrusion. *Proceedings of the Royal Society of London. A. Mathematical and Physical Sciences*, *352*(1671), 523–537.

Ferreira, R. M., Hassan, M. A., & Ferrer-Boix, C. (2015). Principles of bedload transport of non-cohesive sediment in open-channels. *Rivers–Physical, Fluvial and Environmental Processes*, 323–372. https://doi.org/10.1007/978-3-319-17719-9_13

Finotello, A. (2017). *Tidal channel patterns: Field investigations, numerical modelling and laboratory experiments* [Doctoral dissertation]. Università degli studi di Padova.

Forchheimer, H. P. (1908). *Hydraulik*. Springer.

Forchheimer, H. P. (1926). *Grundriss der Hydraulik*. Springer.

Francis, J. (1973). Experiments on the motion of solitary grains along the bed of a water-stream. *Proceedings of the Royal Society of London. A. Mathematical and Physical Sciences*, *332*(1591), 443–471. https://doi.org/10.1098/rspa.1973.0037

Frascati, A., & Lanzoni, S. (2009). Morphodynamic regime and long-term evolution of meandering rivers. *Journal of Geophysical Research: Earth Surface*, *114*(F2). https://doi.org/10.1029/2008JF001101

Frei, S., Piehl, S., Gilfedder, B., Löoder, M. G., Krutzke, J., Wilhelm, L., & Laforsch, C. (2019). Occurence of microplastics in the hyporheic zone of rivers. *Scientific reports*, *9*(1), 15256. https://doi.org/10.1038/s41598-019-51741-5

Gabbott, S., Key, S., Russell, C., Yonan, Y., & Zalasiewicz, J. (2020). The geography and geology of plastics: Their environmental distribution and fate. In *Plastic waste and recycling* (pp. 33–63). Elsevier. https://doi.org/10.1016/B978-0-12-817880-5.00003-7

Garcia, M. (2008). Sedimentation engineering: Processes, measurements, modeling, and practice.

Gaudio, R., Miglio, A., & Dey, S. (2010). Non-universality of von Kármán's κ in fluvial streams. *Journal of Hydraulic Research*, *48*(5), 658–663. https://doi.org/10.1080/00221686.2010.507338

Gilbert, G. K. (1914). *The transportation of debris by running water*. US Government Printing Office.

Gill, T. W., & Pugh, C. A. (2009). Sediment transport similitude for scaled physical hydraulic modeling. *Proceedings of the 33rd IAHR Congress*, 9–14.

González-Fernández, D., Roebroek, C. T., Laufkötter, C., Cózar, A., & van Emmerik, T. H. (2023). Diverging estimates of river plastic input to the ocean. *Nature Reviews Earth & Environment*, 1–3. https://doi.org/10.1038/s43017-023-00448-3

Goral, K. D., Guler, H. G., Larsen, B. E., Carstensen, S., Christensen, E. D., Kerpen, N. B., Schlurmann, T., & Fuhrman, D. R. (2023a). Experimental Study on the Incipient Motion of Microplastic Particles with Different Shapes, Sizes, and Densities on a Live Sediment Bed. In *Coastal sediments 2023: The proceedings of the coastal sediments 2023* (pp. 1149–1155). World Scientific. https://doi.org/10.1142/9789811275135_0106

Goral, K. D., Guler, H. G., Larsen, B. E., Carstensen, S., Christensen, E. D., Kerpen, N. B., Schlurmann, T., & Fuhrman, D. R. (2023b). Settling velocity of microplastic particles having regular and irregular shapes. *Environmental Research*, *228*, 115783. https://doi.org/10.1016/j.envres.2023.115783

Gorrick, S., & Rodrìguez, J. F. (2014). Scaling of sediment dynamics in a laboratory model of a sand-bed stream. *Journal of Hydro-Environment Research*, *8*(2), 77–87. https://doi.org/10.1016/j.jher.2013.12.001

Graf, W., & Pazis, G. (1977). Desposition and erosion in an alluvial channel. *Journal of Hydraulic Research*, *15*(2), 151–166. https://doi.org/10.1080/00221687709499653

Grant, G. E., O'Connor, J. E., & Wolman, M. G. (2013). A river runs through it: Conceptual models in fluvial geomorphology. *Treatise on geomorphology*, *9, Fluvial Geomorphology*, 6–21. https://doi.org/10.1016/B978-0-12-374739-6.00227-X

Grass, A. J. (1970). Initial instability of fine bed sand. *Journal of the Hydraulics Division*, *96*(3), 619–632. https://doi.org/10.1061/JYCEAJ.0002369

Gvelesiani, L. G. (1970). Initial instability of fine bed sand. *Gidrotekhnicheskoe stroitelstvo*, *4*, 28–29.

Hassan, M. A., Parker, G., Hassan, Y., An, C., Fu, X., & Venditti, J. G. (2024). The roles of geometry and viscosity in the mobilization of coarse sediment by finer sediment. *Proceedings of the National Academy of Sciences*, *121*(38), e2409436121. https://doi.org/10.1073/pnas.2409436121

Heathershaw, A., & Thorne, P. (1985). Sea-bed noises reveal role of turbulent bursting phenomenon in sediment transport by tidal currents. *Nature*, *316*(6026), 339–342.

Henry, P., & Aberle, J. (2018). Hydralab+ Deliverable D8. 3 Protocols for scaling morphodynamics in time Zenodo. https://zenodo.org/records/2420824

Hjulström, F. (1932). Das Transportvermögen Der Flüsse: Und Die Bestimmung Des Erosionsbetrages. *Geografiska Annaler*, *14*(3-4), 244–258.

Hodge, R. A., & Buechel, M. E. (2022). The influence of bedrock river morphology and alluvial cover on gravel entrainment. Part 2: Modelling critical shear stress. *Earth Surface Processes and Landforms*, *47*(14), 3348–3360. https://doi.org/10.1002/esp.5462

Horton, A. A. (2022). Plastic pollution: When do we know enough? *Journal of Hazardous Materials*, *422*, 126885. https://doi.org/10.1016/j.jhazmat.2021.126885

Horton, A. A., Walton, A., Spurgeon, D. J., Lahive, E., & Svendsen, C. (2017). Microplastics in freshwater and terrestrial environments: Evaluating the current understanding to identify

the knowledge gaps and future research priorities. *Science of the total environment*, *586*, 127–141. https://doi.org/10.1016/j.scitotenv.2017.01.190

Hosseini-Sadabadi, S. A., Radice, A., & Ballio, F. (2019). On reasons of the scatter of literature data for bed-load particle hops. *Water Resources Research*, *55*(2), 1698–1706. https://doi.org/10.1029/2018WR023350

Houssais, M., & Jerolmack, D. J. (2017). Toward a unifying constitutive relation for sediment transport across environments. *Geomorphology*, *277*, 251–264. https://doi.org/10.1016/j.geomorph.2016.03.026

Hurley, R., Horton, A., Lusher, A., & Nizzetto, L. (2020). Plastic waste in the terrestrial environment. In *Plastic waste and recycling* (pp. 163–193). Elsevier. https://doi.org/10.1016/B978-0-12-817880-5.00007-4

Ippen, A. T., & Verma, R. P. (1955). Motion of particles on bed of a turbulent stream. *Transactions of the American Society of Civil Engineers*, *120*(1), 921–938.

Iuppa, C., Passalacqua, G., & Faraci, C. (2024). An equilibrium criterion for plastic debris fate in wave-driven transport. *Marine Pollution Bulletin*, *206*, 116758. https://doi.org/10.1016/j.marpolbul.2024.116758

Juez, C., Hassan, M. A., & Franca, M. J. (2018). The origin of fine sediment determines the observations of suspended sediment fluxes under unsteady flow conditions. *Water Resources Research*, *54*(8), 5654–5669. https://doi.org/10.1029/2018WR022982

Kennedy, S. K., Meloy, T. P., & Durney, T. (1985). Sieve data; size and shape information. *Journal of Sedimentary Research*, *55*(3), 356–360. https://doi.org/10.1306/212F86CA-2B24-11D7-8648000102C1865D

Keshavarzi, A., & Ball, J. (2011). Stochastic nature of flow turbulence and sediment particle entrainment over the ripples at the bed of open channel using image processing technique. In *Sediment transport, flow processes and morphology* (pp. 69–92). InTechOpen, Croatia.

Keshavarzy, A., & Ball, J. (1999). An application of image processing in the study of sediment motion. *Journal of Hydraulic Research*, *37*(4), 559–576. https://doi.org/10.1080/00221686.1999.9628268

Kirchner, J. W., Dietrich, W. E., Iseya, F., & Ikeda, H. (1990). The variability of critical shear stress, friction angle, and grain protrusion in water-worked sediments. *Sedimentology*, *37*(4), 647–672. https://doi.org/10.1111/j.1365-3091.1990.tb00627.x

Kocyigit, O., Lin, B., & Falconer, R. A. (2005). Modelling sediment transport using a lightweight bed material. *Proceedings of the Institution of Civil Engineers-Maritime Engineering*, *158*(1), 3–14.

Koelmans, A. A., Nor, N. H. M., Hermsen, E., Kooi, M., Mintenig, S. M., & De France, J. (2019). Microplastics in freshwaters and drinking water: Critical review and assessment of data quality. *Water Research*, *155*, 410–422. https://doi.org/10.1016/j.watres.2019.02.054

Komar, P. D. (1985). The hydraulic interpretation of turbidites from their grain sizes and sedimentary structures. *Sedimentology*, *32*(3), 395–407. https://doi.org/10.1111/j.1365-3091.1985.tb00519.x

Komar, P. D. (2007). The entrainment, transport and sorting of heavy minerals by waves and currents. *Developments in sedimentology*, *58*, 3–48. https://doi.org/10.1016/S0070-4571(07)58001-5

Komar, P. D., & Clemens, K. E. (1986). The relationship between a grain's settling velocity and threshold of motion under unidirectional currents. *Journal of Sedimentary Research*. https://doi.org/10.1306/212f88dc-2b24-11d7-8648000102c1865d

Komar, P. D., Morse, A. P., Small, L. F., & Fowler, S. W. (1981). An analysis of sinking rates of natural copepod and euphausiid fecal pellets 1. *Limnology and Oceanography*, *26*(1), 172–180. https://doi.org/10.4319/lo.1981.26.1.0172

Kramer, H. (1935). Sand mixtures and sand movement in fluvial model. *Transactions of the American Society of Civil Engineers*, *100*(1), 798–838.

Krey, H. (1925). Grenzen der Übertragbarkeit der Versuchsergebnisse und Modellähnlichkeit bei praktischen Flussbauversuchen. *Zeitschrift für Angewandte Mathematik und Mechanik*, *5*, 484–486.

Kuhnle, R. A., & Southard, J. B. (1990). Flume experiments on the transport of heavy minerals in gravel-bed streams. *Journal of Sedimentary Research*, *60*(5), 687–696. https://doi.org/10.1306/212F924B-2B24-11D7-8648000102C1865D

Lane, E., & Kalinske, A. (1939). The relation of suspended to bed material in rivers. *Eos, Transactions American Geophysical Union*, *20*(4), 637–641. https://doi.org/10.1029/TR020i004p00637

Lavelle, J. W., & Mofjeld, H. O. (1987). Do critical stresses for incipient motion and erosion really exist? *Journal of Hydraulic Engineering*, *113*(3), 370–385. https://doi.org/10.1061/(ASCE)0733-9429(1987)113:3(370)

Lechner, A. (2020). "Down by the River":(Micro-) Plastic Pollution of Running Freshwaters with Special Emphasis on the Austrian Danube. *Mare Plasticum-The Plastic Sea: Combatting Plastic Pollution Through Science and Art*, 141–185. https://doi.org/10.1007/978-3-030-38945-1_8

Lechner, A., Keckeis, H., Lumesberger-Loisl, F., Zens, B., Krusch, R., Tritthart, M., Glas, M., & Schludermann, E. (2014). The Danube so colourful: a potpourri of plastic litter outnumbers fish larvae in Europe's second largest river. *Environmental pollution*, *188*, 177–181. https://doi.org/10.1016/j.envpol.2014.02.006

Lee, H., & Balachandar, S. (2012). Critical shear stress for incipient motion of a particle on a rough bed. *Journal of Geophysical Research: Earth Surface*, *117*(F1). https://doi.org/10.1029/2011JF002208

Li, B., Mao, R., Chen, Z., Zhang, Y., Song, J., Li, N., Tang, B., Feng, J., & Guan, M. (2024). The competition of heavy metals between hyporheic sediments and microplastics of

driving factors in the Beiluo River Basin. *Journal of Hazardous Materials*, 134538. https://doi.org/10.1016/j.jhazmat.2024.134538

Li, J., Liu, H., & Chen, J. P. (2018). Microplastics in freshwater systems: A review on occurrence, environmental effects, and methods for microplastics detection. *Water Research*, *137*, 362–374. https://doi.org/10.1016/j.watres.2017.12.056

Li, P., Wang, X., Su, M., Zou, X., Duan, L., & Zhang, H. (2021). Characteristics of plastic pollution in the environment: A review. *Bulletin of environmental contamination and toxicology*, *107*, 577–584.

Liedermann, M., Gmeiner, P., Pessenlehner, S., Haimann, M., Hohenblum, P., & Habersack, H. (2018). A methodology for measuring microplastic transport in large or medium rivers. *Water*, *10*(4), 414. https://doi.org/10.3390/w10040414

Liro, M., Zielonka, A., & van Emmerik, T. H. (2023). Macroplastic fragmentation in rivers. *Environment International*, *180*, 108186. https://doi.org/10.1016/j.envint.2023.108186

Lofty, J., Valero, D., Moreno-Rodenas, A., Belay, B. S., Wilson, C., Ouro, P., & Franca, M. J. (2024). On the vertical structure of non-buoyant plastics in turbulent transport. *Water Research*, *254*, 121306. https://doi.org/10.1016/j.watres.2024.121306

Lofty, J., Valero, D., Wilson, C. A., Franca, M. J., & Ouro, P. (2023). Microplastic and natural sediment in bed load saltation: Material does not dictate the fate. *Water Research*, *243*, 120329. https://doi.org/10.1016/j.watres.2023.120329

Longo, S. G. (2022). Physical Models in River Hydraulics. In *Principles and applications of dimensional analysis and similarity* (pp. 329–349). Springer.

Lu, H., Raupach, M. R., & Richards, K. S. (2005). Modeling entrainment of sedimentary particles by wind and water: A generalized approach. *Journal of Geophysical Research: Atmospheres*, *110*(D24). https://doi.org/10.1029/2005JD006418

Luo, X., Wang, Z., Yang, L., Gao, T., & Zhang, Y. (2022). A review of analytical methods and models used in atmospheric microplastic research. *Science of The Total Environment*, *828*, 154487. https://doi.org/10.1016/j.scitotenv.2022.154487

Mantz, P. A. (1977). Incipient transport of fine grains and flakes by fluids—extended shields diagram. *Journal of the Hydraulics division*, *103*(6), 601–615. https://doi.org/10.1061/JYCEAJ.0004766

Maynord, S. T. (2006). Evaluation of the micromodel: An extremely small-scale movable bed model. *Journal of hydraulic engineering*, *132*(4), 343–353. https://doi.org/10.1061/(asce)0733-9429(2006)132:4(343)

Meyering, H. (2012). *Effect of sediment density in bridge pier scour experiments* [Doctoral dissertation, Technische Universität Braunschweig].

Meyer-Peter, E., & Müller, R. (1948). Formulas for bed-load transport. *Proceedings of the 2nd IAHR Congress, Stockholm*, *A2*, 31.

Miller, M. C., McCave, I. N., & Komar, P. (1977). Threshold of sediment motion under unidirectional currents. *Sedimentology*, *24*(4), 507–527. https://doi.org/10.1111/j.1365-3091.1977.tb00136.x

Miura, K., Maeda, K., Furukawa, M., & Toki, S. (1997). Physical characteristics of sands with different primary properties. *Soils and Foundations*, *37*(3), 53–64.

Mrokowska, M. M., & Krztoń-Maziopa, A. (2024). Settling of microplastics in mucus-rich water column: The role of biologically modified rheology of seawater. *Science of The Total Environment*, *912*, 168767. https://doi.org/10.1016/j.scitotenv.2023.168767

Neill, C. R. (1967). Mean-velocity criterion for scour of coarse uniform bed-material. *Proceedings of the 12th Congress of the International Association of Hydraulics Research*, *3*, 46–54.

Neill, C. R., van Der Giessen, N., Blench, T., Mavis, F. T., & Laushey, L. M. (1966). Discussion of "Sediment Transportation Mechanics: Initiation of Motion, Progress Report of the Task Committee on Preparation of Sedimentation Manual, Committee on Sedimentation". *Journal of the Hydraulics Division*, *92*(5), 280–291.

Nelson, J. M., Shreve, R. L., McLean, S. R., & Drake, T. G. (1995). Role of near-bed turbulence structure in bed load transport and bed form mechanics. *Water resources research*, *31*(8), 2071–2086. https://doi.org/10.1029/95WR00976

Nezu, I., & Rodi, W. (1986). Open-channel flow measurements with a laser Doppler anemometer. *Journal of hydraulic engineering*, *112*(5), 335–355. https://doi.org/10.1061/(ASCE)0733-9429(1986)112:5(335)

Nikora, V., Ballio, F., Coleman, S., & Pokrajac, D. (2013). Spatially averaged flows over mobile rough beds: Definitions, averaging theorems, and conservation equations. *Journal of Hydraulic Engineering*, *139*(8), 803–811. https://doi.org/10.1061/(ASCE)HY.1943-7900.0000738

Nikora, V., McEwan, I., McLean, S., Coleman, S., Pokrajac, D., & Walters, R. (2007). Double-averaging concept for rough-bed open-channel and overland flows: Theoretical background. *Journal of hydraulic Engineering*, *133*(8), 873–883. https://doi.org/10.1061/(ASCE)0733-9429(2007)133:8(873)

Nikuradse, J. (1933). Gesetzmäßigkeiten der turbulenten Strömung in glatten Rohren (Nachtrag). *Forschung auf dem Gebiet des Ingenieurwesens*, *4*(1), 44–44.

Niño, Y., Lopez, F., & Garcia, M. (2003). Threshold for particle entrainment into suspension. *Sedimentology*, *50*(2), 247–263. https://doi.org/10.1046/j.1365-3091.2003.00551.x

Nyberg, B., Harris, P. T., Kane, I., & Maes, T. (2023). Leaving a plastic legacy: Current and future scenarios for mismanaged plastic waste in rivers. *Science of the Total Environment*, *869*, 161821. https://doi.org/10.1016/j.scitotenv.2023.161821

Ockelford, A., & Yager, E. (2022). 9.7 The Initiation of Sediment Motion and Formation of Armor Layers. In *Treatise on geomorphology* (pp. 176–199, Vol. 6.1). Elsevier. https://doi.org/10.1016/B978-0-12-818234-5.00005-5

Pähtz, T., Clark, A. H., Valyrakis, M., & Durán, O. (2020). The physics of sediment transport initiation, cessation, and entrainment across aeolian and fluvial environments. *Reviews of Geophysics*, *58*(1), e2019RG000679. https://doi.org/10.1029/2019RG000679

Pähtz, T., & Durán, O. (2020). Unification of aeolian and fluvial sediment transport rate from granular physics. *Physical Review Letters*, *124*(16), 168001. https://doi.org/10.1103/PhysRevLett.124.168001

Paintal, A. (1971). A stochastic model of bed load transport. *Journal of Hydraulic Research*, *9*(4), 527–554. https://doi.org/10.1080/00221687109500371

Paola, C., Straub, K., Mohrig, D., & Reinhardt, L. (2009). The "unreasonable effectiveness" of stratigraphic and geomorphic experiments. *Earth-Science Reviews*, *97*(1-4), 1–43. https://doi.org/10.1016/j.earscirev.2009.05.003

Paphitis, D. (2001). Sediment movement under unidirectional flows: An assessment of empirical threshold curves. *Coastal engineering*, *43*(3-4), 227–245. https://doi.org/10.1016/S0378-3839(01)00015-1

Parker, G., An, C., Lamb, M. P., Garcia, M. H., Dingle, E. H., & Venditti, J. G. (2024). Dimensionless argument: A narrow grain size range near 2 mm plays a special role in river sediment transport and morphodynamics. *Earth Surface Dynamics*, *12*(1), 367–380. https://doi.org/10.5194/esurf-12-367-2024

Parker, G., Klingeman, P. C., & McLean, D. G. (1982). Bedload and size distribution in paved gravel-bed streams. *Journal of the Hydraulics Division*, *108*(4), 544–571. https://doi.org/10.1061/JYCEAJ.0005854

Pektaş, A. O. (2015). Determining the essential parameters of bed load and suspended sediment load. *International Journal of Global Warming*, *8*(3), 335–359. https://doi.org/10.1504/IJGW.2015.072656

Persson, L., Carney Almroth, B. M., Collins, C. D., Cornell, S., De Wit, C. A., Diamond, M. L., Fantke, P., Hassellöv, M., MacLeod, M., Ryberg, M. W., et al. (2022). Outside the safe operating space of the planetary boundary for novel entities. *Environmental science & technology*, *56*(3), 1510–1521. https://doi.org/10.1021/acs.est.1c04158

Peters, J. (1990). Scaling of sediment transport phenomena in large alluvial rivers with very low slopes. In *Movable bed physical models* (pp. 149–158). Springer.

Petit, F. (1994). Dimensionless critical shear stress evaluation from flume experiments using different gravel beds. *Earth Surface Processes and Landforms*, *19*(6), 565–576. https://doi.org/10.1002/esp.3290190608

Petruzzelli, V., Garcia, V. G., Cobos, F. X. G. i., & Petrillo, A. F. (2013). On the use of lightweight materials in small-scale mobile bed physical models. *Journal of Coastal Research*, (65), 1575–1580. https://doi.org/10.2112/SI65-266.1

Pfohl, P., Wagner, M., Meyer, L., Domercq, P., Praetorius, A., Hüffer, T., Hofmann, T., & Wohlleben, W. (2022). Environmental degradation of microplastics: How to measure fragmentation rates to secondary micro-and nanoplastic fragments and dissociation

into dissolved organics. *Environmental Science & Technology*, *56*(16), 11323–11334. https://doi.org/10.1021/acs.est.2c01228

Pokrajac, D., Finnigan, J., Manes, C., McEwan, I., & Nikora, V. (2006). On the definition of the shear velocity in rough bed open channel flows. *River flow*, *1*, 89–98.

Prancevic, J. P., & Lamb, M. P. (2015). Unraveling bed slope from relative roughness in initial sediment motion. *Journal of Geophysical Research: Earth Surface*, *120*(3), 474–489. https://doi.org/10.1002/2014JF003323

Radice, A., Malavasi, S., & Ballio, F. (2008). Sediment kinematics in abutment scour. *Journal of Hydraulic Engineering*, *134*(2), 146–156. https://doi.org/10.1061/(ASCE)0733-9429(2008)134:2(146)

Radice, A., Sarkar, S., & Ballio, F. (2017). Image-based lagrangian particle tracking in bed-load experiments. *JoVE (Journal of Visualized Experiments)*, (125), e55874. https://doi.org/10.3791/55874

Rebai, D., Radice, A., & Ballio, F. (2024). Traveling or jiggling: Particle motion modes and their relative contribution to bed-load variables. *Journal of Geophysical Research: Earth Surface*, *129*(8), e2024JF007637. https://doi.org/10.1029/2024JF007637

Rieux, A., Weill, P., Mouaze, D., Poirier, C., Nechenache, F., Perez, L., & Tessier, B. (2019). Threshold of motion and settling velocities of mollusc shell debris: Influence of faunal composition. *Sedimentology*, *66*(3), 895–916. https://doi.org/10.1111/sed.12521

Rochman, C. M., Hentschel, B. T., & Teh, S. J. (2014). Long-term sorption of metals is similar among plastic types: Implications for plastic debris in aquatic environments. *PLOS one*, *9*(1), e85433. https://doi.org/10.1371/journal.pone.0085433

Rohais, S., Armitage, J. J., Romero-Sarmiento, M.-F., Pierson, J.-L., Teles, V., Bauer, D., Cassar, C., Sebag, D., Klopffer, M.-H., & Pelerin, M. (2024). A source-to-sink perspective of an anthropogenic marker: A first assessment of microplastics concentration, pathways, and accumulation across the environment. *Earth-Science Reviews*, 104822. https://doi.org/10.1016/j.earscirev.2024.104822

Roseberry, J. C., Schmeeckle, M. W., & Furbish, D. J. (2012). A probabilistic description of the bed load sediment flux: 2. Particle activity and motions. *Journal of Geophysical Research: Earth Surface*, *117*(F3). https://doi.org/10.1029/2012JF002353

Roušar, L., Zachoval, Z., & Julien, P. (2016). Incipient motion of coarse uniform gravel. *Journal of Hydraulic Research*, *54*(6), 615–630. https://doi.org/10.1080/00221686.2016.1212286

Rouse, H. (1940). Criteria for similarity in the transportation of sediment. *University of Iowa Studies in Engineering*, *20*, 33–49.

Rubey, W. W. (1933). Settling velocities of gravel, sand and silt particles. *American Journal of Science*, *25*, 325–338.

Rubey, W. W. (1938). *The force required to move particles on a stream bed* (tech. rep.).

Russell, C. E., Fernández, R., Parsons, D. R., & Gabbott, S. E. (2023). Plastic pollution in riverbeds fundamentally affects natural sand transport processes. *Communications Earth & Environment*, *4*(1), 255. https://doi.org/10.1038/s43247-023-00820-7

Russell, C. E., Pohl, F., & Fernández, R. (2024). Plastic as a sediment–a universal and objective practical solution to growing ambiguity in plastic litter classification schemes. *Earth-Science Reviews*, 104994. https://doi.org/10.1016/j.earscirev.2024.104994

Schmidt, C., Krauth, T., & Wagner, S. (2017). Export of plastic debris by rivers into the sea. *Environmental science & technology*, *51*(21), 12246–12253. https://doi.org/10.1021/acs.est.7b02368

Schoklitsch, A. (1914). *Über Schleppkraft und Geschiebebewegung*. W. Engelmann.

Schoklitsch, A. (1926). *Geschiebebewegung in Flüssen und an Stauwerken*. Springer-Verlag Wien Gmbh. https://doi.org/10.1007/978-3-7091-4760-3

Seng Low, H. (1989). Effect of sediment density on bed-load transport. *Journal of Hydraulic Engineering*, *115*(1), 124–138. https://doi.org/10.1061/(ASCE)0733-9429(1989)115:1(124)

Shields, A. (1936). Anwendung der Ähnlichkeitsmechanik und der Turbulenzforschung auf die Geschiebebewegung. *Mitteilungen der Preussische Versuchsanstalt für Wasserbau und Schiffbau, Berlin, Heft*, *26*.

Shvidchenko, A. B., & Pender, G. (2000). Flume study of the effect of relative depth on the incipient motion of coarse uniform sediments. *Water Resources Research*, *36*(2), 619–628. https://doi.org/10.1029/1999WR900312

Shvidchenko, A. B. (2000). *Incipient motion of streambeds* [Doctoral dissertation, University of Glasgow].

Shvidchenko, A. B., Pender, G., & Hoey, T. B. (2001). Critical shear stress for incipient motion of sand/gravel streambeds. *Water Resources Research*, *37*(8), 2273–2283. https://doi.org/10.1029/2000WR000036

Slingerland, R. L. (1977). The effects of entrainment on the hydraulic equivalence relationships of light and heavy minerals in sands. *Journal of Sedimentary Research*, *47*(2), 753–770. https://doi.org/10.1306/212F7243-2B24-11D7-8648000102C1865D

Sutherland, A. J. (1967). Proposed mechanism for sediment entrainment by turbulent flows. *Journal of Geophysical Research*, *72*(24), 6183–6194. https://doi.org/10.1029/JZ072i024p06183

Sutherland, B. (2024, April 4). Transport and Settling of Microplastics in Turbidity Currents. https://doi.org/10.52843/cassyni.b9bpd0

Task Committee on Preparation of Sedimentation Manual Committee on Sedimentation. (1966). Sediment transportation mechanics: Initiation of motion. *Journal of the Hydraulics Division*, *92*(2), 291–314.

Thélusmond, J. R., Chevalier, L. R., & DeVantier, B. A. (2013). The use of plastic media in a movable bed model to study sedimentary processes in rivers. *International Journal of*

Hydrology Science and Technology, *3*(2), 93–110. https://doi.org/10.1504/IJHST.2013.057622

Thompson, R. C., Olsen, Y., Mitchell, R. P., Davis, A., Rowland, S. J., John, A. W., McGonigle, D., & Russell, A. E. (2004). Lost at sea: Where is all the plastic? *Science*, *304*(5672), 838–838. https://doi.org/10.1126/science.1094559

Un plastics treaty: Don't let lobbyists drown out researchers [Editorial]. (2024). https://doi.org/10.1038/d41586-024-01089-2

UNEP. (2022). UNEA Resolution 5/14 entitled " End plastic pollution: Towards an international legally binding instrument". *UNEP/EA. 5/Res. 14*.

USWES. (1936). *Studies of light-weight materials with special reference to their movement and use as model bed material* (tech. rep.). U.S. Waterways Experiment Station, Vicksburg, Mississippi, USA.

Valyrakis, M., Diplas, P., Dancey, C. L., Greer, K., & Celik, A. O. (2010). Role of instantaneous force magnitude and duration on particle entrainment. *Journal of Geophysical Research: Earth Surface*, *115*(F2). https://doi.org/10.1029/2008JF001247

Van Rijn, L. C. (1984). Sediment transport, part I: bed load transport. *Journal of hydraulic engineering*, *110*(10), 1431–1456. https://doi.org/10.1061/(ASCE)0733-9429(1984)110:10(1431)

Vanoni, V. A. (1964). *Measurements of critical shear stress for entraining fine sediments in a boundary layer* (tech. rep. No. Report KH-R-7). California Institute of Technology.

Viparelli, E., Solari, L., & Hill, K. (2015). Downstream lightening and upward heavying: Experiments with sediments differing in density. *Sedimentology*, *62*(5), 1384–1407. https://doi.org/10.1111/sed.12187

Vollmer, S., & Kleinhans, M. G. (2007). Predicting incipient motion, including the effect of turbulent pressure fluctuations in the bed. *Water Resources Research*, *43*(5). https://doi.org/10.1029/2006WR004919

Wagner, M., Scherer, C., Alvarez-Muñoz, D., Brennholt, N., Bourrain, X., Buchinger, S., Fries, E., Grosbois, C., Klasmeier, J., Marti, T., et al. (2014). Microplastics in freshwater ecosystems: What we know and what we need to know. *Environmental Sciences Europe*, *26*(1), 1–9. https://doi.org/10.1186/s12302-014-0012-7

Waldschläger, K., Born, M., Cowger, W., Gray, A., & Schüttrumpf, H. (2020). Settling and rising velocities of environmentally weathered micro-and macroplastic particles. *Environmental Research*, *191*, 110192. https://doi.org/10.1016/j.envres.2020.110192

Waldschläger, K., Brückner, M. Z., Almroth, B. C., Hackney, C. R., Adyel, T. M., Alimi, O. S., Belontz, S. L., Cowger, W., Doyle, D., Gray, A., et al. (2022). Learning from natural sediments to tackle microplastics challenges: A multidisciplinary perspective. *Earth-Science Reviews*, *228*, 104021. https://doi.org/10.1016/j.earscirev.2022.104021

Waldschläger, K., & Schüttrumpf, H. (2019a). Effects of particle properties on the settling and rise velocities of microplastics in freshwater under laboratory conditions. *Environmental science & technology*, *53*(4), 1958–1966. https://doi.org/10.1021/acs.est.8b06794

Waldschläger, K., & Schüttrumpf, H. (2019b). Erosion behavior of different microplastic particles in comparison to natural sediments. *Environmental science & technology*, *53*(22), 13219–13227. https://doi.org/10.1021/acs.est.9b05394

Wang, X., Li, Z., Sun, B., Wang, F., & Gualtieri, C. (2024). Impact of Fenton aging on the incipient motion of microplastic particles in open-channel flow. *Science of The Total Environment*, 176220. https://doi.org/10.1016/j.scitotenv.2024.176220

Weill, P., Mouazé, D., Tessier, B., & Brun-Cottan, J.-C. (2010). Hydrodynamic behaviour of coarse bioclastic sand from shelly cheniers. *Earth Surface Processes and Landforms*, *35*(14), 1642–1654. https://doi.org/10.1002/esp.2004

White, C. (1940). The equilibrium of grains on the bed of a stream. *Proceedings of the Royal Society of London. Series A. Mathematical and Physical Sciences*, *174*(958), 322–338. https://doi.org/10.1098/rspa.1940.0023

Wiberg, P. L., & Smith, J. D. (1987). Calculations of the critical shear stress for motion of uniform and heterogeneous sediments. *Water resources research*, *23*(8), 1471–1480. https://doi.org/10.1029/WR023i008p01471

Wilcock, P. R., & Southard, J. B. (1988). Experimental study of incipient motion in mixed-size sediment. *Water Resources Research*, *24*(7), 1137–1151. https://doi.org/10.1029/WR024i007p01137

Witz, M. J., Cameron, S., & Nikora, V. (2019). Bed particle dynamics at entrainment. *Journal of Hydraulic Research*. https://doi.org/10.1080/00221686.2018.1489898

Wohl, E. (2013). 9.33 Field and Laboratory Experiments in Fluvial Geomorphology. In J. F. Shroder (Ed.), *Treatise on geomorphology* (pp. 679–693). Academic Press. https://doi.org/10.1016/B978-0-12-374739-6.00260-8

Wohlleben, W., Bossa, N., Mitrano, D. M., & Scott, K. (2024). Everything falls apart: How solids degrade and release nanomaterials, composite fragments, and microplastics. *NanoImpact*, *34*, 100510. https://doi.org/10.1016/j.impact.2024.100510

Wolman, M. G., & Brush, L. M. (1961). *Factors controlling the size and shape of stream channels in coarse noncohesive sands*. US Government Printing Office.

Yager, E. M., Schmeeckle, M. W., & Badoux, A. (2018). Resistance is not futile: Grain resistance controls on observed critical shields stress variations. *Journal of Geophysical Research: Earth Surface*, *123*(12), 3308–3322. https://doi.org/10.1029/2018JF004817

Yalin, M. S. (1963). An expression for bed-load transportation. *Journal of the Hydraulics Division*, *89*(3), 221–250.

Yalin, M. S. (1972). Mechanics of sediment transport.

Yalin, M. S., & Karahan, E. (1979). Inception of sediment transport. *Journal of the hydraulics division*, *105*(11), 1433–1443. https://doi.org/10.1061/JYCEAJ.0005306

Yang, C. T. (1973). Incipient motion and sediment transport. *Journal of the hydraulics division*, *99*(10), 1679–1704. https://doi.org/10.1061/JYCEAJ.0003766

Yu, Z., Loewen, M., Guo, S., Guo, Z., & Zhang, W. (2023). Investigation of the Sheltering Effects on the Mobilization of Microplastics in Open-Channel Flow. *Environmental Science & Technology*, *57*(30), 11259–11266. https://doi.org/10.1021/acs.est.3c02500

Yu, Z., Yao, W., Loewen, M., Li, X., & Zhang, W. (2022). Incipient motion of exposed microplastics in an open-channel flow. *Environmental Science & Technology*, *56*(20), 14498–14506. https://doi.org/10.1021/acs.est.2c04415

Zanke, U. C. E. (1977). Neuer Ansatz zur Berechnung des Transportbeginns von Sedimenten unter Stromungseinfluss. *Mitteilungen Des Franzius-Institut*.

Zanke, U. C. E. (2003). On the influence of turbulence on the initiation of sediment motion. *International journal of sediment research*, *18*(1), 17–31.

Zbyszewski, M., & Corcoran, P. L. (2011). Distribution and degradation of fresh water plastic particles along the beaches of Lake Huron, Canada. *Water, Air, & Soil Pollution*, *220*, 365–372. https://doi.org/10.1007/s11270-011-0760-6

Appendices

Appendix A

Glossary

A.1 List of key terms

Herein are listed some frequently recurring terms in this Thesis alongside their definition.

Equilibrium: mutual adjustment of sediment transport and fluid dynamics which does not change topography features (e.g. slope) at the local level.
Incipient motion: The beginning of movement of a bed particle under a forcing flow.
Mobility: The capacity of a particle of being put into motion by a forcing flow.
Morphotype: morphological characterisation for microplastics' shape, where it is considered whether: (i) a microplastic has 1, 2 or 3 main axes (corresponding respectively to fibers, flat fragments or films, and "general" particles), and (ii) its shape has cavities *non-compact shape* or not *compact shape*.
Quasi-equilibrium: short-term equilibrium, in the analysed time window. A combination of quasi-equilibrium conditions can constitute a simplified model for a transient.
Quasi-uniform flow: condition in which, locally, uniform flow can be assumed. In our case, the flow was quasi-uniform as the bed slope and water surface slope were parallel within the accuracy of our measurements ($\pm$ 1 mm). Within this assumption we can apply uniform flow relations.
Remobilisation: motion of particles previously deposited on a bed, differing from the bed material in terms of e.g. size, density.
Threshold conditions: deterministic concept relating a change of state, in this case in terms of kinematics, from static to moving (at equilibrium). Threshold conditions are sought for, and are key points to identify, since the behaviour of the system at study changes as the threshold is surpassed.

Appendix B

Summary tables

Summary tables for HML experiments. For plastics on plastics experiments, the discharge conditions tested were three, with three repetitions each, resulting in nine measured conditions per cross-section. For plastics on a clastic bed, we tested for both PA6 and POM five different discharge conditions, with five increasing surface concentrations of plastics, without repetitions. A tentative dataset, discarded in this work for further analysis, contains HML plastics on clastic bed tests with UB-Lab P device: it consists of five discharge conditions by respectively five and three surface concentrations for POM and PA6 sediments.

B.1 Incipient motion experiments: plastics on plastics bed

PA6: discharge conditions chosen were such that we could observe incipient motion at a depth of around 6 cm. Other parameters in the following tables were derived from the measurements.
Data for XS1 are reported below

test	Q[l/s]	$\bar{y}[cm]$	Re	Flow type	U^* [m/s]	Re*	Near-wall regime
Q1t1	1.9 ±0.02	5.9 ±0.1	7667	turbulent	0.0107	31.96	transitional
Q1t2	1.9 ±0.02	5.9 ±0.1	7667	turbulent	0.0096	28.66	transitional
Q1t3	1.9 ±0.02	5.8 ±0.1	7667	turbulent	0.0113	33.90	transitional
Q2t1	2.0 ±0.02	5.8 ±0.1	8000	turbulent	0.0087	23.26	transitional
Q2t2	2.0 ±0.02	5.9 ±0.1	8000	turbulent	0.0101	30.20	transitional
Q2t3	2.1 ±0.02	5.9 ±0.1	8000	turbulent	0.0103	30.81	transitional
Q3t1	2.1 ±0.02	6.0 ±0.1	8333	turbulent	0.0082	24.61	transitional
Q3t2	2.1 ±0.02	6.0 ±0.1	8333	turbulent	0.0082	24.60	transitional
Q3t3	2.1 ±0.02	6.0 ±0.1	8333	turbulent	0.0093	28.03	transitional

Data for XS2 are reported below

test	Q[l/s]	$\bar{y}[cm]$	Re	Flow type	U^* [m/s]	Re*	Near-wall regime
Q1t1	1.9 ±0.02	6.0 ±0.1	7667	turbulent	0.0096	28.84	transitional
Q1t2	1.9 ±0.02	6.0 ±0.1	7667	turbulent	0.0102	30.66	transitional
Q1t3	1.9 ±0.02	6.0 ±0.1	7667	turbulent	0.0093	27.85	transitional
Q2t1	2.0 ±0.02	5.9 ±0.1	8000	turbulent	0.0087	26.24	transitional
Q2t2	2.0 ±0.02	6.0 ±0.1	8000	turbulent	0.0116	34.90	transitional
Q2t3	2.0 ±0.02	6.0 ±0.1	8000	turbulent	0.0101	30.30	transitional
Q3t1	2.1 ±0.02	6.1 ±0.1	8333	turbulent	0.0095	28.54	transitional
Q3t2	2.1 ±0.02	6.1 ±0.1	8333	turbulent	0.0093	37.81	transitional
Q3t3	2.1 ±0.02	6.1 ±0.1	8333	turbulent	0.0097	29.23	transitional

Data for XS3 are reported below

test	Q[l/s]	$\bar{y}[cm]$	Re	Flow type	U^* [m/s]	Re*	Near-wall regime
Q1t1	1.9 ±0.02	6.1 ±0.1	7667	turbulent	0.0093	27.87	transitional
Q1t2	1.9 ±0.02	6.1 ±0.1	7667	turbulent	0.0095	28.52	transitional
Q1t3	1.9 ±0.02	6.3 ±0.2	7667	turbulent	0.0104	31.34	transitional
Q2t1	2.0 ±0.02	6.0 ±0.1	8000	turbulent	0.0079	23.71	transitional
Q2t2	2.0 ±0.02	6.1 ±0.1	8000	turbulent	0.0105	31.55	transitional
Q2t3	2.0 ±0.02	6.1 ±0.1	8000	turbulent	0.0095	28.38	transitional
Q3t1	2.1 ±0.02	6.2 ±0.1	8333	turbulent	0.0096	28.73	transitional
Q3t2	2.1 ±0.02	6.2 ±0.1	8333	turbulent	0.0095	28.59	transitional
Q3t3	2.1 ±0.02	6.2 ±0.1	8333	turbulent	0.0093	27.82	transitional

Data for XS4 are reported below

test	Q[l/s]	$\bar{y}[cm]$	Re	Flow type	U^* [m/s]	Re*	Near-wal regime
Q1t1	1.9 ±0.02	6.2 ±0.1	7667	turbulent	0.0088	26.42	transitional
Q1t2	1.9 ±0.02	6.2 ±0.1	7667	turbulent	0.0110	33.11	transitional
Q1t3	1.9 ±0.02	6.2 ±0.1	7667	turbulent	0.0115	34.56	transitional
Q2t1	2.0 ±0.02	6.1 ±0.01	8000	turbulent	0.0092	27.66	transitional
Q2t2	2.0 ±0.02	6.2 ±0.1	8000	turbulent	0.0098	29.43	transitional
Q2t3	2.0 ±0.02	6.2 ±0.1	8000	turbulent	0.0113	33.83	transitional
Q3t1	2.1 ±0.02	6.4 ±0.1	8333	turbulent	0.0074	22.21	transitional
Q3t2	2.1 ±0.02	6.3 ±0.1	8333	turbulent	0.0106	31.71	transitional
Q3t3	2.1 ±0.02	6.3 ±0.1	8333	turbulent	0.0101	30.18	transitional

POM: discharge conditions chosen were such that we could observe incipient motion at a depth of around 4.5 cm. Other parameters in the following tables were derived from the measurements.

Data for XS2 are reported below

test	Q[l/s]	$\bar{y}[cm]$	Re	Flow type	U^* [m/s]	Re*	Near-wall regime
Q1t1	2.3 ±0.03	4.4 ±0.1	9333	turbulent	0.0135	40.39	transitional
Q1t2	2.3 ±0.03	4.4 ±0.1	9333	turbulent	0.0165	49.46	transitional
Q1t3	2.3 ±0.03	4.4 ±0.1	9333	turbulent	0.0160	47.99	transitional
Q2t1	2.4 ±0.03	4.4 ±0.1	9667	turbulent	0.0177	53.10	transitional
Q2t2	2.4 ±0.03	4.5 ±0.1	9667	turbulent	0.0172	51.49	transitional
Q2t3	2.4 ±0.03	4.5 ±0.1	9667	turbulent	0.0194	58.06	transitional
Q3t1	2.5 ±0.03	4.4 ±0.1	10000	turbulent	0.0207	62.18	transitional
Q3t2	2.5 ±0.03	4.5 ±0.1	10000	turbulent	0.0183	54.87	transitional
Q3t3	2.5 ±0.03	4.4 ±0.1	10000	turbulent	0.0166	49.74	transitional

Data for XS3 are reported below

test	Q[l/s]	$\bar{y}[cm]$	Re	Flow type	U^* [m/s]	Re*	Near-wall regime
Q1t1	2.3 ±0.03	4.5 ±0.1	9333	turbulent	0.0171	51.31	transitional
Q1t2	2.3 ±0.03	4.5 ±0.1	9333	turbulent	0.0192	57.52	transitional
Q1t3	2.3 ±0.03	4.5 ±0.1	9333	turbulent	0.0190	56.95	transitional
Q2t1	2.4 ±0.03	4.5 ±0.1	9667	turbulent	0.0171	51.28	transitional
Q2t2	2.4 ±0.03	4.5 ±0.1	9667	turbulent	0.0192	57.54	transitional
Q2t3	2.4 ±0.03	4.5 ±0.1	9667	turbulent	0.0184	55.19	transitional
Q3t1	2.5 ±0.03	4.5 ±0.1	10000	turbulent	0.0167	50.17	transitional
Q3t2	2.5 ±0.03	4.6 ±0.1	10000	turbulent	0.0159	47.69	transitional
Q3t3	2.5 ±0.03	4.4 ±0.1	10000	turbulent	0.059	47.75	transitional

Data for XS4 are reported below

test	Q[l/s]	$\bar{y}[cm]$	Re	Flow type	U^* [m/s]	Re*	Near-wall regime
Q1t1	2.3 ±0.03	4.5 ±0.1	9333	turbulent	0.0185	55.63	transitional
Q1t2	2.3 ±0.03	4.5 ±0.1	9333	turbulent	0.0181	54.39	transitional
Q1t3	2.3 ±0.03	4.5 ±0.1	9333	turbulent	0.0173	51.78	transitional
Q2t1	2.4 ±0.03	4.5 ±0.1	9667	turbulent	0.0162	48.57	transitional
Q2t2	2.4 ±0.03	4.5 ±0.1	9667	turbulent	0.0193	57.90	transitional
Q2t3	2.4 ±0.03	4.5 ±0.1	9667	turbulent	0.0160	47.90	transitional
Q3t1	2.5 ±0.03	4.5 ±0.1	10000	turbulent	0.0182	54.49	transitional
Q3t2	2.5 ±0.03	4.7 ±0.1	10000	turbulent	0.0179	53.64	transitional
Q3t3	2.5 ±0.03	4.6 ±0.1	10000	turbulent	0.0168	50.45	transitional

B.2 Incipient motion experiments: plastics on clastic bed

In the following, summary tables for the clastic bed experiments report the hydraulic conditions modelled.

B.2.1 Gravel: PA6

test	Q[l/s]	$\bar{y}[cm]$	Re(R_H)	Flow type	Near-wall regime
Q1c1	1.92 ±0.05	4.7 ±0.1	22244	turbulent	transitional
Q1c2	1.92 ±0.05	4.7 ±0.1	22244	turbulent	transitional
Q1c3	1.92 ±0.05	4.7 ±0.1	22244	turbulent	transitional
Q1c4	1.92 ±0.05	4.7 ±0.1	22244	turbulent	transitional
Q1c5	1.92 ±0.05	4.7 ±0.1	22244	turbulent	transitional
Q2c1	2.0 ±0.03	4.8 ±0.1	23166	turbulent	transitional
Q2c2	2.0 ±0.03	4.8 ±0.1	23166	turbulent	transitional
Q2c3	2.0 ±0.03	4.8 ±0.1	23166	turbulent	transitional
Q2c4	2.0 ±0.03	4.8 ±0.1	23166	turbulent	transitional
Q2c5	2.0 ±0.03	4.8 ±0.1	23166	turbulent	transitional
Q3c1	2.08 ±0.05	4.7 ±0.1	24178	turbulent	transitional
Q3c2	2.08 ±0.05	4.7 ±0.1	24178	turbulent	transitional
Q3c3	2.08 ±0.05	4.8 ±0.1	24178	turbulent	transitional
Q3c4	2.08 ±0.05	4.7 ±0.1	24178	turbulent	transitional
Q3c5	2.08 ±0.05	4.7 ±0.1	24178	turbulent	transitional

B.2.2 Gravel: POM

test	Q[l/s]	$\bar{y}[cm]$	Re(R_H)	Flow type	Near-wall regime
Q1c1	2.50 ±0.02	4.8 ±0.1	28957	turbulent	transitional
Q1c2	2.50 ±0.02	4.8 ±0.1	28957	turbulent	transitional
Q1c3	2.50 ±0.02	4.8 ±0.1	28957	turbulent	transitional
Q1c4	2.50 ±0.02	4.8 ±0.1	28957	turbulent	transitional
Q1c5	2.50 ±0.02	4.8 ±0.1	28957	turbulent	transitional
Q2c1	2.58 ±0.02	4.9 ±0.1	29637	turbulent	transitional
Q2c2	2.58 ±0.02	4.9 ±0.1	29637	turbulent	transitional
Q2c3	2.58 ±0.02	4.9 ±0.1	29637	turbulent	transitional
Q2c4	2.58 ±0.02	4.9 ±0.1	29637	turbulent	transitional
Q2c5	2.58 ±0.02	4.9 ±0.1	29637	turbulent	transitional
Q3c1	2.67 ±0.02	4.7 ±0.1	31008	turbulent	transitional
Q3c2	2.67 ±0.02	4.7 ±0.1	31008	turbulent	transitional
Q3c3	2.67 ±0.02	4.7 ±0.1	31008	turbulent	transitional
Q3c4	2.67 ±0.02	4.7 ±0.1	31008	turbulent	transitional
Q3c5	2.67 ±0.02	4.7 ±0.1	31008	turbulent	transitional

B.2.3 Sand: PA6

test	Q[l/s]	$\bar{y}[cm]$	Re(R_H)	Flow type	Near-wall regime
Q1c1	1.25 ±0.01	6.5 ±0.1	13135	turbulent	transitional
Q1c2	1.25 ±0.01	6.5 ±0.1	13135	turbulent	transitional
Q1c3	1.25 ±0.01	6.5 ±0.1	13135	turbulent	transitional
Q1c4	1.25 ±0.01	6.5 ±0.1	13135	turbulent	transitional
Q1c5	1.25 ±0.01	6.5 ±0.1	13135	turbulent	transitional
Q2c1	1.33 ±0.01	6.6 ±0.1	13937	turbulent	transitional
Q2c2	1.33 ±0.01	6.6 ±0.1	13937	turbulent	transitional
Q2c3	1.33 ±0.01	6.6 ±0.1	13937	turbulent	transitional
Q2c4	1.33 ±0.01	6.6 ±0.1	13937	turbulent	transitional
Q2c5	1.33 ±0.01	6.6 ±0.1	13937	turbulent	transitional
Q3c1	1.42 ±0.01	6.7 ±0.1	14782	turbulent	transitional
Q3c2	1.42 ±0.01	6.7 ±0.1	14782	turbulent	transitional
Q3c3	1.42 ±0.01	6.7 ±0.1	14782	turbulent	transitional
Q3c4	1.42 ±0.01	6.7 ±0.1	14782	turbulent	transitional
Q3c5	1.42 ±0.01	6.7 ±0.1	14782	turbulent	transitional

B.2.4 Sand: POM

test	Q[l/s]	$\bar{y}[cm]$	Re(R_H)	Flow type	Near-wall regime
Q1c1	2.16 ±0.02	7.2 ±0.1	21960	turbulent	transitional
Q1c2	2.16 ±0.02	7.2 ±0.1	21960	turbulent	transitional
Q1c3	2.16 ±0.02	7.2 ±0.1	21960	turbulent	transitional
Q1c4	2.16 ±0.02	7.2 ±0.1	21960	turbulent	transitional
Q1c5	2.16 ±0.02	7.2 ±0.1	21960	turbulent	transitional
Q2c1	2.25 ±0.02	7.3 ±0.1	22727	turbulent	transitional
Q2c2	2.25 ±0.02	7.3 ±0.1	22727	turbulent	transitional
Q2c3	2.25 ±0.02	7.3 ±0.1	22727	turbulent	transitional
Q2c4	2.25 ±0.02	7.3 ±0.1	22727	turbulent	transitional
Q2c5	2.25 ±0.02	7.3 ±0.1	22727	turbulent	transitional
Q3c1	2.33 ±0.02	7.5 ±0.1	23372	turbulent	transitional
Q3c2	2.33 ±0.02	7.5 ±0.1	23372	turbulent	transitional
Q3c3	2.33 ±0.02	7.5 ±0.1	23372	turbulent	transitional
Q3c4	2.33 ±0.02	7.5 ±0.1	23372	turbulent	transitional
Q3c5	2.33 ±0.02	7.5 ±0.1	23372	turbulent	transitional

B.3 Logarithmic fit parameters for different beds

Summary: summary statistics for the logarithmic fits in Sections 2 and 3 for homogeneous beds, and for all tests on all beds.

B.3.1 Homogeneous: PA6

test	U^* [m/s]	MSE [m/s]	R2
Q1XS2T1	0.0089558	2.7186e-06	0.98926
Q1XS2T2	0.0078279	8.537e-07	0.99556
Q1XS2T3	0.0086773	2.3064e-06	0.99028
Q1XS3T1	0.0090737	3.8623e-06	0.98519
Q1XS3T2	0.0072332	7.1675e-07	0.99563
Q1XS3T3	0.0087397	3.1021e-06	0.98716
Q2XS2T1	0.0094806	1.8984e-06	0.99328
Q2XS2T2	0.010925	6.9557e-06	0.98167
Q2XS2T3	0.0086165	4.403e-07	0.99846
Q2XS3T1	0.0090837	2.765e-06	0.98938
Q2XS3T2	0.0099055	6.4433e-07	0.9979
Q2XS3T3	0.0087131	1.6109e-06	0.99325
Q3XS2T1	0.0087082	6.931e-07	0.99708
Q3XS2T2	0.0098947	1.5849e-06	0.99029
Q3XS2T3	0.0094904	3.6667e-06	0.97593
Q3XS3T1	0.0099123	1.5546e-06	0.99496
Q3XS3T2	0.0089373	1.8216e-06	0.99275
Q3XS3T3	0.0086135	4.1974e-06	0.9822

B.3.2 Homogeneous: POM

test	U^* [m/s]	MSE [m/s]	R2
Q1XS2T1	0.011916	0.00023866	0.49544
Q1XS2T2	0.015396	2.6574e-06	0.99325
Q1XS2T3	0.018566	5.306e-06	0.99076
Q1XS3T1	0.015347	7.75e-06	0.98045
Q1XS3T2	0.01497	5.568e-06	0.98517
Q1XS3T3	0.01496	1.256e-05	0.96711
Q2XS2T1	0.01573	2.7054e-06	0.99342
Q2XS2T2	0.01549	5.1326e-06	0.9872
Q2XS2T3	0.017132	9.1245e-06	0.98151
Q2XS3T1	0.017444	9.84e-06	0.98078
Q2XS3T2	0.017123	1.2509e-05	0.9748
Q2XS3T3	0.014801	1.0842e-05	0.97089
Q3XS2T1	0.014465	3.4464e-06	0.99012
Q3XS2T2	0.017754	2.3336e-06	0.99553
Q3XS2T3	0.015687	4.6861e-06	0.98859
Q3XS3T1	0.016901	1.1873e-07	0.99975
Q3XS3T2	0.01688	5.7425e-06	0.98794
Q3XS3T3	0.015086	6.0815e-06	0.98407

B.3.3 Gravel: PA6

test	U^* [m/s]	MSE [m/s]	R2
Q1c1T1	0.0084206	2.7759e-05	0.88957
Q1c1T2	0.0060946	1.0568e-05	0.91736
Q2c1T1	0.0078009	2.346e-05	0.9007
Q2c1T2	0.0086488	2.3343e-05	0.91171
Q3c1T1	0.0078095	1.3269e-05	0.92889
Q3c1T2	0.007793	1.709e-05	0.91305
Q1c2T1	0.0087708	2.1999e-05	0.92368
Q1c2T2	0.008064	1.8224e-05	0.91133
Q2c2T1	0.0074925	1.9097e-05	0.90054
Q2c2T2	0.0069349	1.9839e-05	0.86773
Q3c2T1	0.0081827	1.4844e-05	0.93211
Q3c2T2	0.0084868	1.2893e-05	0.94849
Q1c3T1	0.0078659	1.2613e-05	0.93753
Q1c3T2	0.0077511	1.1081e-05	0.93388
Q2c3T1	0.0073098	1.7699e-05	0.91017
Q2c3T2	0.0068658	1.6706e-05	0.90206
Q3c3T1	0.0071956	2.1526e-05	0.89447
Q3c3T2	0.0065418	1.4003e-05	0.9058
Q1c4T1	0.0079874	8.0795e-06	0.9614
Q1c4T2	0.0069409	1.066e-05	0.93761
Q2c4T1	0.0057641	1.6098e-05	0.86685
Q2c4T2	0.0064279	1.4718e-05	0.90314
Q3c4T1	0.0072109	2.2975e-05	0.87694
Q3c4T2	0.0065499	1.2885e-05	0.89832
Q1c5T1	0.0070223	1.6923e-05	0.89636
Q1c5T2	0.0061586	1.0736e-05	0.92269
Q2c5T1	0.0088161	1.4157e-05	0.9453
Q2c5T2	0.0070668	9.6297e-06	0.94246
Q3c5T1	0.0091775	1.7247e-05	0.93704
Q3c5T2	0.0085777	2.2919e-05	0.91409

B.3.4 Gravel: POM

test	U^* [m/s]	MSE [m/s]	R2
Q1c1	0.0082929	1.0712e-05	0.95385
Q1c1	0.0087729	8.539e-06	0.96569
Q2c1	0.010698	2.9837e-05	0.93057
Q2c1	0.011986	2.5136e-05	0.94633
Q3c1	0.011792	2.5979e-05	0.94419
Q3c1	0.011121	3.7012e-05	0.91543
Q1c2	0.0084737	2.3916e-05	0.90469
Q1c2	0.008389	2.0738e-05	0.92155
Q2c2	0.011252	2.9319e-05	0.93119
Q2c2	0.010705	2.0491e-05	0.94624
Q3c2	0.011453	4.1252e-05	0.90806
Q3c2	0.0098167	6.3931e-05	0.82733
Q1c3	0.0089799	5.0408e-05	0.83291
Q1c3	0.0096459	2.0011e-05	0.93341
Q2c3	0.011024	2.4796e-05	0.9377
Q2c3	0.010023	1.9372e-05	0.94054
Q3c3	0.010833	4.5101e-05	0.89149
Q3c3	0.010731	4.5496e-05	0.88755
Q1c4	0.0089038	2.1446e-05	0.92242
Q1c4	0.0083999	1.6822e-05	0.92637
Q2c4	0.0097388	3.0578e-05	0.90813
Q2c4	0.0093631	1.5305e-05	0.94485
Q3c4	0.012327	2.4619e-05	0.94995
Q3c4	0.01147	3.0072e-05	0.93652
Q1c5	0.0077439	1.8643e-05	0.90611
Q1c5	0.0080939	6.7936e-06	0.96796
Q2c5	0.010352	4.0964e-05	0.89154
Q2c5	0.0095319	1.4486e-05	0.95175
Q3c5	0.011121	4.1831e-05	0.90114
Q3c5	0.011045	4.1762e-05	0.90314

B.3.5 Sand: PA6

test	U^* [m/s]	MSE [m/s]	R2
Q1c1T1	0.0016804	2.1285e-06	0.8254
Q1c1T2	0.0012263	1.442e-06	0.79506
Q2c1T1	0.0014979	1.7877e-06	0.81682
Q2c1T2	0.0012552	9.4635e-07	0.85295
Q3c1T1	0.0023483	3.4962e-06	0.84758
Q3c1T2	0.001307	6.853e-07	0.89452
Q1c2T1	0.0017393	2.3641e-06	0.83387
Q1c2T2	0.0012971	1.3074e-06	0.81348
Q2c2T1	0.0019508	2.4693e-06	0.85131
Q2c2T2	0.0012432	9.2152e-07	0.85131
Q3c2T1	0.0021381	2.6298e-06	0.85544
Q3c2T2	0.0016589	1.0808e-06	0.89972
Q1c3T1	0.0016154	2.2868e-06	0.79916
Q1c3T2	0.0012241	1.7258e-06	0.75431
Q2c3T1	0.0021181	2.6605e-06	0.85291
Q2c3T2	0.0016406	1.7773e-06	0.83575
Q3c3T1	0.0022553	3.8795e-06	0.82443
Q3c3T2	0.0014187	1.8858e-06	0.78217
Q1c4T1	0.0017529	2.8415e-06	0.79604
Q1c4T2	0.0010416	9.1089e-07	0.80725
Q2c4T1	0.0023169	2.4296e-06	0.88501
Q2c4T2	0.0018228	2.6605e-06	0.81272
Q3c4T1	0.0023119	2.4774e-06	0.88639
Q3c4T2	0.0016909	1.7245e-06	0.85126
Q1c5T1	0.0017262	2.2862e-06	0.82086
Q1c5T2	0.0011294	1.3598e-06	0.7586
Q2c5T1	0.0024945	3.1472e-06	0.87259
Q2c5T2	0.0016242	2.7118e-06	0.76906
Q3c5T1	0.0023705	3.516e-06	0.8477
Q3c5T2	0.0014348	1.2255e-06	0.8603

B.3.6 Sand: POM

test	U^* [m/s]	MSE [m/s]	R2
Q1c1	0.0062234	1.0868e-05	0.92919
Q1c1	0.0060796	9.2991e-06	0.93225
Q2c1	0.0061684	6.1144e-06	0.95827
Q2c1	0.0071275	6.2796e-06	0.96592
Q3c1	0.0059145	1.2164e-05	0.9055074
Q3c1	-	-	-
Q1c2	0.006388	1.4574e-05	0.90849
Q1c2	0.0055911	1.1784e-05	0.89962
Q2c2	0.0071016	9.9067e-06	0.94753
Q2c2	0.0067373	1.096e-05	0.93208
Q3c2	0.0061249	1.1929e-05	0.9166
Q3c2	0.0056154	8.1897e-06	0.92992
Q1c3	0.0061663	1.2659e-05	0.9127
Q1c3	0.005619	1.4607e-05	0.88424
Q2c3	0.0064613	5.8068e-06	0.96164
Q2c3	0.0065645	1.8937e-05	0.88914
Q3c3	0.0056959	8.405e-06	0.9295
Q3c3	0.0052897	6.5044e-06	0.93684
Q1c4	0.0059506	9.6711e-06	0.92953
Q1c4	0.0047883	9.9762e-06	0.88932
Q2c4	0.007117	8.1329e-06	0.95507
Q2c4	0.0065446	1.0284e-05	0.93174
Q3c4	0.0059672	1.006e-05	0.92529
Q3c4	0.0044057	1.3311e-05	0.86837
Q1c5	0.0063317	1.1993e-05	0.91694
Q1c5	0.0053076	1.269e-05	0.89401
Q2c5	0.0068156	1.5321e-05	0.91473
Q2c5	0.0066888	1.1062e-05	0.93358
Q3c5	0.0058035	1.5482e-05	0.88482
Q3c5	0.0042687	8.9672e-06	0.88633

Appendix C

Experimental protocol

Flat bed experiments were all performed in a flume at the Hydrodynamic Models Laboratory (HML) at the Institute of Geophysics, Polish Academy of Sciences. The flume is completely made of transparent polycarbonate panels with dimensions 5.1 x 0.25 x 0.4 m^3. It is supported by metal elements and can be operated at different slopes because of a hinge and screw jack. In the following, the protocols for the experiments are listed.

C.1 Movable bed experiments with plastic granules

The homogeneous plastics bed experiments were the first to be performed in the flume, and the velocity measurements apparatus was provided by the company Ubertone® thanks to an agreement with the purpose of testing their new UVP device in laboratory conditions.

C.1.1 Bed layer preparation

1. Cover the flume bed with high-porosity gum mats. They have a dual purpose: decrease the total volume of granular material needed to fill the flume bed up to a given depth and, in the case of light particles bedding, create a rigid matrix which stabilises their positions and avoids immediate mobilisation and washout
2. Cover the gum mats with the granular material up to the desired level (approximately 2-3 cm from the PC bed)
3. Regulate the manual leveller to the right height and level the bed to a planar rough surface
4. Measure bed elevation in 4 (5) sections. These measurements will be needed to check, after filling the flume, that the bed layer depth has not changed more than 1 particle's diameter
5. Place the weir gate at the outlet (now it is up to +3cm from the bed surface)

6. Place a weir gate (3 cm height) at the flume inlet
7. Saturate the bed with water from above with a pressurised nozzle, and from below by manually discharging water with a 1l bucket in the flume inlet
8. When water covers the bed in the entire flume, bed preparation ends

C.1.2 Flume filling up to working conditions

1. Close the valves and start one pump
2. Open the upstream valve to vent the flowmeter pipe, regulate the second valve downstream of the flowmeter (now still spherical) to reach a flowrate of 25 l/min
3. Increase the flow rate stepwise with a step duration around 1 min up to the operational value, this phase should take no longer than 10 mins. If a large amount of grains laying at the bed surface starts to float, use the pressurised nozzle to wet them and enhance their sink
4. Once the operational flow rate is established, wait 5-10 mins for the system to stabilise. Depending on the sediment transport rate, remove elements of the weir gate, one at a time, at the outlet of the flume, up to the desired transport intensity (to be assessed visually)
5. Measure the bed surface level again and check that changes are no higher than 1 grain diameter. Else, the bed is not plane anymore
6. Measure the flowrate at the flowmeter and pressure head at different sections (they can be the same where the bed elevation was measured) to check whether the system is stable.

C.1.3 Flow field characterisation

1. Measure the water depth at the measuring section
2. Position the UVP transducers' holder in the section on the side wall, adjust its elevation according to the first measuring profile, before securing the location, check it is horizontal with the spirit level. This operation now is done by using a suction cup.

   NOTE: The first measured profile will be very close to the bed and the centre of the transducers is approximately 5 mm from the bed surface. The horizontal check with the spirit level is needed only with zero slope bed setup.
3. Locate the transducers in their housing and apply USG gel so that no air is present between the transducer surface and the flume side wall. Fix the transducer position at the wall by screwing firmly at the hinges of its holder
4. Connect the computer to the UVP via its wireless network. Open a browser and enter its IP address (192.168.42.1) to access the GUI (see Figure C.1)

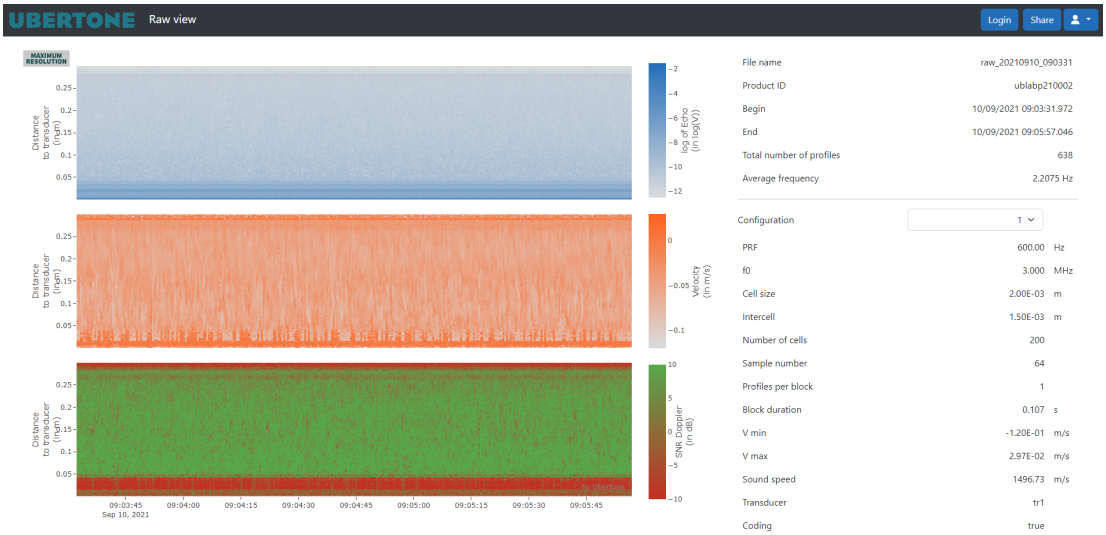

FIGURE C.1: Ubertone® online drive GUI

5. Check the signal correlation on the GUI and setup parameters:

   (a) pulse repetition frequency (it defines the velocity range)

   (b) expected minimal velocity (it shifts the velocity range, it depends on the direction of the transducer with reference to the mean flow)

   (c) sample number (for calculating one profile, its unit should be a power of 2)

   (d) profile number per block ()

   (e) position of the first cell (distance of first measuring point from the transducer)

   (f) distance between cells (distance between cells centres)

   (g) cell size (length of one cell, parallel to the transducer axis)

   (h) cell number (total number of cells making up a profile)

   NOTE: The UVP setup is constant for all profiles (over the vertical in each cross section and over the longitudinal direction along the flume) because we are measuring horizontal velocity profiles (the longitudinal component of the velocity along the horizontal direction). If you need also vertical profiles, you might need to change the setups.

6. Start recording one profile

7. Change the elevation of the transducer, repeat points 2 to 6

C.1.4 Bed movements and cover changes detection

Due to the low density of the materials, and the relatively low depths adopted in the tests (spanning from 4.5 to 6.5 cm), we decided to allow perturbations of the water surface, as not to disturb the flow field too much. We suggest whoever would be willing to replicate these experiments, if possible, to adopt measures to prevent water surface perturbations from affecting the image quality, measures which we could not adopt, and cannot describe hereby, but that are largely available in the recent and less recent literature (e.g. Keshavarzy and Ball, 1999).

1. Use a screen or a foil at the flume inlet to reduce air bubbles on the water surface
2. Position the camera support in the measuring section
3. Fix the camera so that the field of view covers the whole flume width and the lens is at the flume centre. Use the signs on the support as a guide.

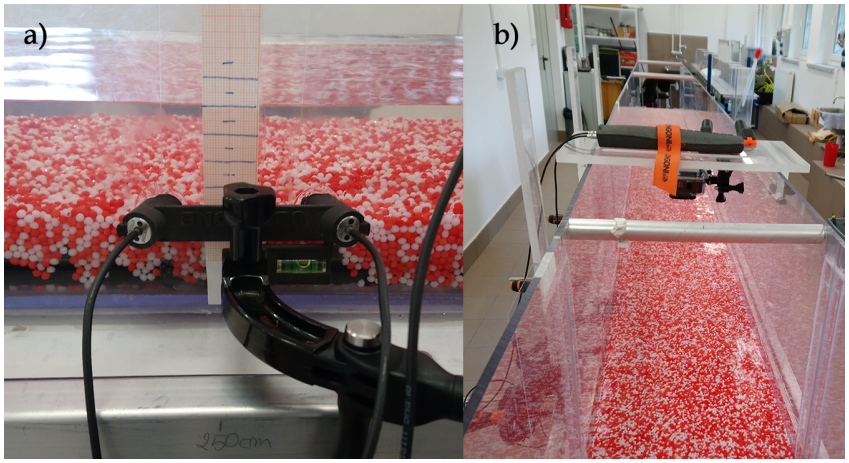

FIGURE C.2: Positioning of the measurement apparatus: a) details on the UBLab P transducers by Ubertone®, b) camera and its support.

4. Cover the area with a lid to reduce to a minimum reflections of light over the water surface
5. Start recording (videos have a duration of 2 - 5 minutes depending on the intensity of bed movements)

C.2 Fixed bed experiments with plastic granules: clastic bed

Experiments are run at fixed hydraulic conditions and increasing the MPs surface concentration, both for gravel- and sand-bed tests. The total duration for each hydraulic condition is around 5 - 6 h.

C.2.1 General protocol for experiments with MPs on clastic beds.

Gravel

The preparation of the bed end experimental condition involves the following steps:

1. Position the weir gate at the flume outlet with an elevation of 6.5 cm.
2. Level the wet bed manually up to an elevation around 3.7-3.5cm from the flume rigid plastic bed.
3. Fill the flume (1 pump) at Q_0 = 30 - 40 l/min up to a depth of 7 - 8 cm, then increase the flow up to 60 - 70 l/min and flow it for 10' to obtain a water-worked bed.
4. Reduce the flow depth to the experimental conditions (around 5cm) and seed with particles, at Qsed 65-70l/min and 100-105l/min with the chosen concentration of PA6 and POM respectively.
5. The seeding scheme is reported in figure (I am drawing it) C.3. The seeding is done by dividing the quantity of MP into parts, with a maximum number of 8, and spreading it manually in diagonal transects covering the whole area 1.5 m long. The remaining quantity is used to fill areas where the least particles are present, so to keep the pattern as randomly uniformly covered as possible.
6. The experiments are run at three fixed discharge conditions, increasing the concentration of the surface MPs in the range 0.05% - 1% (every time repeating the seeding conditions and reducing the discharge to Qsed).
7. After each condition has been run, a visual check on the number of particles mobilised and which exited the area allows eventually to adjust the quantity to seed to meet chosen values (0.05%, 0.1%, 0.2%, 0.5%, 1%).

The duration of each experiment (at fixed flow conditions) is around 5-6h.

Sand

The preparation of the bed end experimental condition involves the following steps:

1. Position the weir gate at the flume outlet with an elevation of 6.5 cm.

2. Level the wet bed manually up to an elevation around 3.7 - 3.5 cm from the flume rigid plastic bed.

3. Fill with water at 20 - 30 l/min up to a depth around 2 - 3 cm: this step is needed to remove air bubbles trapped in the sand surficial layer and ensure all sand is wet.

4. Let the bed drain out the water for 40 mins.

5. Level the wet bed manually up to an elevation around 3.7 cm.

6. Fill the flume slowly, stepwise from 20 to 60 l/min, in 5-minute steps, up to a water depth of around 8 cm.

7. Flow 60 l/min for 15/20 minutes to have a water-worked bed (not anymore influenced by the initial levelling conditions.

8. Seeding of particles is done manually as for gravel bed experiments, at discharges Q_{sed} around - and – for PA6 and POM particles respectively, following the scheme in figure C.3

9. From Q_{sed}, increase the discharge up to experimental conditions stepwise, in 3 - 5 minutes time.

C.2.1.1 Bed layer preparation

The bed is prepared in two steps: (i) filling of the flume with a layer of bed sediments, (ii) modelling the layer to flat bed conditions. The procedure for preparing the bed layer is similar to that outlined in Section C.1.1. Hereon are the main steps:

1. Cover the flume with plastic lining to prevent big scratches of the rigid bottom

2. Cover the bottom with gum mats

3. Pour the granular material to completely cover the mats (gravel was always used also in the case of experiments on sand, to reduce the total weight of the bed layer)

4. Add around 2 cm of material, to have a homogeneous layer of either gravel or sand

5. Regulate the manual leveller to the right height and level the bed to a planar rough surface

6. Measure bed elevation in 4 sections. These measurements will be needed to check if readjustments occurred in the water-filling phase

7. Place the weir gate at the outlet

8. Manually level the (dry) bed to flat conditions

C.2.1.2 Flume filling

The flume is filled slowly, from the upstream end, by manually opening a valve. It requires the following steps:

1. Close the weir gate at the downstream end of the flume up to 7 cm above mean bed elevation
2. Let the water flow and cover the bed up to a depth of 2 cm
3. While checking the bed does not experience movement, gradually open the valve to increase the flow rate, up to depth allowed by the weir gate
4. In case the bed starts to move, reduce the valve opening
5. Regulate the elevation of the weir gate to reach the desired conditions

C.2.1.3 Seeding

The seeding is done by dividing the quantity of MPs into even parts, with a maximum number of 8, and spreading it manually in diagonal transect lines C.3 covering the whole area 1.5 m long. Along the line, seeding follows an oscillatory pattern. The remaining quantity is used to fill areas where the least particles are present, so as to keep the general pattern of MPs on the bed surface as randomly uniformly covered as possible.

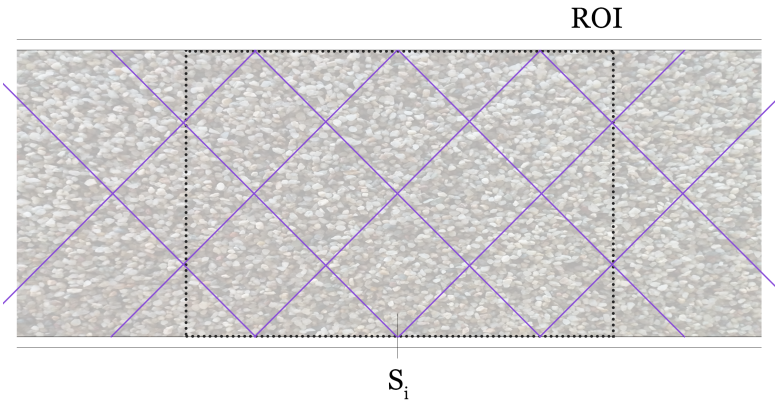

FIGURE C.3: Scheme of manual seeding method: seeding lines (violet) inclined 45° to the longitudinal axis of the flume.

C.2.2 Flow field characterisaton

The characterisation of the flow field requires the following steps:

1. Place the transducer on its support
2. Regulate the support distance from the wall to the desired value

3. Regulate the elevation of the transducer so it just touches the water surface, and does not create a large wake
4. Turn on the UVP measuring apparatus
5. Check the settings, it usually requires regulating the pulse repetition frequency
6. Check the bed is detected in the echo signal (there you have a peak)
7. Set the measurement duration
8. Start measuring

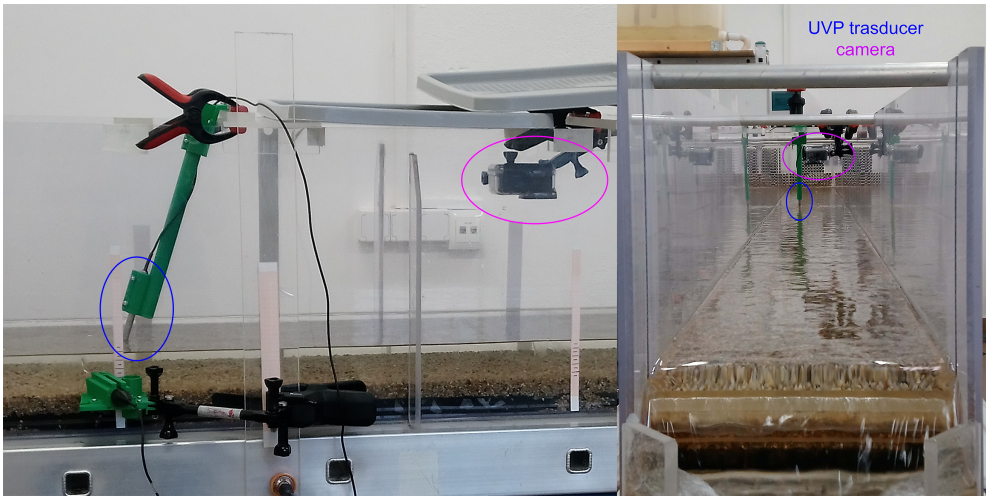

FIGURE C.4: UVP transducer and camera setup during gravel bed experiments. Flume seen from the side.

C.2.3 Bed cover changes detection

To detect the changes in the bed cover, images of the bed are necessary. The procedure requires to have top-view videos, and follows the steps:

1. Prepare the camera support
2. Insert the camera in its support and regulate the camera positioning to cover the whole flume width
3. Cover the camera to avoid light reflections on the surface, and check
4. Start video recording